Characterization of synaptic inputs onto subplate neurons in somatosensory cortex of newborn rat

Inaugural-Dissertation

zur

Erlangung des Doktorgrades der

Mathematisch-Naturwissenschaftlichen Fakultät

der Heinrich-Heine-Universität Düsseldorf

vorgelegt von

Ileana Livia Hanganu

aus Bukarest

Düsseldorf 2002

Gedruckt mit der Genehmigung der Mathematisch-Naturwissenschaftlichen Fakultät der Heinrich-Heine-Universität Düsseldorf

Referent: Prof. Dr. H. J. Luhmann

Korreferent: Prof. Dr. W.-R. Schlue

Tag der mündlichen Prüfung: 10.07.2002

TABLE OF CONTENTS

1. Introduction

1.1 Cerebral cortex

The cerebral cortex is probably the highest achievement of biological evolution and the neural base of remarkable human capacity for reasoning and language. The disproportionate growth relative to the remaining part of the brain, the enormous increase in its surface and the elaboration of functional subdivisions mark the evolution of the cerebral cortex. Ontogenetically, the cerebral cortex emerged from the dorsal telencephalon of the mammalian forebrain and includes the neocortex, paleocortex, archicortex and limbic cortex. In higher mammals, the most prominent and phylogenetically the most recent component of the cerebral cortex is the neocortex. The mature neocortex is composed of six cell layers with different appearance, set of genes and patterns of afferent and efferent axonal connectivity.

1.2 Development of the neocortex

An elaborate sequence of events involving neurogenesis, neuronal migration and differentiation leads to the formation of the six-layered neocortex (Boulder Committee, 1970; Sidman and Rakic, 1973; Allendoerfer and Shatz, 1994; Price and Willshaw, 2000) (Fig. 1). Cortical development begins with the division of the dorsal telencephalic wall into the ventricular zone (VZ), an inner germinal layer which give rise to most of neurons and glia cells of the cerebral cortex, and the preplate (PP) (Marín-Padilla, 1971; Rickmann et al., 1977), an outer layer which contains prospective Cajal-Retzius neurons and other polymorphous cells (Fig. 1A). The neurons forming the cortical plate (CP) are generated in the VZ, migrate toward the pial surface and split the PP into the superficially located marginal zone (MZ) (Boulder Committee, 1970) and the deeply located subplate (Kostovic and Rakic, 1980) (Fig. 1B). During cortical development, neurons forming the deepest layer

(layer VI) are generated first, neurons of the superficial layers (layer II/III) are generated last. This inside-out migration pattern (Angevine and Sidman, 1961; Rakic, 1974) seems to be an unique feature of the mammalian cortex. Migration of the cortical neurons from the VZ to their final destination requires the presence of radial glia cells (Berry and Rogers, 1965) and involves either somal translocation or locomotion depending on the stage of development (Nadarajah et al., 2001). By adulthood (Fig. 1C), the majority of neurons in MZ and subplate have disappeared or transformed themselves into other neuronal shapes (for review Supèr et al., 1998).

The complete development of the neocortex is not restricted to the generation of cortical layers by neurogenesis and neuronal migration, but also involves the formation of specific connections both within and between neocortical areas and with other parts of the nervous system. The organization of complex neuronal networks which are constructed over an extended period, before and after birth, involves activity-independent and activity-dependent processes (for review Goodman and Shatz, 1993). Despite extensive investigation, the mechanisms how genetically programmed molecular cues interact with electrical activity in order to guide axons to their final target and refine patterns of synaptic connectivity remains poorly understood. Generally, the earliest stages of neuronal development, including establishment of cell phenotype and target selection are thought to depend almost exclusively on the genetic program of the cell, while the subsequent stages of development including synaptic refinement are guided by neuronal activity (for review Goodman and Shatz, 1993).

For the investigation of the formation of cortical circuits and of the relationship between the periphery and the cerebral cortex, the somatosensory cortex of small

rodents represents an ideal system, since it is a well studied isomorphic representation of the body surface (Killackey et al., 1995). Sensory information from the peripheric receptors is transmitted via brainstem nuclei to the contralateral thalamus. Finally, topographically ordered thalamocortical projections reach their final destination, the somatosensory cortex (Herkenham, 1980; Chapin and Lin, 1990). The mechanisms by which the crude thalamocortical connections in the developing cortex become topographically ordered in a precise manner and recognize and select their target are not completely understood. During the initial, fetal developmental stage, ingrowing thalamic axons are guided to their appropriate cortical targets by molecular cues intrinsic to the cortex (for review Rakic, 1988; Bolz and Castellani, 1997; Levitt et al., 1997a). In the second, perinatal phase, the thalamocortical innervation is refined in an activity-dependent manner (for review Katz and Shatz, 1996; Feller, 1999; Zhang and Poo, 2001). The topography of the thalamocortical projections seems to be established with the assistance of early generated neurons of the subplate (De Carlos and O'Leary, 1992; Erzurumlu and Jhaveri, 1992; Molnàr and Blakemore, 1995).

1.3 The subplate and its role during neocortical development

Likely co-evolved with neocortex (Aboitiz, 1999), the subplate is a transient structure located directly under the CP and consisting of a heterogeneous population of neurons according to morphology, neurotransmitter identity, content of neuropeptides, growth and death factors (Kostovic and Rakic, 1980; Wahle and Meyer, 1987; Valverde et al., 1989; Allendoerfer and Shatz, 1994). Subplate neurons (SPn) exhibit heterogeneous morphologies (Valverde et al., 1989; Wahle et al., 1987; 1994) and complex arborized dendritic trees (Mrzljak et al., 1992; Del Río et al., 2000). SPn are among the earliest neurons generated during cortical development. Their post-developmental fate remains controversial. In cats and humans, more than 80% of the SPn disappear by cell death,

whereas the remaining SPn transform themselves in other neuronal shapes present in the white matter (WM) (Luskin and Shatz, 1985; Kostovic and Rakic, 1990). In rodents, it is likely that the majority of SPn become incorporated in the mature layer VIb (Valverde et al., 1989; Uylings et al., 1990) and the transient role of SPn in rodents correlates with the loss of specific immunocytochemical markers and not with anatomical degeneration of the neurons (Robertson et al., 2000).

SPn are actively involved in the formation of connections between thalamus and neocortex. They pioneer thalamocortical pathway and guide the selection of the correct cortical area by thalamic axons (for review Allendoerfer and Shatz, 1994). During early development, thalamocortical axons grow towards the cortex and form temporary synapses with SPn (Rakic, 1977; Catalano and Shatz, 1998). Whether these axons "wait" in the subplate (Rakic, 1977; Ghosh and Shatz, 1992a) or directly grow to their final targets in layer IV (Kageyama and Robertson, 1993) remains controversial. However, deletion of the subplate (Ghosh and Shatz, 1992b) or its improper differentiation (Zhou et al., 1999) causes an inappropriate thalamocortical innervation. The growth and guidance of the thalamic axons may in part be due to the presence of specific molecules located in the subplate (Bicknese et al., 1994; Yuasa et al., 1994). However, synaptic interactions between SPn and thalamic axons seem also to be necessary for the achievement of the final pattern of connections (Herrmann et al., 1994). These data indicate that molecular markers as well as electrical activity patterns in the subplate may influence the ingrowing thalamocortical axons.

SPn also play a crucial role in establishing corticothalamic connections (Auladell et al., 2000). Axons of SPn are the first to extend out of the cortex and

influence the growth of cortical efferents through the internal capsule (McConnell et al., 1989; De Carlos and O'Leary, 1992). Not only thalamic and cortical connections seem to interact with SPn, but also catecholaminergic, serotonergic or cholinergic fibers innervate the subplate during early development (Levitt and Moore, 1979; Schlumpf et al., 1980; Kostovic, 1986).

SPn express glutamate (Herrmann, 1996; Smith and Thompson, 1999) and γ-amino-butyric acid type A ($GABA_A$) receptors (Huntley et al., 1990; Meinecke and Rakic, 1992) and exhibit symmetrical as well as asymmetrical synapses with relative mature properties (Chun and Shatz, 1988; Herrmann et al., 1994). These data suggest that SPn are actively involved in glutamatergic and GABAergic synaptic transmission.

1.4 Chemical and electrical synaptic transmission in the developing cortex

1.4.1 Synaptic transmission

Synaptic transmission as communication mode between neurons or between neurons and their effectors is generally required for the formation of neural circuits. According to their operation mechanism, two types of synapses were identified: electrical and chemical synapses. Electrical synapses allow direct electrical coupling between two neurons through low resistance transmembraneous channels referred as gap junctions (Kuffler and Potter, 1964; Bennett et al., 1981; Beyer, 1993). Chemical synapses allow communication between neurons through presynaptic release of neurotransmitters (Millhorn et al., 1989), that activate ion channels in the membrane of the postsynaptic neuron.

1.4.2 Gap junction coupling in the developing neocortex

Gap junctions link neocortical neurons during early developmental stages (Connors et al., 1983; Peinado et al., 1993a) and may form extensive syncitial networks between immature neurons (Peinado, 2001). However, the role played by gap junctions during development remains largely speculative. It seems that they not only allow electrical and metabolic communication between neurons in order to regulate cellular functions (Beyer, 1993), but also establish tight interactions with chemical synaptic transmission, modulating the formation of neuronal connectivity (Rörig and Sutor, 1996).

1.4.3 Neurotransmitter action in the developing cortex

During development, neurotransmitters mediate rapid communication between neurons (Millhorn et al., 1989; Owens and Kriegstein, 2001) and modulate synaptic transmission (Rhoades et al., 1994; Roerig and Katz, 1997; Miller, 1998). Moreover, neurotransmitters are able to regulate morphogenetic events such as proliferation, migration, growth, differentiation, and survival and death of neurons (Hohmann and Berger-Sweeney, 1998; Ma et al., 2000; Behar et al., 1999; Ikonomidou et al., 1999), being essential for correct cortical development.

Excitatory neurotransmission is mainly mediated by glutamate acting on ionotropic and metabotropic glutamate receptors. Ionotropic glutamate receptors are heteromeric ligand-gated ion channels and based on their pharmacological and electrophysiological properties can be subdivided in N-methyl-D-aspartate (NMDA) receptors, (±)-α-amino-3-hydroxy-5-methylisoxazole-4-propionic acid (AMPA) and kainate receptors (Dingledine et al., 1999). NMDA receptors are implicated in important physiological processes such as synaptic plasticity, synapse formation and

learning and memory (for review Mayer and Westbrook, 1987), as well as in pathophysiological processes like ischemia (Kral et al., 1993) and epilepsy (Mikuni et al., 1999; Stone and Burton, 1988). They show during development a high degree of heterogeneity concerning their properties such as the voltage-dependent physiological block by Mg^{2+} (Monyer et al., 1994). Metabotropic glutamate receptors are G-protein coupled and regulate the synthesis of various intracellular second messengers (Pin and Duvoisin, 1995).

In the mature cortex, the inhibitory neurotransmission is mainly mediated by γ-amino-butyric acid (GABA) acting on ionotropic $GABA_A$ receptors and on metabotropic $GABA_B$ receptors (Bormann, 1988). In contrast, during development, GABA acts excitatory due to the relatively high intracellular chloride concentration maintained in immature neurons (Ben-Ari et al., 1989; Luhmann and Prince, 1991; Owens et al., 1996). GABA-induced depolarization is able to upregulate release of neurotrophic factors, which affect cell survival (Ghosh et al., 1994) and synaptic plasticity (Korte et al., 1995).

In addition to glutamate and GABA, acetylcholine (ACh) plays an essential function during cortical development. The cortex receives a widespread cholinergic innervation which originates from the basal forebrain (Kristt et al., 1985; Lehmann et al., 1980; Rye et al., 1984) and seems to interact and mold the thalamocortical sensory inputs to cortex both during development and adulthood (for review Hohmann and Berger-Sweeney, 1998). ACh acts on ionotropic nicotinic and metabotropic muscarinic receptors and is able to modulate visual cortical plasticity (Bear and Singer, 1986), release of glutamate, GABA or monoamines (MacDermott et al., 1999; Aramakis et al., 1999).

1.5 Purpose of the present study

Patch-clamp recordings from visually identified and biocytin labeled SPn in somatosensory cortical slices from newborn rats were performed to identify and study the functional properties of synaptic inputs onto SPn. Detailed analysis of the heterogeneous somatodendritic properties of SPn led to identification of six morphological classes which showed no differences in their electrophysiological properties and synaptic inputs. SPn showed spontaneous synaptic activity mediated by AMPA, NMDA and $GABA_A$ receptors. In order to identify the origin of these synaptic inputs, electrical stimulation of thalamocortical afferents (TA), CP including layers V/VI and subplate was performed and the functional properties of stimulus-evoked synaptic inputs were investigated. The results of the present study show that SPn receive an AMPA and NMDA receptor-mediated input from all three structures and a GABAergic input from other SPn. To addresses the question, whether GABA application has a hyper- or depolarizing effect on SPn, gramicidin perforated patch recordings were performed. In addition, investigation of the effects of nicotinic and muscarinic receptor activation showed that both receptors are functional on SPn and muscarine increased the glutamatergic spontaneous synaptic activity of SPn. Dye-coupling experiments and changes in the membrane properties and synaptic activity in the presence of gap junction blockers led to the conclusion that at least a small fraction of SPn are gap junction coupled . Results of the present study were already published (Luhmann et al., 2000; Hanganu et al., 2000a; Hanganu et al., 2000b; Hanganu et al., 2001a; Hanganu et al., 2001b; Hanganu et al., 2001c; Hanganu et al., 2002, Hanganu et al., in press).

2. Materials and methods

2.1 Preparation of brain slices

Experiments were performed on 400 μm-thick whole brain coronal slices including the somatosensory cortex prepared from 0-3 days old (P0-P3, day of birth = P0) male Wistar rats (Fig. 2A). All experiments were conducted in accordance with the national laws for the use of animals in research and approved by the local ethical committee.

2.1.1 Preparation of tissue for slicing

The rat pups were anaesthetized by hypothermia and decapitated. The skull was opened and a large brain region containing the somatosensory cortex (Fig. 2B) was rapidly removed (<1 min) and immediately immersed in oxygenated ice-cold artificial cerebrospinal fluid (ACSF). Cooling of the tissue minimized damages due to anoxia and improved the texture of tissue for slicing.

2.1.2 Slicing and incubation of slices

Three to four slices were prepared on vibroslicer (TPI, St. Louis, MO). For this purpose the block of tissue containing the somatosensory cortex, trimmed parallel to the desired orientation of the slices, was glued to the stage of the slicer using cyanoacrylat adhesive (Permabond, Eastleigh, UK). The slicing chamber was immediately filled with ice-cold ACSF. After the tissue block was trimmed roughly to the level of primary somatosensory cortex, at least one slice was discarded before slices of uniform 400 μm thickness were obtained. The slicing procedure was monitored continuously and the speed of slicing was adjusted so that the tissue was never pushed by the blade. Moreover, the blade was raised on backwards movement to avoid surface damage of the next slice. The slices were cut in the middle to divide them into two hemispheres and transferred to a holding chamber containing

oxygenated ACSF at 33° C. In order to ensure optimal oxygenation and continuous movement of ACSF, the slices were bubbled from below with 95% O_2/5% CO_2. Slices were transferred into and out of the holding chamber using the large end of the Pasteur pipette. After an incubation period of at least 1 h, slices were transferred one at time to recording chamber (volume < 2 ml), where they were continuously superfused at a rate of 2 ml/min with oxygenated ACSF at 33° C. A grid of parallel nylon threads (10 x 10 mm) in a platinum frame was placed on the slice in the recording chamber to increase mechanical stability. The slices were used up to 7 h without any apparent changes in the electrophysiological properties of the cells.

2.2 Patch-clamp recordings

2.2.1 Introduction to the patch-clamp technique

The patch-clamp technique is an electrophysiological method that allows recording of macroscopic whole-cell or microscopic single-channel currents, flowing across biological membranes through ion channels. Such low-noise recordings are achieved by tightly sealing a glass pipette onto the cell membrane and isolating a small patch (Hamill et al., 1981). The patch clamp technique allows either to experimentally control and manipulate the voltage of membrane patches or whole cell (*voltage-clamp recordings*) or to monitor the changes in membrane potential in response to currents flowing across ion channels (*current-clamp recordings*).

2.2.2 Patch-clamp setup and recording pipettes

2.2.2.1 Patch-clamp setup

The used patch-clamp setup consists of (i) an optical setup including the microscope and the video camera, (ii) a mechanical setup including vibration isolation table,

Faraday cage, micromanipulators, and application-suction system and (iii) an electronic setup consisting of amplifier, stimulators and computer-interface.

2.2.2.1.1 Optical setup

Investigated SPn were visualized with video enhanced infrared Nomarski optics in a recording chamber mounted on the fixed stage of an Axioskop microscope (Zeiss, Oberkochen, Germany) using a 40X water immersion objective. The microscope moved in all three axes driven by a programmable stepping motor (Luigs&Neumann, Ratingen, Germany). The light source was a tungsten lamp powered with a 12-V power supply (Zeiss). The optical pathway used for infrared differential interference contrast (IR-DIC) video microscopy involved the presence of an infrared filter (λ_{max}=780 nm) inserted in the light path prior to the DIC polarizer. An IR-sensitive video camera (CF 8/1, KAPPA, Gleichen, Germany), providing contrast enhancement and shading correction was used to monitor seal formation and possible morphological changes of the investigated cell. The images from camera were displayed on a standard black-and-white video monitor (WV-BM 1410, Hamamatsu, Japan) and were digitized online using a frame grabber card (Screen Machine II, München, Germany).

2.2.2.1.2 Mechanical setup

Since patch-clamp recordings require mechanical stability of all setup components, a low-end air-suspension vibration isolation table (Science Products, Hofheim, Germany) damped up the movements and vibrations disturbing the recording process. To gain additional mechanical stability, the table was placed in a corner of the room and the elastic floor was replaced with a stable base connected to the support structure of the building. The Faraday cage (purpose made) surrounded the patch-clamp setup and shielded the amplifier headstage from electrical noise. The precise control of

position and movement of the recording pipette was realized using a motorized micromanipulator able to move in all three axes (Luigs&Neumann). A second manipulator, manually moved, was used to position the stimulation electrode. Both manipulators were attached to columns that are mounted to the isolation vibration table. Continuous superfusion of the slice in the recording chamber was performed using a purpose-made application-suction system. Within the Faraday cage, brackets were mounted to hold bottles containing the perfusion solutions. These solutions were transported by gravity through thin plastic tubing ending with a metallic tip in the recording chamber. A pump-controlled suction of the solution ensured a constant level of fluid in the recording chamber. The metallic tip of the application system was placed diametrically opposed to the tip of suction system to ensure an optimal circulation of the solution.

2.2.2.1.3 Electronic setup

The used patch-clamp amplifiers (EPC9, Heka, Lambrecht, Germany and SEC-05L, NPI, Tamm, Germany) consisted of a headstage, transforming the recorded current in potential, and the main amplifier amplifying and filtering the signal. The headstage was mounted directly on the micromanipulator in order to position it stable, close to the recording chamber and was separated by a non conducting material from the metallic parts of the micromanipulator. The main amplifier EPC9 is a feedback resistor amplifier with an integrated software for use and collection of data and provided for total digital control with automatic series resistance and capacitance compensation. The SEC05 amplifier is a discontinuous single-electrode voltage-clamp amplifier. The isolated stimulator (purpose made) was used to set the amplitude and the duration of the stimulus and to minimize a capacitive coupling between ground and stimulation electrode. To convert analog signals from amplifier in digital signals

for computer and to deliver control signals to the amplifier and stimulator, an AD/DA converter (Heka) was used. Data were acquired and processed using TIDA 4.11 Software (Heka).

In order to minimize line-frequency interference, all surfaces near the headstage were grounded. The reference electrode represented by a chloride coated silver wire contacting the perfusion solution in the recording chamber, was connected directly to the ground terminal of the headstage. The microscope, Faraday cage, metallic tips of the application-suction system opening in the recording chamber and micromanipulators were grounded by low-resistance ground cables at a central point within Faraday cage.

2.2.2.2 Recording pipettes

Recording pipettes were made from borosilicate glass tubing (2.0 mm OD, 1.16 mm ID; CG200F8P, Science Products, Hofheim, Germany) known to have lower dielectric loss and produce less noise. A vertical puller (PP83, Narishige, Tokio, Japan) used gravitation-controlled two-step mechanism to separate the glass tubing in two pipettes with similar tip diameter. Since the pipettes were perfectly suitable for experiments directly after pulling, they were not further processed by coating or heat polishing. The pipettes were back-filled with filtered (sterile filter with pore size 0.2 µm, Nalgene^{TM}, NY) pipette solution and any bubbles left were removed by tapping the side of the pipette. When filled with pipette solutions, pipette resistance varied from 4 to 14 MΩ. The pipettes were placed in a polycarbonate holder (Science Products) fixed directly at the headstage. Electrical contact between pipette solution and headstage was achieved using a chlorided silver wire. To ensure low-noise recordings, the holder was regularly cleaned with methanol flush, followed by drying with air jet.

2.2.3 Solutions

2.2.3.1 Extracellular solution

During preparation and recording, the slices were superfused with ACSF which contained (in mM): 124 NaCl, 26 $NaHCO_3$, 3 KCl, 1.6 $CaCl_2$, 1.8 $MgCl_2$, 1.3 NaH_2PO_4 and 20 D-glucose (pH 7.4 after equilibration with 95% O_2/5% CO_2, osmolarity 333 mOsm).

2.2.3.2 Pipette solutions

Corresponding to different purposes, several solutions were used and their compositions (in mM) were summarized in Table 1. All pipette solutions were adjusted to pH 7.4 with 1 M KOH and to an osmolarity of 306 mOsm with sucrose. In all experiments 0.5% biocytin was included in the pipette solution.

Table 1. Composition of pipette solutions

Solution	**Composition (mM)**							
	K-gluconate	KCl	$CaCl_2$	$MgCl_2$	EGTA	K-HEPES	NaATP	NaGTP
Gluconate-based solution	117	13	1	2	11	10	2	0.5
High-chloride solution	-	130	1	2	11	10	2	0.5
Perforated patch solution	126	4	1	2	11	10	-	-

EGTA: ethylene glycol-bis(2-aminoethylether)-N,N,N',N'-tetraacetic acid;
HEPES: N-(2-hydroxyethyl) piperazine-N'-(2-ethanesulfonicacid);

The majority of recordings were performed using gluconate-based solution. For determination of the current-voltage relationship of the evoked synaptic currents, 10 mM lidocaine N-ethyl bromide (QX-314), a voltage–dependent sodium channels

blocker, was added to the gluconate-based pipette solution. High-chloride solution was used for the investigation of $GABA_A$ receptor-mediated synaptic currents. For perforated patch recordings gramicidin used as perforation agent, was dissolved in dimethylsulfoxide (DMSO) and added in a final concentration of 1 μM/ml to perforated patch solution.

2.2.4 Patch-clamp procedures

2.2.4.1 Formation of the seal

Patch-clamp recordings on visually identified SPn were performed according to the procedure described by Stuart et al. (1993). The pipette was advanced through the slice at an angle of 20° to horizontal and positive pressure was applied to hinder the obstruction of the pipette tip. The process of high-resistance (>1 GΩ) seal formation was continuously monitored using WinTIDA Software (Heka) while applying voltage pulses of 10 mV to the pipette. Once the pipette tip touched the cell membrane, the pipette resistance increased. Fast capacitance correction was performed using the built-in circuitry of the amplifier and the positive pressure was released. Application of a slight negative pressure until a small patch of membrane was isolated led to seal formation. Hyperpolarization of the recording pipette to –70 mV helped seal formation. Usually, seal formation took less than 1 min and had a success rate higher than 80%. Under these conditions, pipette and neuron formed the *cell-attached configuration* (Fig. 2C) which induced no changes in the second-messenger system or in the ionic concentration of the investigated neuron.

2.2.4.2 Whole-cell recordings

In order to gain access to the cell interior and to voltage-clamp the whole cell, the isolated patch membrane was ruptured by additional negative pressure and rarely by

high-voltage pulses, leading to the formation of *whole-cell configuration* (Fig. 2C). Under these conditions, the recorded neuron was rapidly filled with the pipette solution (Pusch and Neher, 1988). Slow capacitance and series resistances were minimized using the built-in circuitry of the amplifier. During an experiment, the series resistance was continuously controlled. Partial resealing of the patch membrane was prevented by including in the pipette solution high level of Ca^{2+}-buffering capacity (10 mM EGTA).

2.2.4.3 Perforated patch recordings

The main disadvantage of the whole-cell recordings consists in the washout of cytosolic constituents. In order to selectively retain these constituents, the electrical connection between cell and pipette was established by incorporation of a channel forming substance in the pipette solution, leading to the formation of the *perforated patch configuration* (Fig. 2C). In several experiments 1-2 μM gramicidin D, a commercially available mixture (Sigma-Aldrich, Deisenhofen, Germany) of 3 polypeptides produced by *Bacillus brevis*, was used to form chloride-impermeable channels (Kyrozis and Reichling, 1994). The progress of perforation was evaluated by monitoring the capacitative current transient to a 10 mV step in holding potential. Series resistances below 35 MΩ obtained after 5-30 min represented the premise to start the recordings.

2.2.4.4 Liquid junction potentials

Due to different composition of intracellular and extracellular solution, particular attention was paid to junction potentials existing at the tip of the recording pipette. All potentials were corrected for liquid junction potentials with –10 mV for gluconate-

based pipette solution (Mienville and Pesold, 1999) and with –4 mV for the high-chloride pipette solution (Marty and Neher, 1995).

2.2.5 Extracellular stimulation

A bipolar tungsten electrode (5 MΩ, FHC, Bowdoinham, ME) was used for electrical stimulation of the TA, the CP including layers V/VI and the subplate. The positions of the extracellular electrode in cortical and subcortical regions are indicated schematically in Fig. 3. For a precise stimulation of the TA, the path of the thalamocortical projections was determined in ten slices by performing extracellular biocytin injections in rat cortical slices. The revealed characteristic path of TA (Fig. 3 inset) was in accordance with previous anatomical studies (Molnár et al., 1998). For electrical stimulation of the TA, the stimulation electrode (tip separation 600-800 μm) was positioned in the internal capsule approximately 500 μm laterally to the recorded cell. The deeper CP layers including layers V/VI or the subplate were stimulated using a stimulation electrode with a tip separation of 150-200 μm and a horizontal cut was performed directly below the WM to eliminate possible inputs from subcortical regions. Since the connections between the CP and the subplate are organized radially (Antonini and Shatz, 1990), the CP stimulation electrode was positioned in the same vertical axis as the recorded cell. For electrical activation of the subplate, the stimulation electrode was placed approximately 200 μm laterally to the investigated SPn. In all experiments the duration of the electrical stimulus was 70 μs. The intensity of the stimuli varied between 20 and 85 V for stimulation of TA and between 0.5 and 85 V for stimulation of the CP and subplate. Unless otherwise noted, stimuli were delivered at 0.033 Hz.

2.2.6 Data analysis

Data are presented as mean ± SEM. For statistical analyses the two-tailed Student's t-test, one-way ANOVA test and χ^2-test were used. Probability levels of $p<0.05$ (*), $p<0.01$ (**) and $p<0.001$ (***) were considered significant.

2.2.6.1 Analysis of passive and active membrane properties

The passive electrophysiological properties of the SPn were characterized under both voltage- and current-clamp conditions. The resting membrane potential (RMP) was measured either immediately after obtaining the whole-cell configuration or after complete blockade of action potentials (APs) by QX-314 added to the pipette solution (~5-10 min). Unless otherwise indicated, SPn were held at a holding potential between –60 and –70 mV during recordings. For the determination of the input resistance (R_{in}), either hyperpolarizing current pulses of 300 ms duration and 20 pA amplitude or hyperpolarizing voltage pulses of 300 ms duration and 10 mV amplitude were applied from the holding potential. The R_{in} was calculated according to Ohm's law by dividing potential changes by amplitude of injected current.

Active membrane properties and current-voltage relationship were assessed under current-clamp conditions by recording voltage responses to a series of 2 s long hyper- and depolarizing current pulses from the holding potential. Spike amplitude was measured from APs threshold to the peak.

2.2.6.2 Analysis of spontaneous postsynaptic currents

Analysis of spontaneous postsynaptic currents (sPSCs) was performed using Mini Analysis Software (Synaptosoft, Leonia, NJ). The sPSCs were captured using a threshold-crossing detector set above the noise level. Events that did not show a

typical waveform were rejected manually and by optimal settings of the program parameters rise-time, decay-time, area and baseline. Peak amplitude, inter-event interval, rise-time and decay-time of the sPSCs were determined. Rise-time was measured as the time between at 0.5% and peak current amplitude and the decay-time was determined between time points at 100 and 37% of the peak. Decay-time constants (τ) were calculated by fitting single or double exponential functions to averaged sPSCs using a simplex algorithm:

$$I_t = I_0 + a * e^{-(t/\tau)}$$

$$I_t = I_0 + a * e^{-(t/\tau 1)} + b * e^{-(t/\tau 2)}$$

Amplitude or decay-time distribution histograms were displayed using Origin 6 (Microcal Software, Northampton, MA) and correlation coefficients (r) were calculated using a least-squares linear regression analysis.

2.2.6.3 Analysis of evoked postsynaptic currents

The postsynaptic currents (PSCs) were analyzed with WinTida Software (Heka) in their peak amplitude, onset latency, rise-time and decay-time constant. The latency was measured from the beginning of the stimulus artifact to the onset of the PSC. Rise-time was determined as the interval between baseline and peak current amplitude and the decay-time constant (τ) was calculated by fitting a single or double exponential function to averaged currents using a simplex algorithm. Correlation coefficients (r) were calculated using a least-squares linear regression analysis. Voltage steps of 20 mV between –90 and +30 mV were applied to determine the current-voltage relationship of the synaptic inputs. Four to ten stimulus-evoked

responses were recorded under control conditions and after drug application to ensure the action of drugs.

2.2.6.4 Analysis of cholinergic responses

Changes in the membrane potential of SPn in response to cholinergic agonists and antagonists were analyzed with WinTIDA Software (Heka). Peak amplitude, rise-time measured from onset to the peak of response and the duration measured at half maximal amplitude were determined. Analysis of the spontaneous postsynaptic potentials (sPSPs) was performed using MiniAnalysis Software (Synaptosoft). To accurately calculate the effect of muscarine on sPSPs, the time intervals corresponding to ACSF, muscarine and washout were determined for each SPn according to the cumulative time-frequency histogram.

2.3 Cell staining and tracing procedures

2.3.1 Intracellular biocytin staining

For later morphological cell identification, in all experiments biocytin was included in the pipette solution and intracellular diffusion of biocytin from the electrode followed by active transport resulted in adequate filling of the recorded neurons. The slices were processed by a modification of the staining protocol described by Schröder and Luhmann (Schröder and Luhmann, 1997). At the end of the recording session, the electrode was slowly withdrawn and the slice was fixed for >24 h in 4% paraformaldehyde-containing 0.1 M phosphate buffer (pH 7.4). Pre-incubation of slices for 60 min in phosphate-buffered saline (PBS) containing 0.5% H_2O_2 to saturate endogenous peroxidases was followed by incubation overnight in avidin-coupled peroxidase (ABC kit, Vectorlabs, Burlingame, CA). After being rinsed in PBS and TRIS, the slices were incubated for 30 min in 20% 3,3-diaminobenzidine (DAB,

Sigma) and for 10 min in DAB containing 0.01% H_2O_2. The reaction product was intensified by 2-3 min incubation in 0.5% OsO_4. Finally, the slices were rinsed in TRIS and distilled water, dehydrated in ethanol and propylenoxide and embedded in Durcopan (Fluka, Buchs, Switzerland). One to three SPn per slice were recorded and labeled with little or no background staining. This protocol yielded intense staining of the soma as well as of the majority of the dendritic tree and of the axonal projections present in the slice.

In order to determine both the exact location in the slice and the morphological properties of the investigated SPn, combined biocytin and Nissl staining was performed. A similar protocol as above described was used with the difference that cresyl violet was added for staining and the intensification of the reaction product using OsO_4 was omitted.

Biocytin stained neurons were analyzed in their somatodendritic properties using an Axioskop microscope (Zeiss) equipped with a drawing tube and camera lucida reconstructions were made at x250 magnification. An Axiophot II microscope (Zeiss) equipped with a motorized Z-stage was used to take digital photographs (Fig. 2) as Z-stacks with a CoolSNAP CCD-camera (Visitron Systems, Puchheim, Germany). Such stacks were processed with MetaView 4.5 (Universal Imaging Corporation, West Chester, PA) using the minimum-projection in order to achieve an "extended-focus view".

2.3.2 Lucifer yellow labeling

Lucifer yellow CH (Sigma) was added to a final concentration of 0.5% to the intracellular solution and due to its bad solubility, the solution was filtered and

sonicated before use. Lucifer yellow-containing solution was stable at room temperature for weeks. Intracellular diffusion of Lucifer yellow from the electrode resulted in adequate filling of the recorded neurons. Dye injections were performed on SPn identified by their location, morphological and electrophysiological properties and were limited to one per slice in order to ensure unambiguous identification of the coupled neurons. Lucifer yellow was allowed to diffuse into the cell for 20-40 min. Afterwards, the slices were kept in the recording chamber for a minimum of 30 min and were fixed overnight in 4% buffered paraformaldehyde. The filled SPn were viewed under epifluorescence (Stewart, 1978) using a Zeiss Ultraphot microscope (Zeiss) with excitation filter at 546 nm and emission filter at 590 nm.

2.3.3 Extracellular biocytin staining

To determine the path of TA in the slice, biocytin was used as tracer for axonal labeling (Staiger et al., 1999). After preparation (described in section 2.1.2), the coronal slices including the somatosensory cortex were placed into an interface incubation chamber where they were maintained at 34 °C and continuously perfused with oxygenated ACSF. After a short incubation period, a variable sized biocytin crystal was placed in the CP using a fine stainless steel wire. The slices were kept in the chamber for a minimum of 8h and were fixed for >24 h in 4% paraformaldehyde-containing 0.1 M phosphate buffer (pH 7.4). For further processing of the slices, the above described biocytin staining protocol was used.

2.4 Pharmacology

All substances were purchased from Merck with the exception of 6-cyano-7-nitroquinoxaline-2,3-dione (CNQX) and QX-314 which were from Tocris (Ballwin, MO), GABA, carbamylcholine chloride (carbachol), carbenoxolone (CBX) and

nicotine which were from Sigma, atropine sulfate (Braun AG, Melsungen, Germany), and R(-)-3-(2-carboxypiperazin-4-yl)-propyl-1-phosphonic acid (CPP), 2-(3-carboxypropyl)-3-amino-6-(4-methoxyphenyl) pyridazinium bromide (gabazine), cyclothiazide, muscarine and tetrodotoxin citrate (TTX) which were from RBI (Natick, MA). 1-(4-aminophenyl)-4-methyl-7,8-methylenedioxy-5*H*-2,3-benzodiazepine (GYKI 52466) was kindly provided by Dr. I. Világi (Eötvös Loránd University, Budapest, Hungary). Stock solutions of these drugs were prepared as follows: TTX (1 mM), CPP (10-20 mM), GABA (100 mM), CBX (10 mM), muscarine (10 mM), nicotine (100 mM) and carbachol (100 mM) in distilled water, CNQX (10 mM), gabazine (100 mM) and cyclothiazide (100 mM) in DMSO and GYKI 52466 (80 mM) in HCl. Stock solutions were stored at –20° C and diluted in ACSF on the day of experiment. Atropine was commercially available as water-based solution. QX-314 was dissolved directly in the electrode solution on the day of experiment. Maximal concentration of DMSO in the superfusate was 0.1%. The drugs were bath applied after stable control recordings were obtained for at least 6 min and reached synaptic location within the first 5 min of application. During perforated patch recordings GABA was bath applied for 10-30 s. Muscarinic and nicotinic receptors agonists and antagonists were applied for 30-120 s. Generally, a drug-free ACSF wash was applied before and after each drug application. A partial or complete washout was obtained after 5-45 min and up to 4 drugs were tested on the same cell.

3. Results

Whole-cell recordings were performed from 580 SPn identified according to the following criteria. First, under video assisted Nomarski microscopy as well as in Nissl-stained section, SPn were identified by their location within the subplate between the densely cell-packed layer VI and the cell-sparse WM (Fig. 4A). Second, the form of the soma and the orientation of primary dendrites observed under video assisted Nomarski microscopy (Fig. 4B, C) and the morphological properties after histological processing for biocytin (Fig. 5) served as main criteria to identify the SPn. And third, the electrophysiological properties of the recorded neurons (depolarized RMP, high R_{in} and firing pattern) contributed to the final identification of SPn.

3.1 Morphological characterization of subplate neurons

The morphology of 324 SPn was investigated in detail. According to previous described morphological criteria (i.e. the form of the soma and the orientation of the dendritic tree (Wahle et al., 1987; 1994; deAzevedo et al., 1997), six morphological classes of SPn were characterized. Horizontal bitufted SPn (Fig. 5A, n=75) showed a spindle-like, horizontally oriented soma with primary dendrites extending parallel to the pial surface in opposite directions. Horizontal monotufted SPn (Fig. 5B, n=41) showed a spindle-like, horizontally oriented soma with primary dendrites extending parallel to the pial surface in only one direction. Neurons with a round or ovoid soma and multiple primary dendrites with no preferential orientation were classified as multipolar SPn (Fig. 5C, n=90). Inverted pyramid SPn (Fig. 5D, n=59) showed a triangular or round soma with a major dendrite oriented toward the WM. Tripolar (pyramid-like) SPn (Fig. 5E, n=54) have a triangular or round soma and a major dendrite oriented to the pial surface. Five SPn showed a vertically oriented soma and radial dendrites and were classified as vertical SPn. Independent to the morphological

class, SPn showed a ramified dendritic tree (Fig. 6). The majority of SPn extended processes in the WM (72% of horizontal bitufted SPn, 61% of horizontal monotufted SPn, 77% of multipolar SPn, 84% of inverted pyramid SPn and 72% of tripolar SPn), in the CP (63%, 42%, 57%, 61% and 67%) as well as in layers V/VI (84%, 78%, 84%, 83% and 96%). To a lesser extent the processes reached the internal capsule (24%, 20%, 19%, 25% and 22%) and the MZ (8%, 12%, 12%, 18% and 11%). All SPn extended more or less arborized processes within the subplate. The destination of projections was not significantly different (χ^2-test) between morphological classes. Without being object of systematic investigation, the presence of spines on the processes of SPn was observed (Fig. 6 inset). Since we could not detect any statistically significant differences between the six morphological classes of SPn in their electrophysiological properties (one-way ANOVA test) or synaptic inputs (χ^2-test), data from these morphologically distinct SPn were pooled.

3.2 Passive and active membrane properties of subplate neurons

SPn exhibited relatively uniform passive membrane properties. Using gluconate-based pipette solution, the average RMP and R_{in} were –55.4 ± 0.3 mV and 1267 ± 25 MΩ (n=453), respectively. Similar values were measured when using high-chloride pipette solution (RMP=-54.3 ± 0.6 mV, R_{in}=1207 ± 69 MΩ, n=74) or QX-314-containing pipette solution (RMP=-55.3 ± 0.8 mV, R_{in}=1279 ± 72.3, n=53). All SPn were able to fire overshooting APs in response to sustained depolarization by intracellular current injection. At RMP, almost 50% of the investigated neurons showed spontaneous APs. SPn revealed different firing patterns in response to injection of suprathreshold current pulses. Repetitive firing at frequencies between 4.5 and 13 Hz could be observed in 60 % of the investigated SPn. In accordance with Friauf *et al.* (1990), these neurons were classified as *regular spiking* SPn (Fig. 7A). The remaining 40% of the neurons,

which were classified as *single spiking* SPn (Friauf et al., 1990), responded to suprathreshold current injection with a single AP at the beginning of the depolarizing pulse followed by membrane oscillation (Fig. 7C). Neither the passive membrane properties, nor the APs amplitudes were significantly different between *regular spiking* (RMP=-56 ± 0.8 mV, R_{in}=1181 ± 59 MΩ, n=88, 52 ± 1.6 mV, n=35) and *single spiking* SPn (RMP=-54.3 ± 0.8 mV, R_{in}=1146 ± 57 MΩ, n=43, 49.9 ± 2.9 mV, n=10). The firing patterns of the SPn were independent of the used pipette solution. In both groups the voltage deflection showed either linear dependence or time-independent inward rectification from the injected current (Fig. 7B, D). No significant correlation could be noted between the firing type and the presence of inward rectification. Since within the investigated age-group (P0-P3) no significant age-dependent differences in the passive membrane properties (Fig. 7E) or in the proportion of SPn showing *regular spiking* and *single spiking* discharge (Fig. 7F) could be observed, data from these age groups were pooled.

3.3 Spontaneous synaptic activity of subplate neurons

3.3.1 Characterization of spontaneous postsynaptic currents

Voltage-clamp recordings at a holding potential of -70 mV revealed in 89% of the 131 investigated SPn sPSCs (Fig. 8A). The frequencies of these sPSCs varied considerably among the neurons, ranging from 0.1 to 0.9 Hz (0.27 ± 0.02 Hz, n=117 cells). The average amplitude of the sPSCs was 15 ± 0.6 pA (n=117 cells). The peak-to-peak noise level varied between 2 and 7 pA, and was below the smallest sPSCs amplitude. In 68% of the SPn that showed sPSCs, the decay-times of the sPSCs were either fast or slow (Fig. 8B), and across the neurons gave rise to a bimodal distribution (Fig. 8C). In these neurons, decay-time distribution histograms served to determine the limit between fast and slow sPSCs, which was between 10 and 20 ms for all investigated

SPn. The properties of the fast and slow sPSCs are summarized in Table 2. In comparison to the slow sPSCs, fast sPSCs occurred approximately twice as often and revealed a significantly smaller average amplitude and faster rise-time. The fast sPSCs decay could be best fitted with a monoexponential function, while the slow sPSCs decay was fitted with a biexponential function (Fig. 8B). Fast and slow sPSCs showed an unimodal amplitude distribution (Fig. 8D) and could be observed in *regular spiking* as well as in *single spiking* SPn.

Table 2. Properties of fast and slow sPSCs recorded in 80 SPn

Property	**Fast sPSCs**	**Slow sPSCs**	**Significance level**
Decay-time (ms)	6.3 ± 0.2	51.2 ±3	***
Frequency (Hz)	0.2 ± 0.02	0.1 ± 0.01	***
Amplitude (pA)	14 ± 0.6	18 ± 1.4	**
Rise-time (ms)	2.6 ± 0.1	3.9 ± 0.1	***
Decay-time constants (ms)	4.9 ± 0.2	17.5 ± 1.2 104 ± 6.1	***

Significant differences between fast and slow sPSCs are indicated by **(t-test, $p<0.01$) and ***(t-test, $p<0.001$).

The remaining 32% of the SPn showing sPSCs gave rise to an unimodal decay-time distribution of sPSCs. The fast decay of these sPSCs (mean decay-time 6.3 ± 0.5 ms, n=37 cells) which could be fitted with a monoexponential function, as well as their average frequency (0.22 ± 0.02 Hz), amplitude (13.7 ± 1 pA) and fast rise-time (2.3 ± 0.2 ms) led to the conclusion that these sPSCs belong to the fast population.

A possible effect of dendritic cable filtering on sPSCs was examined in 21 SPn by plotting the rise-time versus amplitude (Fig. 8E) and the rise-time versus decay-time (Fig. 8F) for fast as well as for slow sPSCs (Burgard and Hablitz, 1993). No significant correlation could be observed between rise-time and amplitude and between rise-time and decay-time, indicating that dendritic filtering does not profoundly influence the kinetics of the sPSCs.

In order to investigate the role of action potential-dependent transmitter release on the generation of sPSCs, the effects of TTX were studied in 8 SPn (Fig. 9). Bath application of 1 μM TTX reduced significantly (t-test, $p<0.001$) the frequency of the fast sPSCs by 46 ± 7% and had no significant effect on the amplitude, rise- or decay-time of the remaining fast sPSCs. These results indicate that about half of the fast sPSCs were mediated by action potential dependent transmitter release. The slow sPSCs were completely blocked by TTX. TTX effects on slow sPSCs indicate that these currents required action potential-dependent transmitter release. For both populations of currents, the TTX effects were reversible within 5 min.

3.3.2 Glutamate receptor-mediated spontaneous postsynaptic currents

Previous studies have shown that SPn express AMPA, kainate and NMDA receptors (Herrmann, 1996; Smith and Thompson, 1999). In order to study their contribution to the mediation of fast and slow sPSCs, the effects of the AMPA/kainate receptor antagonist CNQX (Honoré et al., 1988) and of NMDA receptor antagonist CPP (Lehmann et al., 1987) on sPSCs were investigated. Application of CNQX (10 μM) significantly (t-test, $p<0.001$) reduced the frequency of fast sPSCs by 95 ± 2.5% (n=19 cells) (Fig. 10A, B) without having any effects on the slow sPSCs. The effects of CNQX were not accompanied by any changes in the holding current or R_{in} and were

reversible. These results indicate that the fast sPSCs were mediated by AMPA/kainate receptors. In order to discriminate between AMPA and kainate receptors, modulation of the sPSCs by cyclothiazide, a drug known to slow the desensitization of AMPA, but not of kainate receptors (Partin et al., 1993) was investigated in 6 SPn. Bath application of 100 μM cyclothiazide in the presence of CPP (20 μM) and the $GABA_A$ receptor antagonist gabazine (50 μM) caused a significant (t-test, $p<0.001$) and reversible prolongation in the decay-time of the fast sPSCs to 348 ± 43% of the control value (Fig. 10C, D). Cyclothiazide had no significant effect on the frequency of the fast sPSCs, but unexpectedly significantly (t-test, $p<0.05$) increased their amplitude from 7.4 ± 0.6 pA to 9 ± 0.8 pA. Cyclothiazide effects were reversible. According to these results, it is likely that AMPA but not kainate receptors mediate the fast sPSCs.

In 9 SPn bath application of 10-20 μM CPP, a potent and selective NMDA receptor antagonist significantly (t-test, $p<0.01$) reduced the frequency of the fast sPSCs by 34 ± 10.2% (n=9 cells) (Fig. 10E, F) and had no effect on their amplitude, rise- and decay-time. In contrast, CPP blocked almost completely the slow sPSCs, their frequency being significantly (t-test, $p<0.001$) reduced by 96 ± 1.5% (Fig. 10E, F). Since CPP dissociates slowly from NMDA receptors (Benveniste and Mayer, 1991), only a partial recovery could be observed upon washout of CPP. These results indicate that the slow sPSCs were mediated by NMDA receptors. This conclusion is also supported by the long decay-time constants of the slow sPSCs (Table 2), which seems to be a typical feature of NMDA receptor-mediated synaptic events (Forsythe and Westbrook, 1988, Bellingham et al., 1998). In 8 SPn combined application of CPP and CNQX caused a complete blockade of the fast sPSCs and a 98 ± 1.5% reduction in the frequency of the slow sPSCs, indicating that the spontaneous activity observed

in these neurons using gluconate-based solution was mediated by AMPA and NMDA receptors (Fig. 10G). After washout of CPP and CNQX the frequency of the fast and slow sPSCs recovered to 45 ± 14.6% and 37.3 ± 15.9% of the control values (n=8 cells).

3.3.3 $GABA_A$ receptor-mediated spontaneous postsynaptic currents

Since previous studies have shown the expression of benzodiazepine binding sites (Schlumpf et al., 1983), $GABA_A$ receptors (Huntley et al., 1990) and $GABA_A$ receptor subunits (Meinecke and Rakic, 1992) in the subplate, the contribution of $GABA_A$ receptors to the mediation of sPSCs was investigated. The lack of $GABA_A$ receptor-mediated sPSCs, when a gluconate-based pipette solution was used (n=11 cells), may result from the small driving force at an estimated equilibrium potential for chloride of about –60 mV. Using high-chloride pipette solution, the chloride equilibrium potential was shifted to approximately 0 mV, allowing to detect $GABA_A$ receptor-mediated inward currents at the holding potential. Under these conditions, bath application of 10 μM CNQX and 20 μM CPP reduced the frequency of the sPSCs to 47.9 ± 7.5% (n=8 cells). The remaining sPSCs were blocked by bath application of 100 μM gabazine, a potent $GABA_A$ receptor antagonist (Wermuth and Bizière, 1986) (Fig 11A), indicating that they were mediated by $GABA_A$ receptors. The $GABA_A$-mediated sPSCs were characterized by their low frequency (0.07 ± 0.009 Hz, n=8 cells), variable amplitudes (34.4 ± 4.7 pA) and long rise- (6.1 ± 0.9 ms) and decay-times (123.4 ± 13 ms) (Fig. 11B). In agreement with previous studies (Edwards et al., 1990), their decay could be fitted with a biexponential function with average decay-time constants of 40.5 ± 4.8 ms and 211.5 ± 22.5 ms (n=8 cells). All properties of the GABAergic sPSCs were significantly different (ANOVA test, $p<0.001$) from those of the fast and slow sPSCs.

Gabazine showed a very slow washout rate and a complete recovery could be observed in only 3 cells after 45 min washout. Despite the fact that the slow kinetic could indicate that GABAergic sPSCs originate from electrotonically distant sites and are influenced by cable filtering, neither decay-time versus rise-time nor amplitude versus rise-time were correlated (n=12 cells). However, it should be noted that the relatively small number of GABAergic events recorded per neuron precluded a complete analysis for each cell. Since the slow kinetic seems not to be the result of dendritic filtering, developmental differences (Hollrigel and Soltesz, 1997) related to a certain subunit composition of the $GABA_A$ receptors (Laurie et al., 1992) may account for the slow rise- and decay-time of the GABAergic sPSCs.

In order to investigate the involvement of action potential-dependent transmitter release on the generation of GABAergic sPSCs, TTX effects were investigated in 5 SPn. Bath application of 1 μM TTX reduced the frequency of $GABA_A$ receptor-mediated sPSCs by 89.8 ± 1.5%, indicating that the majority of $GABA_A$ receptor-mediated sPSCs were dependent on presynaptic action potentials.

Blockade of the $GABA_A$ receptor-mediated sPSCs by bath application of gabazine (n=5 cells), led to isolation of NMDA and AMPA receptor-mediated sPSCs with similar properties as when recorded with gluconate-based pipette solution. A combined application of gabazine, CPP and CNQX completely blocked the spontaneous synaptic activity in 4 out of 4 SPn tested.

Summarizing, these results indicate that SPn show spontaneous synaptic inputs mediated by AMPA, NMDA and $GABA_A$ receptors.

3.4 Functional synaptic projections onto subplate neurons

In order to identify the origin of the synaptic inputs onto SPn, cortical and subcortical regions were electrically stimulated, since axons from thalamus (Rakic, 1977; Catalano and Shatz, 1998) and cortical layers IV and VI project to SPn (Callaway and Katz, 1992; Callaway and Lieber, 1996) and SPn extensively project within the subplate (Wahle et al., 1987; Meinecke and Rakic, 1992).

3.4.1 Postsynaptic currents evoked by stimulation of the thalamocortical afferents

In order to specifically stimulate the TA, the stimulation electrode was placed in the internal capsule, laterally to the recorded SPn. At a holding potential of –70 mV, postsynaptic currents in response to electrical stimulation of the TA (TA-PSCs) could be obtained in 68% of the 59 investigated SPn (Fig. 12A) and were completely abolished by bath application of 1 µM TTX (n=8 cells) (Fig. 12B). The short onset latency (5.7 ± 0.3 ms, n=40 cells) and the unimodal distribution of the latencies (Fig. 12A inset) argue for the monosynaptic character of the TA-PSCs. The amplitudes of the TA-PSCs varied considerably among the cells, ranging from 12 to 79 pA (29.7 ± 2.7 pA, n=40 cells). The TA-PSCs had a rise-time of 2.5 ± 0.1 ms (n=40 cells) and their decay could be best fitted with a monoexponential function (mean decay-time constant 5.4 ± 0.7 ms, n=40 cells) (Fig. 12A). This fast kinetic represents a typical feature of AMPA/kainate receptor-mediated PSCs (Trussell et al., 1988; Colquhoun et al., 1992) and is comparable to the kinetic of AMPA receptor-mediated sPSCs recorded on SPn. The properties of TA-PSCs were summarized in Table 3. Bath application of 10 µM CNQX (n=8 cells) blocked the TA-PSCs (Fig. 12C), supporting the assumption that these responses were mediated by activation of AMPA/kainate receptor. CNQX effect was partially reversible in 5 SPn.

Table 3. Properties of synaptic inputs onto SPn

Results	***Thalamocortical afferents (TA-PSCs)***	***Cortical plate and layer V/VI (CP-monoPSCs)***	***Subplate (SP-monoPSCs)***
			Dual-component PSCs Mono-component PSCs
Percentage of SPn receiving monosynaptic input	68% (59)	72% (82)	79% (43)
Onset latency (ms)	5.7 ± 0.3 (40)	5.2 ± 0.4 (59)	**3.9 ± 0.2 (29)** 5.6 ± 0.8 (5)
Amplitude at –70 mV (pA)	29.7 ± 2.7 (40)	34.9 ± 3.4 (59)	**35.8 ± 3.4 (29)** 28.1 ± 6.4 (5)
Rise-time at –70 mV (ms)	2.5 ± 0.1 (40)	2.4 ± 1.1 (59)	**2.9 ± 0.2 (29)** 2.9 ± 0.6 (5)
Decay-time constant at –70 mV (ms)	5.4 ± 0.7 (40)	5.2 ± 0.4 (59)	**5.5 ± 0.7 (29)** **92.5 ± 15.7 (29)** 4.7 ± 0.5 (5)
Relationship with increasing frequency of stimulation	No fatigue	Fatigue	Fatigue
Percentage of SPn with NMDA receptor mediated PSCs at –70 mV	0% (40)	0% (59)	**100% (29)** 0% (5)
Percentage of SPn with NMDA receptor mediated PSCs at –30 mV	45% (11)	80% (10)	**?** 42% (7)
Decay-time constant of NMDA receptor mediated PSCs at +10 mV (ms)	68.7 ± 7.7 (4)	125.5 ± 10.5 (6)	**110.7 ± 36 (5)** 90.5 ± 9.5 (7)
Percentage of SPn receiving polysynaptic input	0% (59)	56% (82)	11% (43)
Percentage of SPn with GABAergic input	0% (11)	0% (7)	68% (19)

In order to discriminate between AMPA and kainate receptors, TA-PSCs modulation by cyclothiazide was investigated in 6 SPn. Bath application of 100 μM cyclothiazide caused a significant (t-test, $p<0.05$) and reversible prolongation in the decay-time constants of the TA-PSCs to 339 ± 107% of the control value (Fig. 12D). Furthermore, the TA-PSCs were completely blocked in 5 out 5 cells by 80 μM GYKI 52466 (Fig. 12E), a selective AMPA receptor antagonist (Paternain et al., 1995). These results indicate that at a holding potential of –70 mV TA-PSCs are mediated by AMPA receptors.

TA-PSCs were not elicited until a critical threshold of stimulus intensity (varying between 20 V and 85 V) was reached and a further increase of stimulus strength did not significantly modify their amplitude or shape (Fig. 13A, B). Therefore, it is likely that SPn respond to stimulation in an all-or-none manner, depending on whether TA fire or not. Antidromic APs could never be observed in SPn in response to TA stimulation, even at maximal intensities. This result may indicate that the axonal pathway of the SPn corticothalamic projection differs from the thalamocortical projection. Increasing the frequency of TA stimulation from 0.03 to 1 Hz (n=7 cells) did not significantly affect the amplitude of the recorded PSCs (Fig. 13C, D), but increased in 5 out 7 cells the failure rate from 8.5% to 28.6%. However, failures of presynaptic transmitter release cannot be unambiguously distinguished from failures of the stimulus to trigger an action potential in the TA (Debanne et al., 1996). To asses the influence of dendritic filtering on the kinetic of the TA-PSCs, the relationship between rise-time and decay-time constants and between amplitude and decay-time constants was examined. Regression analyses revealed a lack of correlation between these parameters ($r=0.15$ and $r=0.09$, respectively), suggesting that dendritic filtering did not profoundly influence the kinetics of the TA-PSCs.

Analysis of the current-voltage relationship of the TA-PSCs performed with QX-314-containing pipette solution indicates that NMDA receptors may also contribute to the thalamocortical inputs onto SPn. At membrane potentials positive to –50 mV an additional slow component could be identified in 5 out of 11 SPn upon TA stimulation (Fig. 13E). This CNQX-insensitive component (Fig. 13F) was blocked by CPP, indicating that NMDA receptors activated at depolarized membrane potentials are implicated in the mediation of TA-PSCs. Isolated NMDA receptor-mediated TA-PSCs, recorded in the presence of 10 μM CNQX, reversed at +6 mV and showed a mean decay-time constant of 68.7 ± 7.7 ms (n=4 cells) when measured at +10 mV. The remaining 6 SPn showed PSCs with linear current-voltage relationship and were completely abolished by CNQX even at depolarized membrane potentials, indicating that these PSCs were exclusively mediated by AMPA receptors.

TA stimulation did not elicit GABAergic synaptic activity in SPn. When high-chloride pipette solution was used, the amplitude and the kinetics of the TA-PSCs (amplitude 40.9 ± 8 pA, rise-time 2.5 ± 0.2 ms, decay-time constant 7.9 ± 2 ms and latency 4.9 ± 0.5 ms, n=11 cells) were not significantly different from those measured with gluconate-based pipette solution. Gabazine (100 μM), had no effect on the TA-PSCs in 6 out of 6 SPn when gluconate-based pipette solution was used and in 5 out of 5 SPn when high-chloride intracellular solution was used (Fig. 12F). These results indicate that stimulation of the TA did not activate the $GABA_A$ receptors on SPn.

Summarizing, electrical stimulation of TA elicited monosynaptic AMPA receptor mediated PSCs with an additional NMDA receptor-mediated component at depolarized membrane potentials.

3.4.2 Postsynaptic currents evoked by stimulation in the cortical plate

At a holding potential of –70 mV, electrical stimulation of the lower CP including layers V/VI elicited in 59 of 82 investigated SPn PSCs with unimodal latency distribution peaking at 5.2 ± 0.4 ms (n=59 cells) and with fast rise-time and decay-time constants (2.4 ± 1.1 ms and 5.2 ± 0.4 ms) (Fig. 14A). According to these results, the PSCs elicited by CP stimulation are most likely to be monosynaptic (CP-monoPSCs). The mean amplitude of the CP-monoPSCs was 34.9 ± 3.4 pA (n=59). The properties of CP-monoPSCs were summarized in Table 3. The initial CP-monoPSCs were followed in 23 out of the 59 cells by long-lasting (60-450 ms) multiphasic PSCs with peak latencies ranging from 10 to 80 ms (Fig. 14A). These PSCs are likely to be of polysynaptic origin (CP-polyPSCs). Ten additional SPn exhibited CP-polyPSCs not preceded by a CP-monoPSC. The CP-polyPSCs showed variable maximal amplitudes ranging from 10 to 100 pA (mean 38.8 ± 3.7 pA, n=33 cells). The remaining 13 SPn showed no response to electrical stimulation. In 7 out of 82 neurons maximal stimulation intensities elicited antidromic APs, indicating that these SPn possess an ascending axonal projection into the CP including layers V/VI. Both CP-monoPSCs (n=8 cells) and CP-polyPSCs (n=4 cells) were completely blocked by 1 μM TTX (Fig. 14B).

At –70 mV the CP-monoPSCs were abolished by 10 μM CNQX (n=8 cells) (Fig. 14C), while the NMDA receptor antagonist CPP (20 μM) had no significant effect on the amplitude or the kinetics of the monosynaptic responses (n=11 cells) (Fig. 14F). The significant (t-test, $p<0.001$) prolongation of the decay-time constants of the CP-monoPSCs to 337 ± 34% (n=7 cells) of the control values in cyclothiazide (100 μM) (Fig. 14D) and the complete blockade of CP-monoPSCs by GYKI 52466 (80 μM) in 5

SPn (Fig. 14E) indicate that at –70 mV the CP-monoPSCs are mediated by AMPA receptors.

The CP-polyPSCs were blocked by 20 μM CPP (n=6 cells) (Fig. 14F), indicating that NMDA receptors are critically involved in the generation of this polysynaptic activity. CNQX (10 μM) significantly (t-test, $p<0.05$) reduced the maximal amplitudes of the CP-polyPSCs by 40.8 ± 13.9% (n=5 cells) (Fig. 14C). In a bathing solution containing CNQX and CPP (n=6 cells), no synaptic responses were observed.

In contrast to the TA-PSCs, the CP-monoPSCs and particularly the CP-polyPSCs showed a pronounced sensitivity to stimulus frequencies >0.03 Hz. Whereas the CP-monoPSCs gradually decreased in their maximal amplitudes at frequencies between 0.03 and 1 Hz, the CP-polyPSCs were already abolished at >0.03 Hz (Fig. 15A). When 10 stimuli were applied at a constant frequency of 0.03 Hz, the CP-polyPSCs gradually diminished (n=6 cells), whereas the CP-monoPSCs were relatively stable (n=7 cells) (Fig. 15B). Similar results have been previously reported for immature rat cortical neurons (Kriegstein et al., 1987; Luhmann and Prince, 1990). The lack of a positive correlation between rise- and decay-time constants (r=0.17) and between amplitude and decay-time constants (r=0.38) of the CP-monoPSCs indicate that dendritic filtering does not profoundly influence the kinetic of CP-monoPSCs.

In 8 out of 10 SPn recorded using QX-314-containing pipette solution, membrane depolarization to potentials positive to –50 mV uncovered an additional monosynaptic component (Fig. 15C) which was CNQX-insensitive (Fig. 15D) and blocked by CPP. This NMDA-receptor mediated component of the CP-monoPSCs reversed at +7 mV and revealed a mean decay-time constant of 125.5 ± 10.5 ms (n=6 cells) when

measured at +10 mV. The remaining 2 SPn showed PSCs with linear current-voltage dependence which were mediated exclusively by AMPA receptors.

In order to reveal possible $GABA_A$ receptor-mediated synaptic inputs arising from the CP, we investigated in 7 cells the effects of 100 μM gabazine on CP-monoPSCs and CP-polyPSCs. Using high-chloride pipette solution, neither the amplitude nor the kinetics of the CP-monoPSCs were affected by gabazine (n=7 cells) (Fig. 15E), indicating that $GABA_A$ receptors are not involved in their mediation. However, gabazine reduced significantly (t-test, $p<0.01$) the maximal amplitudes of the CP-polyPSCs by 63% (n=5 cells) (Fig. 15E, F), suggesting a contribution of $GABA_A$ receptors to the polysynaptic activity elicited by CP stimulation.

Summarizing, electrical stimulation of CP including layers V/VI elicited monosynaptic PSCs mediated by AMPA receptors with an additional NMDA receptor-mediated component at depolarized membrane potentials as well as polysynaptic PSCs depending on NMDA and $GABA_A$ receptors.

3.4.3 Postsynaptic currents evoked by stimulation in the subplate

At a holding potential of –70 mV, electrical stimulation of the subplate elicited in 34 of the 43 investigated SPn monosynaptic PSCs (SP-monoPSCs). In 29 SPn the SP-monoPSCs were dual-component (Fig. 16A) and in 5 SPn they were single-component (Fig. 18A). In addition, at high stimulation intensities, 5 SPn revealed polysynaptic responses (SP-polyPSCs) with similar properties to those determined for CP-polyPSCs (latency 52.8 ± 18 ms, amplitude 39.4 ± 8 pA, duration from 245 to 312 ms). These SP-polyPSCs were also critically dependent on NMDA receptors, as they were completely abolished in the presence of 20 μM CPP (n=2 cells).

The dual-component SP-monoPSCs (Fig. 16A) showed unimodal latency distribution with a peak at 3.9 ± 0.2 ms, average amplitude of 35.8 ± 3.4 pA, mean rise-time of 2.9 ± 0.2 ms and their decay could be best fitted with a biexponential function (mean decay-time constants 5.5 ± 0.7 ms and 92.5 ± 15.7 ms, n=29 cells). The properties of dual-component SP-monoPSCs were summarized in Table 3. These PSCs were characterized in more detail by bath application of AMPA/kainate and NMDA receptor antagonists. Application of 20 μM CPP abolished in all 21 investigated SPn the slow decaying component (CPP trace in Fig. 16B). The remaining response revealed an average onset latency of 3.7 ± 0.2 ms (n=21 cells), a mean amplitude of 41.8 ± 5.4 pA, a fast rise-time and decay-time constants of 2.3 ± 0.1 ms and 5.8 ± 1 ms, respectively. This remaining fast decaying component was blocked by CNQX (n=11 cells) (Fig. 16B) and TTX (n=4 cells) (Fig. 16C), indicating that it was mediated by AMPA/kainate receptors and is action potential-dependent. Since in 4 out 4 SPn cyclothiazide (100 μM) caused a significant (t-test, $p<0.01$) prolongation in the decay-time constant to 290 ± 33% of the control (Fig. 16D) and GYKI 52466 (80 μM) blocked the response in 5 out of 5 SPn (Fig. 16E), the fast decaying component of the dual-component SP-monoPSCs is most likely mediated by AMPA receptors.

Application of 10 μM CNQX abolished in all 7 investigated SPn the fast decaying component of the SP-monoPSCs (CNQX trace in Fig 16F). The remaining response revealed an onset latency of 4.9 ± 0.4 ms, an amplitude of 14.6 ± 3.2 pA and significantly (t-test, $p<0.005$) longer rise-time and decay-time constants (4.7 ± 0.5 ms and 69.5 ± 9.5 ms, n=7 cells) as compared to the AMPA receptor-mediated fast decaying component. This slow decaying component was blocked by 20 μM CPP

(n=3 cells) (Fig. 16F) and 1 μM TTX (n=4 cells) (Fig. 16G), indicating that it is mediated by NMDA receptors and required action potential-dependent transmitter release. Since the recordings were performed at –70 mV, NMDA receptors with a reduced Mg^{2+}-sensitivity (Burgard and Hablitz, 1994; Kirson et al., 1999) seem to mediate the slow decaying component recorded at hyperpolarized holding potentials. Upon membrane depolarization, the NMDA receptor-mediated component revealed a complex current-voltage relationship (Fig. 17A), reversed at +8.1 mV and showed a mean decay-time constant of 110.7 ± 36 ms (n=5 cells) when measured at +10 mV.

Electrical stimulation of the subplate at frequencies >0.03 Hz caused a gradual decrease in the amplitude of the AMPA receptor-mediated fast decaying component (n=5 cells) and at >0.2 Hz abolishment of the NMDA receptor-mediated slow decaying component (n=3 cells) (Fig. 17B). Since no correlation between rise-time and decay-time constants and between amplitude and decay-time constants for the AMPA receptor-mediated component (r=0.02 and r=0.11, n=21 cells) as well as for the NMDA receptor-mediated component (r=0.3 and r= 0.04, n=7 cells) could be detected, dendritic filtering did not profoundly influence the kinetics of the fast and slow decaying components of the dual-component SP-monoPSCs.

The single-component SP-monoPSCs showed an unimodal latency distribution peaking at 5.6 ± 0.8 ms, an average amplitude of 28.1 ± 6.4 pA, a rise-time of 2.9 ± 0.6 ms and their decay-time could be best fitted with a monoexponential function (mean decay-time constant 4.7 ± 0.5 ms, n=5 cells) (Fig. 18A). The properties of single-component SP-monoPSCs were summarized in Table 3. Since the single-component SP-monoPSCs were completely abolished by 10 μM CNQX (n=5 cells) (Fig. 18B) as well as by 80 μM GYKI 52466 (n=5 cells), it is likely that at –70 mV

they are mediated by AMPA receptors. Analysis of the current-voltage relationship in 3 out of 7 SPn recorded with QX-314-containing pipette solution, revealed an additional CNQX-insensitive component at membrane potentials positive to –50 mV (Fig. 18C, D). This component was blocked by CPP, indicating that it is mediated by NMDA receptors activated at depolarized membrane potentials. The NMDA receptor-mediated component reversed at +12.6 mV and showed a mean decay-time constant of 90.5 ± 9.5 ms (n=3 cells) when measured at +10 mV. The remaining 4 SPn showed single-component SP-monoPSCs with linear current-voltage dependence which were mediated exclusively by AMPA receptors. The single-component SP-monoPSCs revealed similar properties as the CP-monoPSCs. The possibility that these PSCs were elicited by activation of axonal projections arising from the layers V/VI and traversing the subplateshould not be neglected.

The contribution of $GABA_A$ receptors to SP-monoPSCs was studied using high-chloride pipette solution and in the continuous presence of 10 μM CNQX and 10 μM CPP. Under this condition, 13 out of 19 investigated SPn revealed PSCs which were blocked by 100 μM gabazine (n=9 cells) (Fig. 19A) and by 1 μM TTX (n=4 cells) (Fig. 19B), indicating that they were mediated by $GABA_A$ receptors and required action potential-dependent transmitter release. These $GABA_A$ receptor-mediated PSCs showed large amplitudes (51.5 ± 8.3 pA), long rise-times (4.5 ± 0.6) and decay-time constants (67.6 ± 11.3 ms) and an unimodal latency distribution with a peak at 4.3 ± 0.4 ms (n=13 cells), suggesting a monosynaptic origin of the GABAergic PSCs. According to the lack of correlation between decay-time constants and amplitude (r=0.2, n=13 cells) and between decay-time constants and rise-time (r=0.4, n=13 cells) dendritic filtering did not profoundly influence the kinetics of the $GABA_A$ receptor-mediated SP-monoPSCs. Similar to GABAergic sPSCs, $GABA_A$ receptor-mediated

SP-monoPSCs showed slow kinetics, likely to be determined by the subunit composition of the $GABA_A$ receptor during early development (Hollrigel and Soltesz, 1997; Laurie et al., 1992). In contrast to the glutamatergic SP-monoPSCs, increasing stimulation frequencies did neither affect the kinetics nor the amplitudes of the $GABA_A$-mediated SP-monoPSCs (n=4 cells) (Fig. 19C), indicating stable GABAergic connections between SPn.

3.4.4 Depolarizing action of GABA in subplate neurons

$GABA_A$ receptor activation was reported to depolarize immature cortical neurons due to the high intracellular chloride concentration in these neurons (Luhmann and Prince, 1991). To study the effects of GABA without altering the intracellular chloride concentration, gramicidin-perforated patch recordings (Kyrozis and Reichling, 1995) were performed on 11 SPn. At –70 mV, bath application of 1 mM GABA for 10 to 30 s caused a membrane depolarization to –40 ± 3.4 mV (n=11 cells) and evoked APs in 5 out 11 cells (Fig. 19D). In all 4 tested SPn, this GABA effect was abolished by 100 μM gabazine. In 6 neurons the perforated patch recordings were converted to whole-cell recordings, allowing the precise morphological identification of SPn. Taken together, these data demonstrate that GABA depolarizes SPn and evokes or facilitates the firing of APs.

3.5 Effects of cholinergic innervation on subplate neurons

3.5.1 Direct effects of nicotinic and muscarinic receptor activation

Previous autoradiographic studies demonstrated the accumulation of nicotinic binding sites (Naeff et al., 1992) and the presence of muscarinic receptors (Schlumpf et al., 1991) at the level of the subplate. In order to investigate to which extent these receptors are functional during postnatal development, activation of nicotinic and

muscarinic receptors using specific agonists was performed. Bath application of carbachol (100 μM), a non-selective cholinergic receptor agonist induced membrane depolarization in 9 out of 9 current-clamped SPn. The carbachol-induced membrane depolarization to –42.8 ± 2.6 mV (n=9 cells) triggered a barrage of APs lasting for several minutes (n=9 cells) (Fig. 20A). Blockade of APs with 1 μM TTX and of glutamatergic synaptic activity with 10 μM CNQX and 20 μM CPP significantly (t-test, $p<0.001$) reduced the carbachol-induced membrane depolarization from –42.8 ± 2.6 mV to –52.8 ± 1.7 mV (n=9 cells) (Fig. 20B), demonstrating a contribution of presynaptic activity to carbachol-induced response. A slight reduction of the response duration from 250 ± 21 s to 213 ± 21 s was also detected in the presence of the mixture CNQX, CPP and TTX, but this effect was not at significantly different. In voltage-clamped SPn, the transient carbachol-induced inward current showed a rise-time of 37.9 ± 4 s (n=26 cells) and reached a mean peak of 54.4 ± 5 pA (n=26 cells). A high degree of variability was observed in the duration of the response ranging from 90 to 680 s.

Since carbachol activates both muscarinic and nicotinic receptors, several subtype specific agonists and antagonists were used to determine which receptor type is functional on SPn. Bath application of the non-selective muscarinic receptor antagonist atropine (10 μM) on voltage-clamped SPn reduced significantly (t-test, $p<0.01$) the amplitude of the carbachol-induced inward current from 66.9 ± 9.5 pA to 32.7 ± 2.3 pA (n=9 cells) with no significant effects on the duration of the response. Since atropine did not completely block the carbachol-induced response, it is likely that both muscarinic and nicotinic receptors are functional on SPn.

Bath application of 100 μM nicotine depolarized 24 out of 27 current-clamped SPn from –70 mV to –47 ± 1.6 mV, whereas the remaining 3 SPn showed no response to nicotine. In 15 SPn the depolarization was of enough amplitude to trigger APs (Fig. 20C). The nicotine-induced response was characterized by a relatively fast rising phase (14 ± 1.5 s, n=24 cells) and by a long duration (450 ± 45 s, n=24 cells), several SPn being not able to return to holding potential even after 800 s (Fig. 20C). The significant (t-test, $p<0.01$) smaller depolarization (from –70 mV to –63 mV, n=7 cells), as well as the absence of APs in response to a second application of nicotine on SPn completely recovered to the holding potential argue for strong desensitization of nicotinic receptors.

In contrast to the uniform response of SPn to nicotine, bath application of 10 μM muscarine induced heterogeneous responses in 21 out of 29 investigated SPn. The most common response observed in 16 out of 21 responding SPn was a long lasting membrane depolarization from –70 mV to –58.3 ± 1.8 mV which triggered no APs (Fig. 20D). Muscarine-induced depolarization was relatively slow (mean rise-time of 25.9 2 ± 3.6 s) and in contrast to the nicotine response, the membrane potential recovered completely within 46-275 s after muscarine application. Two out of 21 responding SPn showed a different muscarine-induced response which consisted of oscillation-like changes in the membrane potential showing low frequency (0.02 Hz) and sufficient amplitude to evoke a train of APs during the depolarizing phase (Fig. 20E). The remaining 3 out of 21 responding SPn responded to muscarine with both long lasting depolarization (from –70 mV to –63 mV) and slow oscillation-like changes (frequency 0.025 Hz) in the membrane potential (Fig. 20F).

3.5.2 Muscarine-induced modulation of spontaneous synaptic activity

Activation of muscarinic receptors was reported to have not only a direct effect on the membrane potential, but also a modulatory effect on the neurotransmitter release at presynaptic sites (Jones, 1993). Carbachol (n=9 cells) and nicotine (n=24 cells) increased the noise but had no significant effect on spontaneous synaptic activity of SPn (Fig. 20A, C). In addition, bath application of the nicotine receptor antagonist tubocurarine (100 μM) had no significant effect on the frequency, amplitude or kinetic of the sPSCs (n=7 cells). In contrast, muscarine was able to modulate the spontaneous synaptic activity of SPn. In 10 out of 29 current-clamped SPn muscarine increased the frequency of the sPSPs (Fig. 20G, H) from a mean frequency of 0.2 ± 0.03 Hz to 0.8 ± 0.06 Hz (n=10 cells), with no significant effect on the sPSPs decay-time. The absence of muscarine-induced effects on the decay of sPSPs as well as the previously reported results indicating that fast spontaneous synaptic events are mediated by AMPA and slow synaptic events by NMDA receptors, led to the suggestion that both AMPA and NMDA receptor-mediated synaptic transmission is modulated by muscarine.

3.6 Electrical synapses between subplate neurons

Since the extensive presence of electrical synapses between cortical neurons during development was associated with their essential role in modulating the formation of neuronal connectivity, the presence of gap junctions between SPn was investigated.

3.6.1 Dye-coupling within the subplate

In order to identify the presence of dye-coupling within the subplate, injections of Lucifer Yellow CH (Stewart, 1978; Gutnick and Prince, 1981) into SPn were performed. In 7 out of 9 successfully recovered injections only the injected SPn was stained. The remaining two injections led to intense staining of the injected SPn and to

weaker staining of 2 or 3 neighboring neurons located within the subplate (Fig. 21A), indicating the presence of gap junctions between these SPn. In all 9 successfully recovered injections, Lucifer Yellow filled the soma and enough of the dendritic tree to permit morphological characterization of the injected SPn.

However, dye-coupling using Lucifer yellow was reported to be subject of ambiguous interpretation (Peinado et al., 1993a). Therefore, further investigation of electrical coupling was performed using as gap junctional tracer the biotinylated compound biocytin (Vaney, 1991) which due to its smaller size crosses different classes of gap junctions more readily (Yuste et al., 1992). In 66 out of 324 investigated SPn, injections of biocytin stained more than one neuron. The majority of the dye-coupled aggregates consisted of more than two and less than 20 neurons located within subplate and CP including layers V/VI (Fig. 21B, C). The great majority of coupled SPn were distributed consistently in the vicinity of the injected SPn's dendritic tree. No significant (χ^2-test) morphology- (horizontal bitufted 13.3%, horizontal monotufted 21.9%, multipolar 19.8%, inverted pyramid 30% and tripolar 16.7%) or age-dependent (P0 15%, P1 25%, P2 18.3% and P3 21%) differences in the proportion of dye-coupled SPn could be observed. The remaining 258 out of 324 biocytin-injected SPn showed no dye-coupling, only the injected SPn being stained in the slice.

3.6.2 Electrophysiological attempts to detect the presence of gap junctions

In order to detect the presence of gap junctions, R_{in} and spontaneous synaptic activity of SPn were investigated in the presence of the gap junction blocker carbenoxolone (CBX). CBX, a glycyrrhetic acid derivate, was reported to decrease dye transfer between cells (Davidson and Baumgarten, 1988) and increase the R_{in} of the investigated cells by blocking gap junctions (for review Roerig and Feller, 2000).

However, bath application of 10 μM CBX had no effect on the R_{in} of 22 investigated SPn. When depolarizing and hyperpolarizing voltage pulses of 2 s were applied from a holding potential of –70 mV, no significant changes in the corresponding current in CBX (Fig. 21D) could be observed and the linear current-voltage relationship was not modified by CBX (Fig. 21E). However, CBX affected the spontaneous synaptic activity in 16 investigated SPn. Bath application of CBX significantly (t-test, $p<0.001$) decreased the frequency of both fast and slow sPSCs by 15.5 ± 11.2% (n=16 cells) and 56.2 ± 13.6% (n=9 cells), respectively (Fig. 21F) and had no effect on the amplitude, rise-and decay-time of the sPSCs.

According to dye-coupling and electrophysiological recordings it is most likely that few SPn are coupled through gap junctions. However, the presence of this small fraction of electrically-coupled SPn did not allow identification of significant differences in their electrophysiological properties and precluded a more detailed analysis of the electrical coupling within the subplate.

4. Discussion

The present *in vitro* electrophysiological study on visually identified and morphologically characterized SPn in newborn rat somatosensory cortex demonstrates the presence and characterizes for the first time the properties of synaptic inputs onto SPn, indicating that SPn are able to integrate and process information from cortical and subcortical regions. SPn show spontaneous synaptic activity and three populations of sPSCs were identified: fast AMPA receptor-mediated sPSCs, slow NMDA receptor-mediated sPSCs and chloride-driven $GABA_A$ receptor-mediated sPSCs. The synaptic inputs onto SPn arise from cortical and subcortical regions and are mediated by AMPA, NMDA and $GABA_A$ receptors. Monosynaptic inputs arising from the thalamus and the CP are mediated by AMPA receptors and "classical" NMDA receptors activated at depolarized membrane potentials. In contrast, monosynaptic inputs from neighboring SPn are mediated by AMPA receptors, NMDA receptors activated at –70 mV, and by $GABA_A$ receptors mediating a depolarizing action. Beside these monosynaptic inputs, SPn also receive upon electrical stimulation of the CP or subplate polysynaptic inputs mediated by glutamate and $GABA_A$ receptors. SPn express functional muscarinic and nicotinic receptors mediating a depolarizing action. In addition to direct effects on membrane potential, muscarine increases glutamatergic spontaneous synaptic activity of SPn. Beside chemical synaptic transmission, at least a small fraction of SPn show gap junctional communication.

4.1 Electrophysiological properties of subplate neurons

The passive membrane properties of SPn (depolarized RMP and high R_{in}) were similar to those reported for Cajal-Retzius cells (Mienville and Pesold, 1999) and cortical neurons during early postnatal development (LoTurco et al., 1991; Kim et al., 1995; Luhmann et al., 2000). It seems unlikely that the depolarized RMP resulted from poor

recording quality since gigaohm seals were achieved before obtaining the whole-cell configuration and cells exhibited a high R_{in} throughout the recording. Although a depolarized RMP may be a typical feature of immature cortical neurons, it cannot be excluded that the depolarized RMP of SPn contributes to the induction or progression of programmed cell death, as it has been suggested for Cajal-Retzius neurons (Mienville and Pesold, 1999). In agreement with previous observations in fetal and early postnatal cat visual cortex (Friauf et al., 1990), SPn showed different firing patterns to injection of depolarizing current pulses and were classified as *regular spiking* or *single spiking* neurons. *Single spiking* SPn did not differ in their passive and active membrane properties from *regular spiking* SPn, indicating that poor cell health or recording quality does not account for the lack of repetitive firing in *single spiking* SPn. It is also unlikely that *single spiking* neurons represent a population of immature cells, which during further development will transform into *regular spiking* SPn or vice versa, since the relative proportion of SPn showing *regular* or *single spiking* remained constant during the investigated period (P0-3). It is highly likely that two distinct classes of SPn with different firing patterns but without obvious differences in their morphology and synaptic inputs may exist in the subplate of the newborn rat. The absence of correlation between the firing pattern and morphology has been previously reported for cat SPn (Friauf et al., 1990). Similar with results from SPn in embryonic turtle cerebral cortex (Blanton and Kriegstein, 1991), SPn were also able to fire spontaneous APs, which may contribute to the spontaneous synaptic activity observed in these neurons.

4.2 Functional synaptic inputs onto subplate neurons

4.2.1 Spontaneous synaptic activity of subplate neurons

The present study demonstrates for the first time that the majority of SPn shows spontaneous synaptic activity mediated by AMPA, NMDA and $GABA_A$ receptors. Although the low frequency and moderate amplitude of the sPSCs indicate a small number of synapses and a low density of channels devoted to them, the high R_{in} and the depolarized RMP of SPn may amplify the efficiency of these synapses. The sPSCs mediated by AMPA and NMDA receptors, as well as the GABAergic sPSCs had a depolarizing action and elicited APs in SPn. The frequency of spontaneous synaptic activity observed in SPn is relatively low. Similar results were reported also for other neonatal neurons (Hollrigel and Soltesz, 1997; Owens et al., 1999; Kilb and Luhmann, 2001), suggesting that the low frequency of spontaneous synaptic activity is a general feature of immature cortical neurons.

Although the basic organization of the cerebral cortex seems to be specified by molecular cues, the role of spontaneous synaptic activity in the cortical development should not be neglected (Goodman and Shatz, 1993). As previously reported (Weliky and Katz, 1999), spontaneous synaptic activity may supply an input which contains sufficient information to refine the formation of connections during development. Therefore, several cellular processes, including the strength and location of synapses, the expression of genes and the electrophysiological properties of SPn may be influenced by spontaneous activity.

4.2.2 Thalamocortical inputs onto subplate neurons

The present results on the thalamocortical input onto SPn are in good agreement with previous observations by Friauf et al. (1990) and Friauf and Shatz (1991) in fetal cat

visual cortex. The short onset latency, the all-or-none character and the unimodal latency distribution of the PSCs strongly argue for a monosynaptic input. As already reported by Friauf et al. (1990), electrical stimulation of the TA never elicited any polysynaptic activity. The present observation, that the thalamocortical input onto SPn is mediated by AMPA and NMDA receptors is in good agreement with previous observations by Agmon and O'Dowd (1992) on thalamocortical synaptic input onto layer IV neurons in somatosensory cortex of P3-P8 mice. A participation of NMDA and AMPA receptors to thalamocortical inputs onto SPn is supported by immunohistochemical studies demonstrating intense NMDAR1 immunoreactivity (Catalano et al., 1997) and high levels of the AMPA receptor-assembling subunits GluR1 and GluR2/3 in SPn (Herrmann, 1996; Furuta and Martin, 1999), whereas the density of kainate receptors remains relatively low (Smith and Thompson, 1999). Due to the voltage-dependent block by extracellular Mg^{2+}, the NMDA receptors mediating thalamocortical input onto SPn were activated only at depolarized membrane potentials and could be referred to as "classical" NMDA receptors. This property together with their fast decay-time constants argue for the presence of NR1 and NR2A subunit at the thalamocortical synapse (Feldmeyer and Cull-Candy, 1996; for review Cull-Candy et al., 2001). The reliability of the responses to higher stimulus frequencies may indicate a more mature structure and function of the thalamocortical synapse onto SPn, as it has been documented by Herrmann et al. (1994) in their ultrastructural analyses.

The lack of any antidromic activity in neonatal rat SPn may indicate that the corticothalamic axons follow a different trajectory as the thalamocortical afferents to the somatosensory cortex. In the developing cortex of mice and rats, a spatial separation of these two axonal projections has been documented (De Carlos and

O'Leary, 1992; Agmon et al., 1993; Bicknese et al., 1994) and in the hamster both projection systems are separated through much of the internal capsule ((Miller et al., 1993)). Therefore, it is most likely that corticothalamic axons could not be stimulated under experimental conditions of the present study.

4.2.3 Synaptic interactions between cortical plate and subplate

Previous morphological studies in kitten and ferret visual cortex have demonstrated axonal projections from layer IV spiny neurons (Callaway and Katz, 1992) and layer VI pyramidal cells (Callaway and Lieber, 1996) to the underlying subplate (Shering and Lowenstein, 1994). Consistent with these findings, the present data in neonatal rat cortex indicate that CP and layers V/VI neurons form functional synapses with SPn. These monosynaptic connections are fragile and mediated by AMPA receptors and by "classical" NMDA receptors. Since electrical stimulation of the CP including layers V/VI elicited antidromic spikes in SPn, the results of the present study are in accordance with previous anatomical studies documenting axonal projections from SPn to the CP (Assal and Innocenti, 1993; Galuske and Singer, 1996; Finney et al., 1998; Clancy et al., 2001). Functional projections of SPn to CP neurons have been previously demonstrated by Friauf and Shatz (1991) in visual cortical slices of fetal cats using current-source density analyses. Immunohistochemical data (Finney et al., 1998) in ferrets indicate that about half of cortically projecting SPn are glutamatergic.

4.2.4 Synaptic interactions within the subplate

As previously reported, SPn extend long-range tangential axonal collaterals (Assal and Innocenti, 1993; Galuske and Singer, 1996) and are able to form a dense, long-distance axonal network within the subplate (Wahle et al., 1987; Van Eden et al., 1989; Antonini and Shatz, 1990; Meinecke and Rakic, 1992). According to these data,

the present results demonstrated that the connections between SPn are functional. Electrical stimulation of the subplate elicited monosynaptic PSCs mediated by AMPA, NMDA and $GABA_A$ receptors, suggesting that SPn are interconnected via a dense synaptic network using these three ionotropic receptors.

The results of the present study indicate that the majority of the glutamatergic synapses between SPn contain AMPA receptors and NMDA receptors. In contrast to the "classical" NMDA receptors, the NMDA receptors mediating synaptic responses from other SPn showed a relatively weak voltage dependence of magnesium blockade as previously reported in neonatal rat hippocampus and neocortex (Burgard and Hablitz, 1994; Kirson et al., 1999). Since a substantial NMDA component with a slow decay-time constant at membrane potentials negative to -50 mV was observed, NMDA receptors containing preferentially the NR1/NR2C subunit combination may be expressed at these synapses (for review Cull-Candy et al., 2001; Feldmeyer and Cull-Candy, 1996). However, the presence of NR1-1a (exon-5-lacking) subunits with slow deactivation rates, triheteromeric NMDA receptors or extrasynaptic receptors cannot be excluded (for review see Cull-Candy et al., 2001). Since *in situ* hybridization studies concerning the expression of distinct NMDA receptor subunits during development were limited to the whole cortex (Monyer et al., 1994; Wenzel et al., 1996), the exact molecular basis for the distinct NMDA receptors present on SPn has to be determined.

Electrical stimulation of the subplate revealed also monosynaptic glutamatergic PSCs mediated by "classical" NMDA receptors activated at depolarized membrane potentials. This result suggests that SPn may express at least two variations in NMDA receptor subunit combination as it has been described for other cell types. It may well

be that NMDA receptors with different subunit compositions function within a single neuron in a synapse-selective manner (Ito et al., 1997).

In agreement with earlier studies in the hippocampus (Ben-Ari et al., 1989) and neocortex (Luhmann and Prince, 1991; Yuste and Katz, 1991; LoTurco et al., 1995; Owens et al., 1996), the perforated patch recordings from SPn indicate that $GABA_A$ receptor activation had a depolarizing effect. Therefore SPn are easily excited by network activity involving $GABA_A$, AMPA and NMDA receptors. However, the rapid fatigue of AMPA and especially NMDA receptor-mediated PSCs during on-going activity may prevent a pathophysiological hyperexcitation of this immature network. The present data indicate that the mono- and polysynaptic components involving $GABA_A$ receptor activation are generated within the subplate, since monosynaptic GABAergic inputs arising from the CP and layers V/VI or from the thalamus were never observed. As suggested by Kostovic and Rakic (1980), synaptic inputs forming symmetrical synapses originate from GABAergic SPn. Furthermore, the restriction of monosynaptic GABAergic PSCs to activation of the subplate indicates that the electrical stimulation procedure preferentially activates indigenous neuronal elements (for discussion of this issue see Hirsch, 1995). This assumption is also supported by the fact that electrical stimulation of the CP and layers V/VI elicited monosynaptic glutamatergic PSCs with a different kinetic and voltage-dependence as compared to those evoked by SP stimulation.

Polysynaptic PSCs mediated by AMPA, NMDA and $GABA_A$ receptors were also observed upon electrical stimulation of the CP including layers V/VI. Previous recordings from immature neocortical neurons already demonstrated long-lasting polysynaptic responses mediated by NMDA and non-NMDA receptors (Kim et al.,

1995; Agmon et al., 1996; Luhmann et al., 1999). However, since monosynaptic connections from CP including layers V/VI to the subplate were exclusively mediated by "classical" NMDA receptors and by AMPA receptors, this polysynaptic activity comprising GABAergic components is generated most likely by antidromic activation of ascending axons originating from SPn.

4.2.5 Activation of muscarinic and nicotinic receptors of subplate neurons

The present results show for the first time that activation of both nicotinic and muscarinic receptors elicited depolarizing responses in SPn and argues for the functional role of cholinergic afferents densely accumulating in the subplate by birth (Kostovic, 1986; Clinton and Ebner, 1988; Nyakas et al., 1994).

Previous autoradiographic data showed the appearance of nicotinic binding sites at the level of subplate shortly before birth and speculated on the presence of transient functional synapses between cholinergic forebrain projections and SPn (Naeff et al., 1992). According to these results, the majority of SPn responded with depolarization and firing of APs to nicotine. The nicotinic receptors on SPn showed slow desensitization, which may suggest the incorporation of α_7 subunit in their structure (Couturier et al., 1990; Zhang et al., 1994).

In contrast to the distribution of nicotinic receptors, muscarinic receptors are diffusely present during development across the entire depth of the cortex without being accumulated in the subplate (Schlumpf et al., 1991). According to these data, SPn responded to a less extent to muscarine and the effects induced by activation of muscarinic receptors were complex and diversified. In the majority of SPn, muscarine induced depolarization not sufficient to evoke APs. Similar effect of muscarine was

reported for cortical neurons (Benardo and Prince, 1982; Chessell and Humphrey, 1995). In few SPn muscarine was able to induce slow oscillation-like changes in the membrane potential accompanied by firing of APs. The small fraction of SPn showing this type of response precluded statistical analysis to identify if the morphology and the type of muscarine-induced response are correlated. Oscillation-like changes in the membrane potential in response to muscarine were previously described in hippocampal interneurons (McQuiston and Madison, 1999). These large-amplitude changes in the membrane potential were to slow to range in the frequency interval of behaviorally relevant oscillations like hippocampal theta-rhythm oscillations (4-12 Hz) involved in the mnemonic processing (Buzsàki, 1997). However, the slow frequency of the oscillation-like changes may be due to the slow application of muscarine. As previously reported for metabotropic glutamate receptors (Whittington et al., 1995), the presence of muscarine-induced oscillatory responses may suggest the role of muscarinic receptors on SPn in synchronizing oscillations in developing neocortical network.

The results of the present study show that muscarine not only acts directly on the membrane potential, but also had indirect effects on SPn by modulating their synaptic activity. The muscarine-induced increase in the frequency of glutamatergic spontaneous synaptic inputs indicates that muscarine elevates the firing rate of presynaptic neurons from thalamus, CP or subplate, the regions from where glutamatergic synaptic inputs onto SPn arise. The complex effects of muscarine onto SPn provide further support for the modulatory role of cholinergic input (MacDermott et al., 1999).

4.3 Gap junctions and their interactions with synaptic circuits

A small percent of SPn showed dye-coupling when biocytin or Lucifer yellow were used as tracers. Despite the data which stipulate the advantages of smaller biotinylated components as biocytin (molecular weight, MW 373 Da) upon Lucifer yellow (MW 457 Da) in crossing different classes of gap junctions (Vaney, 1991; Peinado et al., 1993b), similar fraction of SPn (22% for Lucifer yellow and 20% for biocytin) showed dye-coupling. A significant difference between both dyes was observed only in the number of neurons forming the dye-coupled aggregates. Since 2 to 3 neurons were present in Lucifer yellow-stained aggregates, up to 20 neurons were stained by a single biocytin injection. However, it should be noted that Lucifer yellow generates both false negative as well as false positive results (Peinado et al., 1993b).

The small fraction of SPn presenting dye-coupling may account for the absence of significant effects of CBX on R_{in}. However, CBX affected the spontaneous synaptic activity, leading to a significant decrease in the frequency of the glutamatergic sPSCs arising from thalamus, CP and subplate. Since in the rodent neocortex gap junctions and chemical synaptic transmission coexist and strongly interact with each other during early postnatal period (Roerig and Feller, 2000), modulation of synaptic transmission by blockade of gap junctions seems to account for CBX effects on sPSCs frequency. Gap junction may interact with synaptic activity by influencing electrotonic structure of neurons (Rörig et al., 1996) or synchronizing neuronal activity by coordinating biochemical activity (Kandler and Katz, 1998). Moreover, glutamatergic synaptic inputs, such as the thalamocortical input were reported to control gap junction permeability in the developing neocortex (Rörig and Sutor, 1996). The effect of CBX on synaptic activity due to the direct effect on the neurotransmitter receptors should not be neglected. Several gap junctions blockers like 1-octanol influence synaptic

transmission even during developmental stages when gap junction coupling disappeared (Rörig et al., 1996).

4.4 Functional role of the subplate during cortical development

Although early events in corticogenesis (e.g. regional specification, neurogenesis, migration and establishment of crude connections) depend on genetic information and molecular cues (for review Levitt et al., 1997b; Rubenstein et al., 1999), the refinement of the initial crude connectivity during a later stage of development requires neuronal activity (for review Katz and Shatz, 1996; Feller, 1999; Zhang and Poo, 2001). SPn probably play an important role in this activity-dependent refinement process (for review Allendoerfer and Shatz, 1994), being actively involved in synaptic processes. Our data indicate that the subplate integrates and processes synaptic inputs from cortical and subcortical structures in an input-specific manner. Thalamic activity is transmitted to the subplate via reliable AMPA and NMDA receptor-mediated synapses and subsequently processed in the cortical plate. Whereas monosynaptic feedback connections from the CP to the subplate are AMPA and NMDA receptor-mediated, the subplate itself contains an intrinsic network of long-range axonal connections acting via AMPA, NMDA and depolarizing $GABA_A$ synapses (Fig. 22). Moreover, SPn are depolarized by activation of cholinergic receptors and their spontaneous synaptic inputs mediated by AMPA and NMDA receptors is enhanced by muscarine.

As suggested by Finney et al. (1998), SPn may provide the cortex with a general level of excitation necessary to produce neurotrophins. Neurotrophins are regulated in an activity-dependent manner and participate in activity-induced modifications of synaptic transmission (for review Schinder and Poo, 2000). Therefore, afferent inputs

as well as spontaneous synaptic activity in the subplate may be required for the formation of normal connections, as it has been demonstrated for the activity-dependent maturation of thalamocortical connections in cat visual cortex (Herrmann and Shatz, 1995). Voigt et al. (2001) (Voigt et al., 2001) recently demonstrated that a subpopulation of large GABAergic SPn generates synchronous $[Ca^{2+}]_i$ oscillations, which can be blocked by either glutamate or $GABA_A$ receptor antagonists. This interconnected network of large GABAergic SPn may synchronize thalamocortical inputs, intracortical activity and modulatory inputs from subcortical sources to form early cortical ensembles. In addition, cholinergic input may be an important mediator of the neurotrophins action on cortical plasticity and shaping cortical connections as reported for visual cortex (Rossi et al., 2002). Moreover, the cholinergic input seems to have a crucial role for the fate of SPn. SPn survival is promoted by the p75 neurotrophin receptor (p75NTR) (DeFreitas et al., 2001) which undergoes a dramatic reduction in the absence of cholinergic input (Rossi et al., 2002).

GABA and glutamate released from SPn may regulate neuronal proliferation in the ventricular zone (VZ) and subventricular zone (SVZ) (LoTurco et al., 1995). Interestingly, both amino acids increase cell proliferation in the VZ by shortening the cell cycle, but decrease proliferation in the SVZ (Haydar et al., 2000). SPn are ideal candidates to influence proliferation, because (i) they are located close to the VZ and SVZ, (ii) they are immunoreactive for GABA and glutamate, and (iii) they can generate long-lasting network activity involving GABAergic and glutamatergic synaptic transmission.

As already emphasized by Ghosh and Shatz (1992a), the subplate represents more than a passive “waiting station” for afferent systems. SPn are able to integrate and

process information during development and play an active role in the maturation of the cortex.

6. Summary

1. Patch-clamp recordings and dye tracing experiments were performed from visually identified and biocytin labeled subplate neurons (SPn) in coronal somatosensory cortical slices from postnatal day (P) P0-P3 Wistar rats to investigate the morphological and electrophysiological properties, synaptic inputs and gap junctional coupling of SPn.

2. A detailed investigation of the somatodendritic properties of 324 biocytin-stained SPn allowed their classification in six morphological classes: horizontal bitufted (23% of the investigated SPn), horizontal monotufted (13%), multipolar (28%), inverted pyramid (18%), tripolar (pyramid-like) (17%) and vertical (0.02%). Independent of their morphology, SPn extend their processes in the white matter, cortical plate (CP) including layers V/VI as well as within the subplate. No significant correlation between morphology and electrophysiological properties or synaptic inputs could be detected.

3. SPn exhibited relatively uniform membrane properties with an average resting membrane potential of –55 ± 0.3 mV and an input resistance of 1267 ± 25 MΩ (n=453) when gluconate-based pipette solution was used. All SPn were able to fire action potentials (APs) in response to suprathreshold current injection. 60% of the investigated SPn are repetitively firing and were classified as *regular spiking* and the remaining 40% showed only one AP followed by membrane oscillations and were classified as *single spiking* SPn. In both groups the voltage deflection showed either linear dependence or time-independent inward rectification from the injected current. No significant age-dependent changes in the passive and active membrane properties were determined in SPn.

4. Three populations of spontaneous postsynaptic currents (sPSCs) could be identified in SPn: (i) fast sPSCs, which could be fitted with a monoexponential function and showed a 95% decrease in their frequency during AMPA/kainate receptor blockade by CNQX. Cyclothiazide caused a 3.5-fold increase in their decay-time, indicating that the fast sPSCs were mediated by AMPA receptors. (ii) slow sPSCs, which could be fitted with a biexponential function. The NMDA receptor antagonist CPP blocked almost completely the slow sPSCs, indicating that they are mediated by NMDA receptors. (iii) chloride-driven sPSCs, which were blocked by the $GABA_A$ receptor antagonist gabazine, indicating that they are mediated by $GABA_A$ receptors. While TTX completely blocked the slow NMDA receptor-mediated sPSCs, the frequency of the fast AMPA receptor-mediated sPSCs and of the GABAergic sPSCs was reduced by 55% and 90%, respectively.

5. In order to identify the origin of these synaptic inputs onto SPn, electrical stimulation of the subcortical and cortical regions using a bipolar electrode was performed. (i) Stimulation of the thalamocortical afferents (TA) was performed according to their path in the coronal slice determined by extracellular biocytin staining. At holding potential of –70 mV, electrical stimulation of the TA elicited in 68% of the SPn monosynaptic, unitary and CNQX-sensitive postsynaptic currents (PSCs). These fast PSCs were mediated by AMPA receptors, since they were prolonged by cyclothiazide and blocked by the selective AMPA receptor antagonist GYKI 52466. Upon membrane depolarization, stimulation of TA elicited in 50% of the SPn an additional slow monosynaptic component, which was mediated by NMDA receptors. (ii) Stimulation of the CP including layers V/VI evoked in 72% of the SPn monosynaptic PSCs followed in 40% of the investigated SPn by long-lasting polysynaptic PSCs. The monosynaptic PSCs were mediated by AMPA receptors and

showed in 80% of the SPn an additional NMDA receptor-mediated component at depolarized membrane potentials. The polysynaptic PSCs were dependent on NMDA and $GABA_A$ receptors, since they were completely blocked by CPP and their maximal amplitude was significantly reduced by gabazine. (iii) Stimulation of the subplate elicited in 67% of the investigated SPn monosynaptic dual-component PSCs and in 12% of the investigated SPn monosynaptic single-component PSCs. The dual-component PSCs were mediated by AMPA receptors and by NMDA receptors active at –70 mV, since the fast decaying component of the dual-component PSC was completely blocked by CNQX and GYKI 52466 and the slow decaying component was blocked by CPP. The single-component PSCs were mediated by AMPA receptors and showed an additional slow monosynaptic component mediated by NMDA receptors at depolarized membrane potentials. In addition, using high-chloride pipette solution and an extracellular solution supplied with CNQX and CPP, stimulation of the subplate elicited monosynaptic slow GABAergic PSCs in 68% of the investigated SPn. In gramicidin-perforated patch recordings, bath application of GABA caused a membrane depolarization from –70 to –40 mV and elicited APs, indicating that GABA plays a depolarizing role in SPn.

6. In order to investigate the effects of cholinergic innervation on membrane properties and synaptic inputs of SPn, nicotinic and muscarinic receptors agonists were bath-applied. Carbachol a non-selective cholinergic agonist depolarized the SPn by almost 27 mV and triggered a barrage of APs. Nicotine induced a long-lasting depolarization to -47 ± 1.6 mV (n=24 cells) of sufficient magnitude to trigger a barrage of APs. In contrast, muscarine-induced depolarization to –58.3 ± 1.6 mV (n=16 cells) did not trigger APs. Moreover, muscarine was able to induce oscillation-like changes in the membrane potentials of sufficient amplitude to trigger APs. These

results indicate that SPn expressed both functional nicotinic and muscarinic receptors. The synaptic activity of SPn was affected neither by carbachol nor by nicotine. Moreover, nicotinic receptor antagonist tubocurarine had no significant effects on the spontaneous synaptic activity of SPn. In contrast, muscarine increased the frequency of glutamatergic spontaneous synaptic potentials from 0.2 ± 0.03 Hz to 0.8 ± 0.006 Hz, with no effect on their amplitude.

7. Intracellular dye tracing experiments using Lucifer yellow and biocytin as well as whole-cell recordings were performed to determine if SPn are coupled by gap junctions. The presence of a small amount of SPn showing dye coupling (22% using Lucifer yellow and 20% using biocytin) was accompanied by the absence of significant changes in the input resistance of the SPn and in the current-voltage relationship in the presence of gap junction blocker carbenoxolone. These results suggest that the presence of gap junctions is restricted to few SPn precluding significant effects of carbenoxolone. However, carbenoxolone affected the spontaneous synaptic activity of SPn, decreasing the frequency of both fast and slow sPSCs by 15.5 ± 11.2% and 56.2 ± 13.6%, respectively.

8. The results of the present study demonstrate that SPn receive distinct functional synaptic inputs and integrate and process information from cortical and subcortical regions. Integrated in a synaptic circuit transiently expressed during development, SPn may play an active role in the maturation of the cerebral cortex.

6. References

Aboitiz F (1999) Comparative development of the mammalian isocortex and the reptilian dorsal ventricular ridge. Evolutionary considerations. Cereb Cortex 9: 783-791.

Agmon A, O'Dowd DK (1992) NMDA receptor-mediated currents are prominent in the thalamocortical synaptic response before maturation of inhibition. J Neurophysiol 68: 345-349.

Agmon A, Yang LT, O'Dowd DK, Jones EG (1993) Organized growth of thalamocortical axons from the deep tier of terminations into layer IV of developing mouse barrel cortex. J Neurosci 13: 5365-5382.

Agmon A, Hollrigel G, O'Dowd DK (1996) Functional GABAergic synaptic connection in neonatal mouse barrel cortex. J Neurosci 16: 4684-4695.

Allendoerfer KL, Shatz CJ (1994) The subplate, a transient neocortical structure: Its role in the development of connections between thalamus and cortex. Annu Rev Neurosci 17: 185-218.

Angevine JB, Sidman RL (1961) Autoradiographic study of cell migration during histogenesis of cerebral cortex in mouse. Nature 192: 766-768.

Antonini A, Shatz CJ (1990) Relation between putative transmitter phenotypes and connectivity of subplate neurons during cerebral cortical development. Eur J Neurosci 2: 744-761.

Aramakis VB, Bandrowski AE, Ashe JH (1999) Role of muscarinic receptors, G-proteins, and intracellular messengers in muscarinic modulation of NMDA receptor-mediated synaptic transmission. Synapse 32: 262-275.

Assal F, Innocenti GM (1993) Transient intra-areal axons in developing cat visual cortex. Cereb Cortex 3: 290-303.

Auladell C, Perez-Sust P. Supèr H, Soriano E (2000) The early development of thalamocortical and corticothalamic projections in the mouse. Anat Rmbryol (Berlin) 201: 169-179.

Bear MF, Singer W (1986) Modulation of visual cortical plasticity by acetylcholine and noradrenaline. Nature 320: 172-176.

Behar TN, Scott CA, Greene CL, Wen XL, Smith SV, Maric D, Liu QY, Colton CA, Barker JL (1999) Glutamate acting at NMDA receptors stimulates embryonic cortical neuronal migration. J Neurosci 19: 4449-4461.

Bellingham MC, Lim R, Walmsley B (1998) Developmental changes in EPSC quantal size and quantal content at a central glutamatergic synapse in rat. J Physiol (Lond) 511: 861-869.

Ben-Ari Y, Cherubini E, Corradetti R, Gaiarsa J-L (1989) Giant synaptic potentials in immature rat CA3 hippocampal neurones. J Physiol (Lond) 416: 303-325.

Benardo LS, Prince DA (1982) Ionic mechanisms of cholinergic excitation in mammalian hippocampal pyramidal cells. Brain Res 249: 333-344.

Bennett MVL, Spray DC, Harris AL (1981) Electrical coupling in development. Amer Zool 21: 413-427.

Benveniste M, Mayer ML (1991) Kinetic analysis of antagonist action at N-methyl-D-aspartic acid receptors. Two binding sites each for glutamate and glycine. Biophys J 59: 560-573.

Berry M, Rogers AW (1965) The migration of neuroblasts in the developing cerebral cortex. J Anat 99: 691-709.

Beyer EC (1993) Gap junctions. Int Rev Cytol 137C: 1-37.

Bicknese AR, Sheppard AM, O'Leary DD, Pearlman AL (1994) Thalamocortical axons extend along a chondroitin sulfate proteoglycan- enriched pathway coincident with the neocortical subplate and distinct from the efferent path. J Neurosci 14: 3500-3510.

Blanton MG, Kriegstein AR (1991) Spontaneous action potential activity and synaptic currents in the embryonic turtle cerebral cortex. J Neurosci 11: 3907-3923.

Bolz J, Castellani V (1997) How do wiring molecules specify cortical connections? Cell Tissue Res 290: 307-314.

Bormann J (1988) Electrophysiology of GABAA and GABAB receptor subtypes. Trends Neurosci 11: 112-116.

Boulder Committee (1970) Embryonic vertebrate central nervous system: revised terminology. Anat Rec 166: 257-261.

Burgard EC, Hablitz JJ (1993) NMDA receptor-mediated components of miniature excitatory synaptic currents in developing rat neocortex. J Neurophysiol 70: 1841-1852.

Burgard EC, Hablitz JJ (1994) Developmental changes in the voltage-dependence of neocortical NMDA responses. Dev Brain Res 80: 275-278.

Buzsàki G (1997) Functions for interneurons nets in the hippocampus. Can J Physiol Pharmacol 75: 508-515.

Callaway EM, Katz LC (1992) Development of axonal arbors of layer 4 spiny neurons in cat striate cortex. J Neurosci 12: 570-582.

Callaway EM, Lieber JL (1996) Development of axonal arbors of layer 6 pyramidal neurons in ferret primary visual cortex. J Comp Neurol 376: 295-305.

Catalano SM, Chang CK, Shatz CJ (1997) Activity-dependent regulation of NMDAR1 immunoreactivity in the developing visual cortex. J Neurosci 17: 8376-8390.

Catalano SM, Shatz CJ (1998) Activity-dependent cortical target selection by thalamic axons. Science 281: 559-562.

Chapin JK, Lin C-S (1990) The somatic sensory cortex of the rat. In: The cerebral cortex of the rat (Kolb B, Tees RC, eds), pp 341-380. Cambridge: MIT Press.

Chessell IP, Humphrey PP (1995) Nicotinic and muscarinic receptor-evoked depolarizations recorded from a novel cortical brain slice preparation. Neuropharmacol 34: 1289-1296.

Chun JJ, Shatz CJ (1988) A fibronectin-like molecule is present in the developing cat cerebral cortex and is correlated with subplate neurons. J Cell Biol 106: 857-872.

Clancy B, Silva M, Friedlander MJ (2001) Structure and projections of white matter neurons in the postnatal rat visual cortex. J Comp Neurol 434: 233-252.

Clinton RJ, Ebner FF (1988) The time course of neocortical graft innervation by AchE-positive fibers. J Comp Neurol 277: 557-577.

Colquhoun D, Jonas P, Sakmann B (1992) Action of brief pulses of glutamate on AMPA/kainate receptors in patches from different neurones of rat hippocampal slices. J Physiol (Lond) 458: 261-287.

Connors BW, Bernardo LS, Prince DA (1983) Coupling between neurons of the developing rat neocortex. J Neurosci 3: 773-782.

Couturier S, Bertrand D, Matter JM, Hernandez MC, Bertrand S, Millar N, Valera S, Barkas T, Ballivet M (1990) A neuronal nicotinic acetylcholine receptor subunit (alpha 7) is developmentally regulated and forms a homo-oligomeric channel blocked by alpha-BTX. Neuron 5: 847-856.

Cull-Candy S, Brickley S, Farrant M (2001) NMDA receptor subunits: diversity, development and disease. Curr Opin Neurobiol 11: 327-335.

Davidson JS, Baumgarten IM (1988) Glycyrrhetinic acid derivatives: a novel class of inhibitors of gap-junctional intercellular communication. A structure-activity relationship. J Pharmacol Exp Ther 246: 1104-1107.

De Carlos JA, O'Leary DDM (1992) Growth and targeting of subplate axons and establishment of major cortical pathways. J Neurosci 12: 1194-1211.

deAzevedo LC, Hedin-Pereira C, Lent R (1997) Callosal neurons in the cingulate cortical plate and subplate of human fetuses. J Comp Neurol 386: 60-70.

Debanne D, Guérineau NC, Gähwiler BH, Thompson SM (1996) Paired-pulse facilitation and depression at unitary synapses in rat hippocampus: Quantal fluctuation affects subsequent release. J Physiol (Lond) 491: 163-176.

DeFreitas MF, McQuillen PS, Shatz CJ (2001) A novel p75NTR signaling pathway promotes survival, not death, of immunopurified neocortical subplate neurons. J Neurosci 21: 5121-5129.

Del Río JA, Martínez A, Auladelland C, Soriano E (2000) Developmental history of the subplate and developing white matter in the murine neocortex. Neuronal organization and relationship with the main afferent systems at embryonic perinatal stages. Cereb Cortex 10: 784-801.

Dingledine R, Borges K, Bowie D, Traynelis SF (1999) The glutamate receptor ion channels. Pharmacol Rev 51: 7-61.

Edwards FA, Konnerth A, Sakmann B, Busch C (1990) Quantal analysis of inhibitory synaptic transmission in the dentate gyrus of rat hippocampal slices: A patch-clamp study. J Physiol (Lond) 430: 213-249.

Erzurumlu RS, Jhaveri S (1992) Emergence of connectivity in the embryonic rat parietal cortex. Cereb Cortex 2: 336-352.

Feldmeyer D, Cull-Candy S (1996) Functional consequences of changes in NMDA receptor subunit expression during development. J Neurocytol 25: 857-867.

Feller MB (1999) Spontaneous correlated activity in developing neural circuits. Neuron 22: 653-656.

Finney EM, Stone JR, Shatz CJ (1998) Major glutamatergic projection from subplate into visual cortex during development. J Comp Neurol 398: 105-118.

Forsythe ID, Westbrook GL (1988) Slow excitatory postsynaptic currents mediated by N-methyl-D- aspartate receptors on cultured mouse central neurones. J Physiol (Lond) 396: 515-533.

Friauf E, McConnell SK, Shatz CJ (1990) Functional synaptic circuits in the subplate during fetal and early postnatal development of cat visual cortex. J Neurosci 10: 2601-2613.

Friauf E, Shatz CJ (1991) Changing patterns of synaptic input to subplate and cortical plate during development of visual cortex. J Neurophysiol 66: 2059-2071.

Furuta A, Martin LJ (1999) Laminar segregation of the cortical plate during corticogenesis is accompanied by changes in glutamate receptor expression. J Neurobiol 39: 67-80.

Galuske RAW, Singer W (1996) The origin and topography of long-range intrinsic projections in cat visual cortex: A developmental study. Cereb Cortex 6: 417-430.

Ghosh A, Shatz CJ (1992a) Pathfinding and target selection by developing geniculocortical axons. J Neurosci 12: 39-55.

Ghosh A, Shatz CJ (1992b) Involvement of subplate neurons in the formation of ocular dominance columns. Science 255: 1441-1443.

Ghosh A, Carnahan J, Greenberg ME (1994) Requirement for BDNF in activity-dependent survival of cortical neurons. Science 263: 1618-1623.

Goodman CS, Shatz CJ (1993) Developmental mechanisms that generate precise patterns of neuronal connectivity. Cell 72: 77-98.

Gutnick MJ, Prince DA (1981) Dye coupling and possible electronic coupling in the guinea pig neocortical slice. Science 211: 67-70.

Hamill OP, Marty A, Neher E, Sakmann B, Sigworth FJ (1981) Improved patch-clamp techniques for high-resolution current recording from cells and cell-free membrane patches. Pflügers Arch 391: 85-100.

Hanganu IL, Kilb W, Luhmann HJ (2000a) Spontaneous synaptic events in subplate cells of neonatal rat neocortex. Pflügers Archiv 439 (Suppl.): R430.

Hanganu IL, Kilb W, Luhmann HJ (2000b) Subplate neurones of neonatal rat neocortex show excitatory and inhibitory spontaneous synaptic events. Eur J Neurosci 12 (Suppl 11): 280.

Hanganu IL, Kilb W, Luhmann HJ (2001a) Spontaneous synaptic activity of subplate neurons in neonatal rat somatosensory cortex. Cereb Cortex 11: 400-410.

Hanganu IL, Kilb W, Luhmann HJ (2001b) AMPA-receptor mediated thalamocortical projection to the neonatal rat subplate. Göttinger Neurobiology Report 2001: Proceedings of the 4th Meeting of German Neuroscience Society. Thieme Verlag: 927

Hanganu IL, Kilb W, Luhmann HJ (2001c) Subplate neurons are implicated in early neocortical networks. Online published.

Hanganu IL, Kilb W, Luhmann HJ (2002) Functional microcircuitry of the developmental cerebral cortex: evidence for a synaptic network in the subplate. Eur J Neurosci 443 (Suppl): S166.

Hanganu IL, Kilb W, Luhmann HJ (in press) Functional synaptic projections onto subplate neurons in neonatal rat somatosensory cortex.

Haydar TF, Wang F, Schwartz ML, Rakic P (2000) Differential modulation of proliferation in the neocortical ventricular and subventricular zones. J Neurosci 20: 5764-5774.

Herkenham M (1980) Laminar organization of thalamic projections to the rat neocortex. Science 207: 532-535.

Herrmann K (1996) Differential distribution of AMPA receptors and glutamate during pre- and postnatal development in the visual cortex of ferrets. J Comp Neurol 375: 1-17.

Herrmann K, Antonini A, Shatz CJ (1994) Ultrastructural evidence for synaptic interactions between thalamocortical axons and subplate neurons. Eur J Neurosci 6: 1729-1742.

Herrmann K, Shatz CJ (1995) Blockade of action potential activity alters initial arborization of thalamic axons within cortical layer 4. Proc Natl Acad Sci USA 92: 11244-11248.

Hirsch JA (1995) Synaptic integration in layer IV of the ferret striate cortex. J Physiol (Lond) 483: 183-190.

Hohmann CF, Berger-Sweeney J (1998) Cholinergic regulation of cortical development and plasticity. New twists to an old story. Perspect Dev Neurobiol 5: 401-425.

Hollrigel GS, Soltesz I (1997) Slow kinetics of miniature IPSCs during early postnatal development in granule cells of the dentate gyrus. J Neurosci 17: 5119-5128.

Honore T, Davies SN, Drejer J, Fletcher EJ, Jacobsen P, Lodge D, Nielsen FR (1988) Quinoxalinediones: potent competitive non-NMDA glutamate receptor antagonists. Science 241: 701-703.

Huntley GW, De Blas AL, Jones EG (1990) $GABA_A$ receptor immunoreactivity in adult and developing monkey sensory-motor cortex. Exp Brain Res 82: 519-535.

Ikonomidou C, Bosch F, Miksa M, Bittigau P, Vöckler J, Dikranian K, Tenkova TI, Stefovska V, Turski L, Olney JW (1999) Blockade of NMDA receptors and apoptotic neurodegeneration in the developing brain. Science 283: 70-74.

Ito I, Futai K, Katagiri H, Watanabe M, Sakimura K, Mishina M, Sugiyama H (1997) Synapse-selective impairment of NMDA receptor functions in mice lacking NMDA receptor ε1 or ε2 subunit. J Physiol (Lond) 500: 401-408.

Jones SV (1993) Muscarinic receptor subtypes: modulation of ion channels. Life Sci 52: 457-464.

Kageyama GH, Robertson RT (1993) Development of geniculocortical projections to visual cortex in rat: Evidence for early ingrowth and synaptogenesis. J Comp Neurol 335: 123-148.

Kandler K, Katz LC (1998) Coordination of neuronal activity in developing visual cortex by gap junction-mediated biochemical communication. J Neurosci 18: 1419-1427.

Katz LC, Shatz CJ (1996) Synaptic activity and the construction of cortical circuits. Science 274: 1133-1138.

Kilb W, Luhmann HJ (2001) Spontaneous GABAergic postsynaptic currents in Cajal-Retzius cells in neonatal rat cerebral cortex. Eur J Neurosci 13: 1387-1390.

Killackey HP, Rhoades RW, Bennett-Clarke CA (1995) The formation of a cortical somatotopic map. Trends Neurosci 18: 402-407.

Kim HG, Fox K, Connors BW (1995) Properties of excitatory synaptic events in neurons of primary somatosensory cortex of neonatal rats. Cereb Cortex 5: 148-157.

Kirson ED, Schirra C, Konnerth A, Yaari Y (1999) Early postnatal switch in magnesium sensitivity of NMDA receptors in rat CA1 pyramidal cells. J Physiol (Lond) 521: 99-111.

Korte M, Carroll P, Wolf E, Brem G, Thoenen H, Bonhoeffer T (1995) Hippocampal long-term potentiation is impaired in mice lacking brain-derived neurotrophic factor. Proc Natl Acad Sci USA 92: 8856-8860.

Kostovic I (1986) Prenatal development of nucleus basalis complex and related fiber systems in man: a histochemical study. Neuroscience 17: 1047-1077.

Kostovic I, Rakic P (1980) Cytology and time of origin of interstitial neurons in the white matter in infant and adult human and monkey telencephalon. J Neurocytol 9: 219-242.

Kostovic I, Rakic P (1990) Developmental history of the transient subplate zone in the visual and somatosensory cortex of the macaque monkey and human brain. J Comp Neurol 297: 441-470.

Kral T, Luhmann HJ, Mittmann T, Heinemann U (1993) Role of NMDA receptors and voltage-activated calcium channels in an in vitro model of cerebral ischemia. Brain Res 612: 278-288.

Kriegstein AR, Suppes T, Prince DA (1987) Cellular and synaptic physiology and epileptogenesis of developing rat neocortical neurons in vitro. Dev Brain Res 34: 161-171.

Kristt DA, McGowan RA Jr, Martin-MacKinnon N, Solomon J (1985) Basal forebrain innervation of rodent neocortex: studies using acetylcholineesterase histochemistry, Golgi and lesion strategies. Brain Res 337: 19-39.

Kuffler SW, Potter DD (1964) Glia in the leech central nervous system: physiological properties and neuron-glia relationship. J Neurophysiol 27: 290-320.

Kyrozis A, Reichling DB (1995) Perforated-patch recording with gramicidin avoids artifactual changes in intracellular chloride concentration. J Neurosci Methods 57: 27-35.

Laurie DJ, Wisden W, Seeburg PH (1992) The distribution of thirteen $GABA_A$ receptor subunit mRNAs in the rat brain. III. Embryonic and postnatal development. J Neurosci 12: 4151-4172.

Lehmann J, Nagy JI, Atmadia S, Fibiger HC (1980) The nucleus basalis magnocellularis: the origin of a cholinergic projection to the neocortex of the rat. Neuroscience 5: 1161-1174.

Lehmann J, Schneider J, McPherson S, Murphy DE, Bernard P, Tsai C, Bennett DA, Pastor G, Steel DJ, Boehm C, Cheney DL, Liebman JM, Williams M, Wood PL

(1987) CPP, a selective N-methyl-D-aspartate (NMDA)-type receptor antagonist: characterization in vitro and in vivo. J Pharmacol Exp Ther 240: 737-746.

Levitt P, Moore RY (1979) Development of the noradrenergic innervation of neocortex. Brain Res 162: 243-259.

Levitt P, Harvey JA, Friedman E, Simansky K, Murphy EH (1997a) New evidence for neurotransmitter influences on brain development. Trends Neurosci 20: 269-274.

Levitt P, Barbe MF, Eagleson KL (1997b) Patterning and specification of the cerebral cortex. Annu Rev Neurosci 20: 1-24.

LoTurco JJ, Blanton MG, Kriegstein AR (1991) Initial expression and endogenous activation of NMDA channels in early neocortical development. J Neurosci 11: 792-799.

LoTurco JJ, Owens DF, Heath MJS, Davis MBE, Kriegstein AR (1995) GABA and glutamate depolarize cortical progenitor cells and inhibit DNA synthesis. Neuron 15: 1287-1298.

Luhmann HJ, Prince DA (1990) Transient expression of polysynaptic NMDA receptor-mediated activity during neocortical development. Neurosci Lett 111: 109-115.

Luhmann HJ, Prince DA (1991) Postnatal maturation of the GABAergic system in rat neocortex. J Neurophysiol 65: 247-263.

Luhmann HJ, Schubert D, Kötter R, Staiger JF (1999) Cellular morphology and physiology of the perinatal rat cerebral cortex. Dev Neurosci 21: 298-309.

Luhmann HJ, Reiprich RA, Hanganu I, Kilb W (2000) Cellular physiology of the neonatal rat cerebral cortex: Intrinsic membrane properties, sodium and calcium currents. J Neurosci Res 62: 574-584.

Luskin MB, Shatz CJ (1985) Neurogenesis of the cat's primary visual cortex. J Comp Neurol 242: 611-631.

Ma W, Maric D, Li BS, Hu Q, Andreadis JD, Grant GM, Liu QY, Shaffer KM, Chang YH, Zhang L, Pancrazio JJ, Pant HC, Stenger DA, Barker JL (2000) Acetylcholine stimulates cortical precursor cell proliferation *in vitro* via muscarinic receptor activation and MAP kinase phosphorylation. Eur J Neurosci 12: 1227-1240.

MacDermott AB, Role LW, Siegelbaum SA (1999) Presynaptic ionotropic receptors and the control of transmitter release. Annu Rev Neurosci 22: 443-485.

Marín-Padilla M (1971) Early prenatal ontogenesis of the cerebral cortex (neocortex) of the cat (Felis domestica). A Golgi study. I. The primordial neocortical organization. Z Anat Entwickl -Gesch 134: 117-145.

Marty A, Neher E (1995) Tight-seal whole-cell recordings. In: Single-channel recording (Sakmann B, Neher E, eds), pp 31-52. New York: Plenum.

Mayer ML, Westbrook GL (1987) The physiology of excitatory amino acids in the vertebrate central nervous system. Prog Neurobiol 28: 197-276.

McConnell SK, Ghosh A, Shatz CJ (1989) Subplate neurons pioneer the first axon pathway from the cerebral cortex. Science 245: 978-982.

McQuiston AR, Madison DV (1999) Muscarinic receptor activity has multiple effects on the resting membrane potentials of CA1 hippocampal interneurons. J Neurosci 19: 5693-5702.

Meinecke DL, Rakic P (1992) Expression of GABA and $GABA_A$ receptors by neurons of the subplate zone in developing primate occipital cortex: Evidence for transient local circuits. J Comp Neurol 317: 91-101.

Mienville JM, Pesold C (1999) Low resting potential and postnatal upregulation of NMDA receptors may cause Cajal-Retzius cell death. J Neurosci 19: 1636-1646.

Mikuni N, Babb TL, Ying Z, Najm I, Nishiyama K, Wylie C, Yacubova K, Okamoto T, Bingaman W (1999) NMDA-receptors 1 and 2A/B coassembly increased in human epileptic focal cortical dysplasia. Epilepsia 40: 1683-1687.

Miller B, Chou L, Finlay BL (1993) The early development of thalamocortical and corticothalamic projections. J Comp Neurol 335: 16-41.

Miller RJ (1998) Presynaptic receptors. Annu Rev Pharmacol Toxicol 38: 201-227.

Millhorn DE, Bayliss DA, Erickson JT, Gallwan EA, Szymeczek CL, Czyzyk-Krzesky M, Dean JB (1989) Cellular and molecular mechanisms of chemical synaptic transmission. Am J Physiol 257: L289-L310.

Molnàr Z, Blakemore C (1995) How do thalamic axons find their way to the cortex. Trends Neurosci 18: 389-397.

Molnár Z, Adams R, Blakemore C (1998) Mechanisms underlying the early establishment of thalamocortical connections in the rat. J Neurosci 18: 5723-5745.

Monyer H, Burnashev N, Laurie DJ, Sakmann B, Seeburg PH (1994) Developmental and regional expression in the rat brain and functional properties of four NMDA receptors. Neuron 12: 529-540.

Mrzljak L, Uylings HBM, Kostovic I, Van Eden CG (1992) Prenatal development of neurons in the human prefrontal cortex. II. A quantitative Golgi study. J Comp Neurol 316: 485-496.

Nadarajah B, Brunstrom JE, Grutzendler J, Wong ROL, Pearlman AL (2001) Two modes of radial migration in early development of the cerebral cortex. Nat Neurosci 4: 143-150.

Naeff B, Schlumpf M, Lichtensteiger W (1992) Pre- and postnatal development of high-affinity [^{3}H]nicotine binding sites in rat brain regions: An autoradiographic study. Dev Brain Res 68: 163-174.

Nyakas C, Buwalda B, Kramers RJK, Traber J, Luiten PGM (1994) Postnatal development of hippocampal and neocortical cholinergic and serotonergic innervation in rat: Effects of nitrite- induced prenatal hypoxia and nimodipine treatment. Neuroscience 59: 541-559.

Owens DF, Boyce LH, Davis MBE, Kriegstein AR (1996) Excitatory GABA responses in embryonic and neonatal cortical slices demonstrated by gramicidin perforated-patch recordings and calcium imaging. J Neurosci 16: 6414-6423.

Owens DF, Liu XL, Kriegstein AR (1999) Changing properties of $GABA_A$ receptor-mediated signaling during early neocortical development. J Neurophysiol 82: 570-583.

Owens DF, Kriegstein AR (2001) Maturation of channels and receptors: consequences for excitability. Int Rev Neurobiol 45: 43-87.

Partin KM, Patneau DK, Winters CA, Mayer ML, Buonanno A (1993) Selective modulation of desensitization at AMPA versus kainate receptors by cyclothiazide and concanavalin A. Neuron 11: 1069-1082.

Paternain AV, Morales M, Lerma J (1995) Selective antagonism of AMPA receptors unmasks kainate receptor- mediated responses in hippocampal neurons. Neuron 14: 185-189.

Peinado A (2001) Immature neocortical neurons exist as extensive syncitial networks linked by dendrodendritic electrical connections. J Neurophysiol 85: 620-629.

Peinado A, Yuste R, Katz LC (1993a) Extensive dye coupling between rat neocortical neurons during the period of circuit formation. Neuron 10: 103-114.

Peinado A, Yuste R, Katz LC (1993b) Gap junctional communication and the development of local circuits in neocortex. Cereb Cortex 3: 488-498.

Pin J-P, Duvoisin R (1995) The metabotropic glutamate receptors: Structure and functions. Neuropharmacology 34: 1-26.

Price DJ, Willshaw DJ (2000) Early development of the telencephalon. In: Mechanisms of cortical development (Monographs of the Physiological society, 47). pp 9-49. New York: Oxford University Press.

Pusch M, Neher E (1988) Rates of diffusional exchange between small cells and a measuring patch pipette. Pflügers Arch 411: 204-211.

Rakic P (1974) Neurons in the rhesus monkey visual cortex: systematic relationship between time of origin and eventual disposition. Science 182: 425-427.

Rakic P (1977) Prenatal development of the visual system in rhesus monkey. Philos Trans R Soc Lond B Biol Sci 278: 245-260.

Rakic P (1988) Specification of cerebral cortical areas. Science 241: 170-176.

Rhoades RW, Bennett-Clarke CA, Shi M-Y, Mooney RD (1994) Effects of 5-HT on thalamocortical synaptic transmission in the developing rat. J Neurophysiol 72: 2438-2450.

Rickmann M, Chronwall BM, Wolff JR (1977) On the development of non-pyramidal neurons and axons outside the cortical plate: the early marginal zone as a pallial anlage. Anat Embryol (Berl) 151: 285-307.

Robertson RT, Annis CM, Baratta J, Haraldson S, Ingeman J, Kageya GH, Kimm E, Yu J (2000) Do subplate neurons comprise a transient population of cells in developing neocortex of rats? J Comp Neurol 426: 632-650.

Roerig B, Feller MB (2000) Neurotransmitters and gap junctions in developing neural circuits. Brain Res Rev 32: 86-114.

Roerig B, Katz LC (1997) Modulation of intrinsic circuits by serotonin 5-HT_3 receptors in developing ferret visual cortex. J Neurosci 17: 8324-8338.

Rossi FM, Sala R, Maffei L (2002) Expression of the nerve growth factor receptors TrkA and $p75^{NTR}$ in the visual cortex of the rat: development and regulation by the cholinergic input. J Neurosci 22: 912-919.

Rörig B, Klausa G, Sutor B (1996) Intracellular acidification reduced gap junction coupling between immature rat neocortical pyramidal neurones. J Physiol (Lond) 490: 31-49.

Rörig B, Sutor B (1996) Regulation of gap junction coupling in the developing neocortex. Mol Neurobiol 12: 225-249.

Rubenstein JLR, Anderson S, Shi LM, Miyashita-Lin E, Bulfone A, Hevner R (1999) Genetic control of cortical regionalization and connectivity. Cereb Cortex 9: 524-532.

Rye DB, Wainer BH, Mesulam MM, Mufson EJ, Saper CB (1984) Cortical projections arising from the basal forebrain: a study of cholinergic and noncholinergic components employing combined retrograde tracing and immunohistochemical localization of choline acetyltransferase. Neuroscience 13: 627-643.

Schinder AF, Poo MM (2000) The neurotrophin hypothesis for synaptic plasticity. Trends in Neurosciences 23: 639-645.

Schlumpf M, Shoemaker WJ, Bloom FE (1980) Innervation of embryonic rat cerebral by catecholamine containing fibers. J Comp Neurol 192: 361-376.

Schlumpf M, Richards JG, Lichtensteiger W, Mohler H (1983) An autoradiographic study of the prenatal development of benzodiazepine-binding sites in rat brain. J Neurosci 3: 1478-1487.

Schlumpf M, Palacios JM, Cortes R, Lichtensteiger W (1991) Regional development of muscarinic cholinergic binding sites in the prenatal rat brain. Neuroscience 45: 347-357.

Schröder R, Luhmann HJ (1997) Morphology, electrophysiology and pathophysiology of supragranular neurons in rat primary somatosensory cortex. Eur J Neurosci 9: 163-176.

Shering AF, Lowenstein PR (1994) Neocortex provides direct synaptic input to interstitial neurons of the intermediate zone of kittens and white matter of cats: A light and electron microscopic study. J Comp Neurol 347: 433-443.

Sidman RL, Rakic P (1973) Neuronal migration, with special reference to developing human brain: a review. Brain Res 62: 1-35.

Smith AL, Thompson ID (1999) Spatiotemporal patterning of glutamate receptors in developing ferret striate cortex. Eur J Neurosci 11: 923-934.

Staiger JF, Kötter R, Zilles K, Luhmann HJ (1999) Connectivity in the somatosensory cortex of the adolescent rat: an in vitro biocytin study. Anat Embryol (Berl) 199: 357-365.

Stewart WW (1978) Functional connections between cells as revealed by dye-coupling with a highly fluorescent naphthalimide tracer. Cell 14: 741-759.

Stone TW, Burton NR (1988) NMDA receptors and ligands in the vertebrate CNS. Prog Neurobiol 30: 333-368.

Stuart GJ, Dodt HU, Sakmann B (1993) Patch-clamp recordings from the soma and dendrites of neurons in brain slices using infrared video microscopy. Pflügers Arch 423: 511-518.

Supèr H, Soriano E, Uylings HB (1998) The functions of the preplate in development and evolution of the neocortex and hippocampus. Brain Res Rev 27: 40-64.

Trussell LO, Thio LL, Zorumski CF, Fischbach GD (1988) Rapid desensitization of glutamate receptors in vertebrate central neurons. Proc Natl Acad Sci USA 85: 2834-2838.

Uylings HBM, Van Eden CG, Parnavelas JG, Kalsbeek A (1990) The prenatal and postnatal development of rat cerebral cortex. In: The cerebral cortex of the rat (Kolb B, Tees RC, eds), pp 35-76. Cambridge: MIT Press.

Valverde F, Facal Valverde MV, Santacana M, Heredia M (1989) Development and differentiation of early generated cells of sublayer VIb in the somatosensory cortex of the rat: a correlated Golgi and autoradiographic study. J Comp Neurol 290: 118-140.

Van Eden CG, Mrzljak L, Voorn P, Uylings HBM (1989) Prenatal development of GABA-ergic neurons in the neocortex of the rat. J Comp Neurol 289: 213-227.

Vaney DI (1991) Many diverse types of retinal neurons show tracer coupling when injected with biocytin or Neurobiotin. Neurosci Lett 125: 187-190.

Voigt T, Opitz T, De Lima AD (2001) Synchronous oscillatory activity in immature cortical network is driven by GABAergic preplate neurons. J Neurosci 21: 8895-8905.

Wahle P, Meyer G (1987) Morphology and quantitative changes of transient NPY-ir neuronal populations during early postnatal development of the cat visual cortex. J Comp Neurol 261: 165-192.

Wahle P, Meyer G, Wu JY, Albus K (1987) Morphology and axon terminal pattern of glutamate decarboxylase- immunoreactive cell types in the white matter of the cat occipital cortex during early postnatal development. Brain Res 433: 53-61.

Wahle P, Lübke J, Naegele JR (1994) Inverted pyramidal neurons and interneurons in cat cortical subplate zone are labelled by monoclonal antibody SP1. Eur J Neurosci 6: 1167-1178.

Weliky M, Katz LC (1999) Correlational structure of spontaneous neuronal activity in the developing lateral geniculate nucleus in vivo. Science 285: 599-604.

Wenzel A, Villa M, Mohler H, Benke D (1996) Developmental and regional expression of NMDA receptor subtypes containing the NR2D subunit in rat brain. J Neurochem 66: 1240-1248.

Wermuth CG, Bizière K (1986) Pyridazinyl-GABA derivates: a new class of synthetic GABA-A antagonists. Trends Pharmacol Sci 7: 421-424.

Whittington MA, Traub RD, Jefferys JG (1995) Synchronized oscillations in interneuron networks driven by metabotropic glutamate receptor activation. Nature 373: 612-615.

Yuasa S, Kitoh J, Kawamura K (1994) Interactions between growing thalamocortical afferent axons and the neocortical primodium in normal and reeler mutant mice. Anat Embryol (Berlin) 190: 137-154.

Yuste R, Katz LC (1991) Control of postsynaptic Ca^{2+} influx in developing neocortex by excitatory and inhibitory neurotransmitters. Neuron 6: 333-344.

Yuste R, Peinado A, Katz LC (1992) Neuronal domains in developing neocortex. Science 257: 665-669.

Zhang LI, Poo MM (2001) Electrical activity and development of neural circuits. Nat Neurosci 4: 1207-1214.

Zhang ZW, Vijayaraghavan S, Berg DK (1994) Neuronal acetylcholine receptors that bind alpha-bungarotoxin with high affinity function as ligand-gated ion channels. Neuron 12: 167-177.

Zhou C, Qiu YH, Pereira FA, Crair MC, Tsai SY, Tsai MJ (1999) The nuclear orphan receptor COUP-TFI is required for differentiation of subplate neurons and guidance of thalamocortical axons. Neuron 24: 847-859.

7. Figures

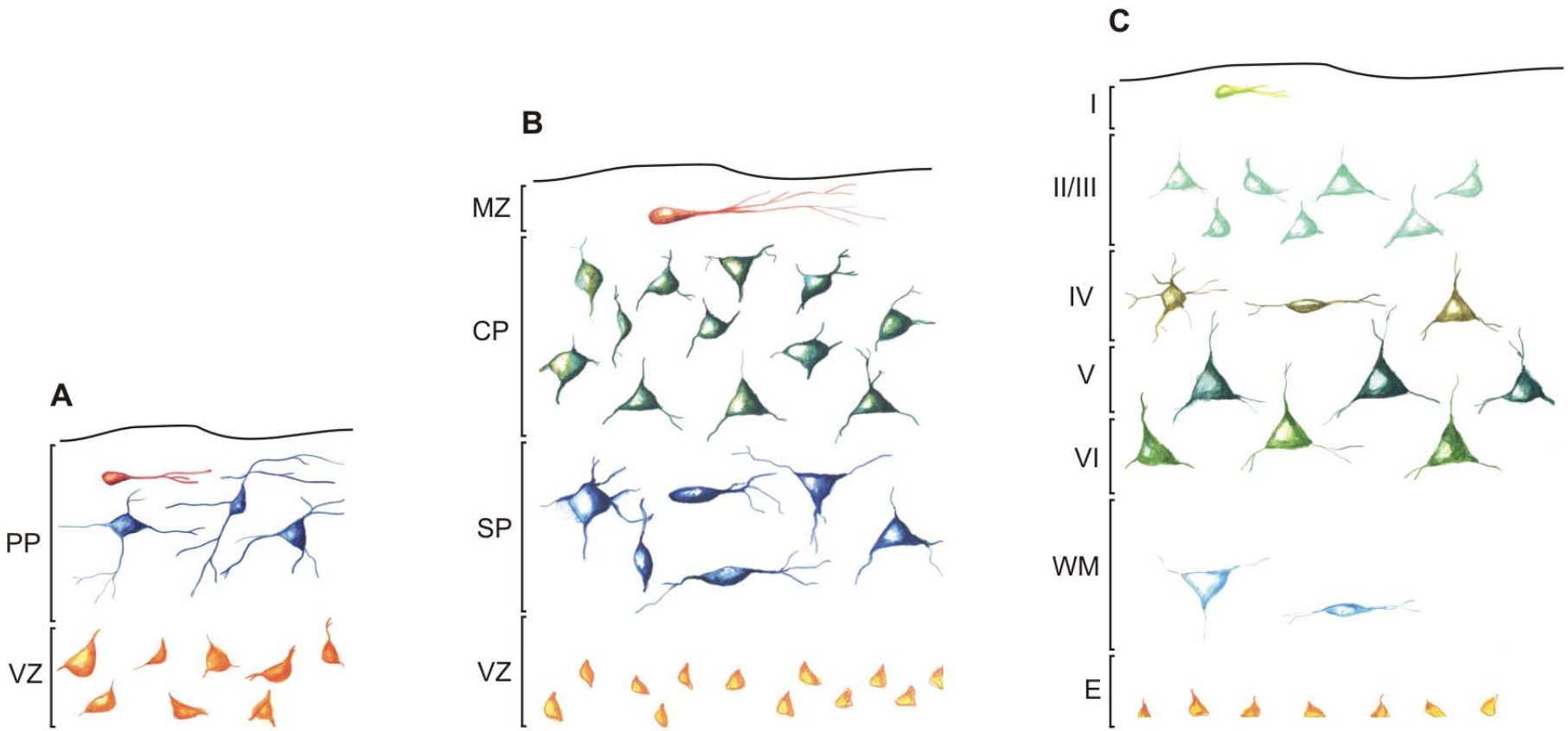

Figure 1. Diagram of the major histological changes in the cerebral wall during neocortical development. **A.** Cortical development begins with formation of the ventricular zone (VZ) and of the preplate (PP) containing prospective Cajal-Retzius neurons (red cell) and polymorphous neurons (blue cells). **B.** With on-going neurogenesis and migration, the cortical plate (CP) neurons split the PP in marginal zone (MZ) and subplate (SP). **C.** By adulthood, the six-layered cortex generated in an inside-out manner is completely developed. The majority of neurons in the SP have disappeared or transformed themselves in interstitial neurons present in the white matter (WM). VZ was substituted by an ependymal layer (E). Modified from Allendoerfer and Shatz, (1994).

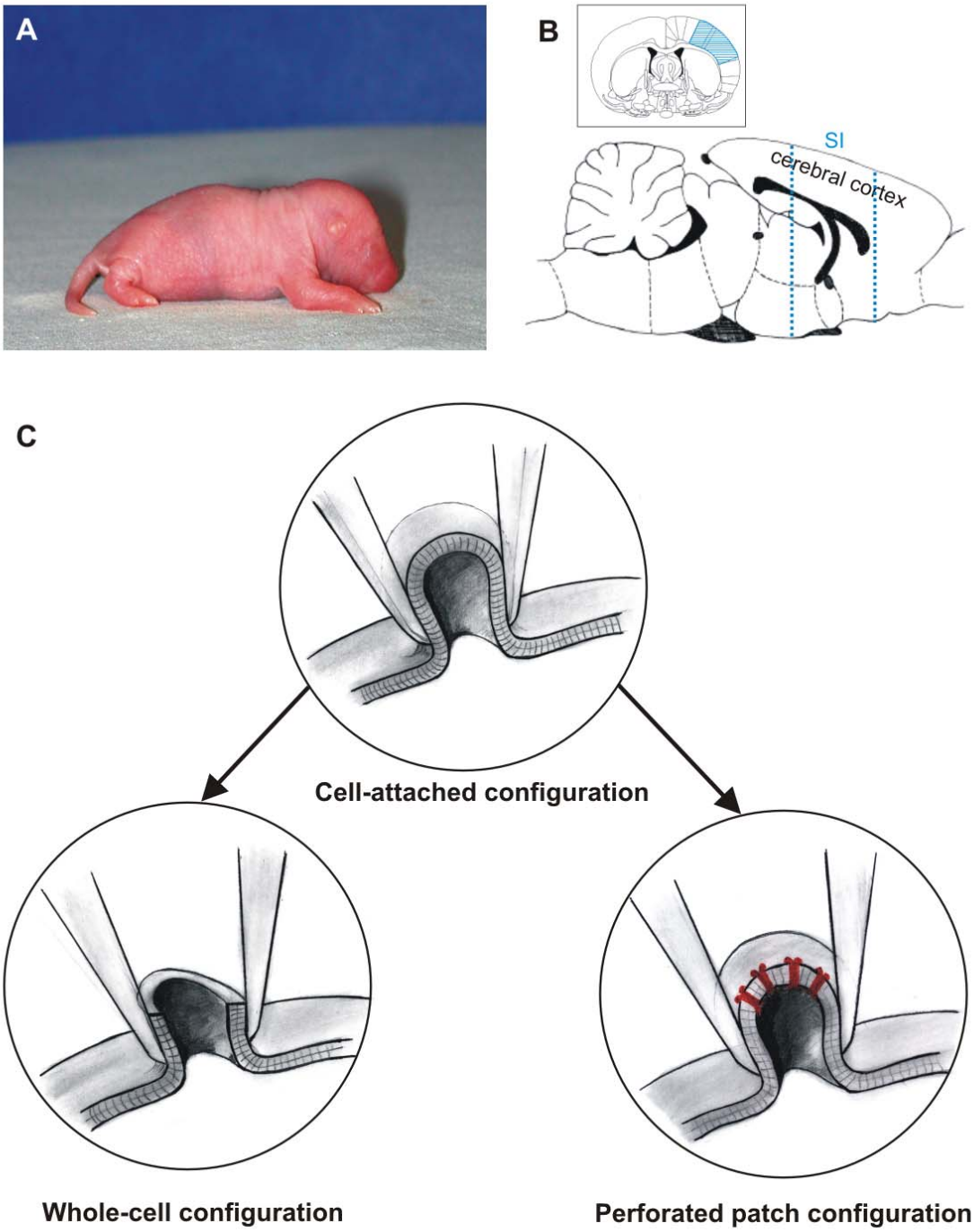

Figure 2. Diagram showing the location of rat somatosensory cortex in coronal slices and the patch-clamp configurations used for recordings from SPn. **A.** Photograph of a two days-old Wistar rat. **B.** Outline drawing of rat brain showing the location of the region containing the somatosensory cortex (delimitated by blue doted lines). In the inset, outline drawing shows the location of somatosensory cortex (blue hatched region) in a coronal slice. Modified from Paxinos, (1999). **C.** Schematic drawing of the used patch-clamp configurations. Cell-attached configuration obtained by tightly sealing the pipette onto the membrane of the cell is the precursor of all patch-clamp configurations. Electrical connection between pipette and cell may be achieved either by rupture of the membrane using brief pulses of suction applied to the pipette (whole-cell configuration) or by incorporation of a channel-forming substance (marked in red) in the pipette (perforated patch configuration). Modified from Numberger and Draguhn, (1996).

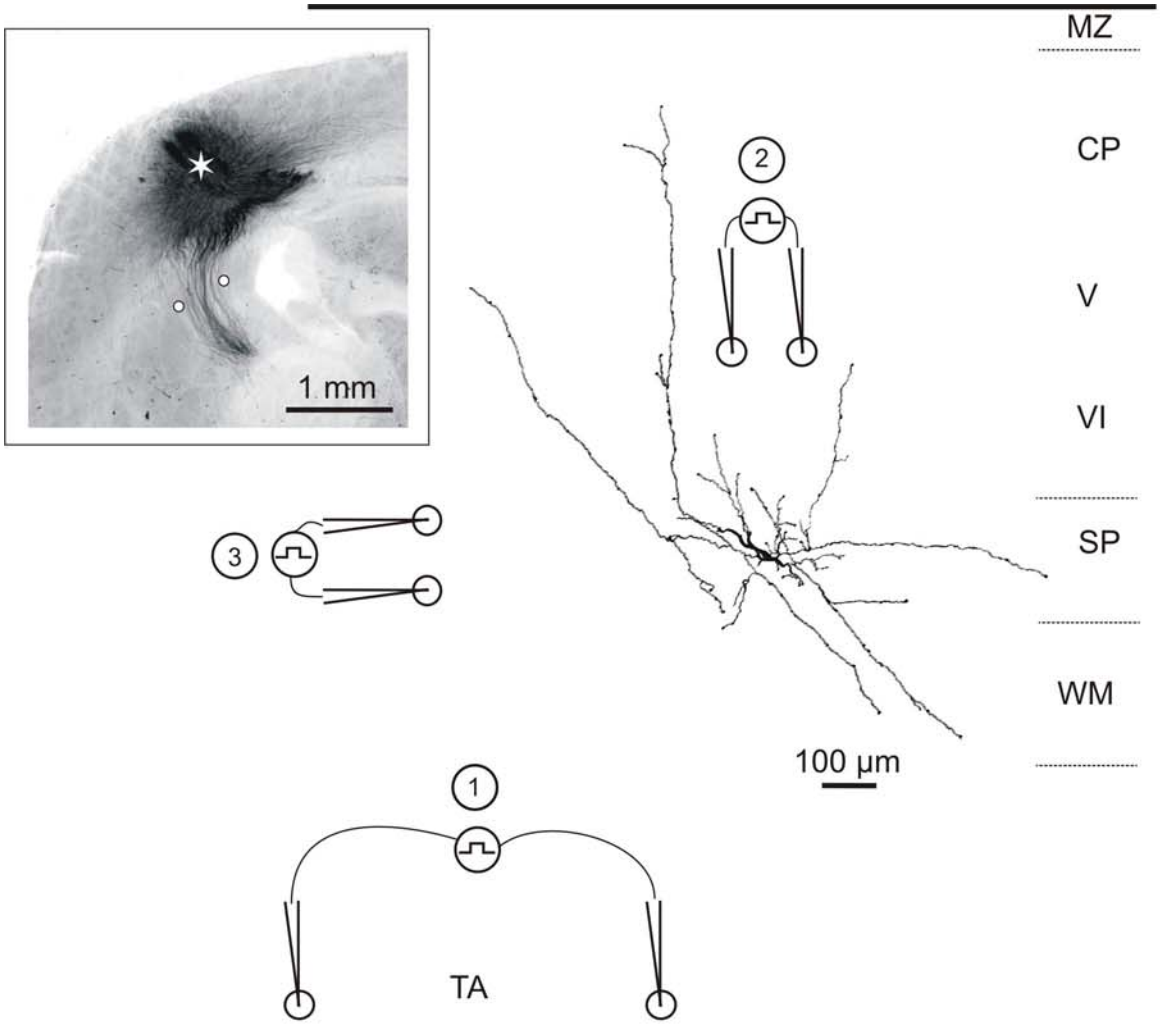

Figure 3. Morphology of a P2 SPn reconstructed with camera lucida and schematic illustration showing the location of the bipolar tungsten electrode used for electrical stimulation of the thalamocortical afferents (TA,①), cortical plate (CP) and layers V/VI (②), and the subplate (SP,③). Note larger interpole distance of electrode ① as compared to electrode ② and ③. The inset shows photomicrograph of biocytin-stained thalamocortical projections in a 400 µm thick coronal slice from a P1 rat. Asterisk shows extracellular injection of biocytin crystal and white circles mark position of TA stimulating electrodes.

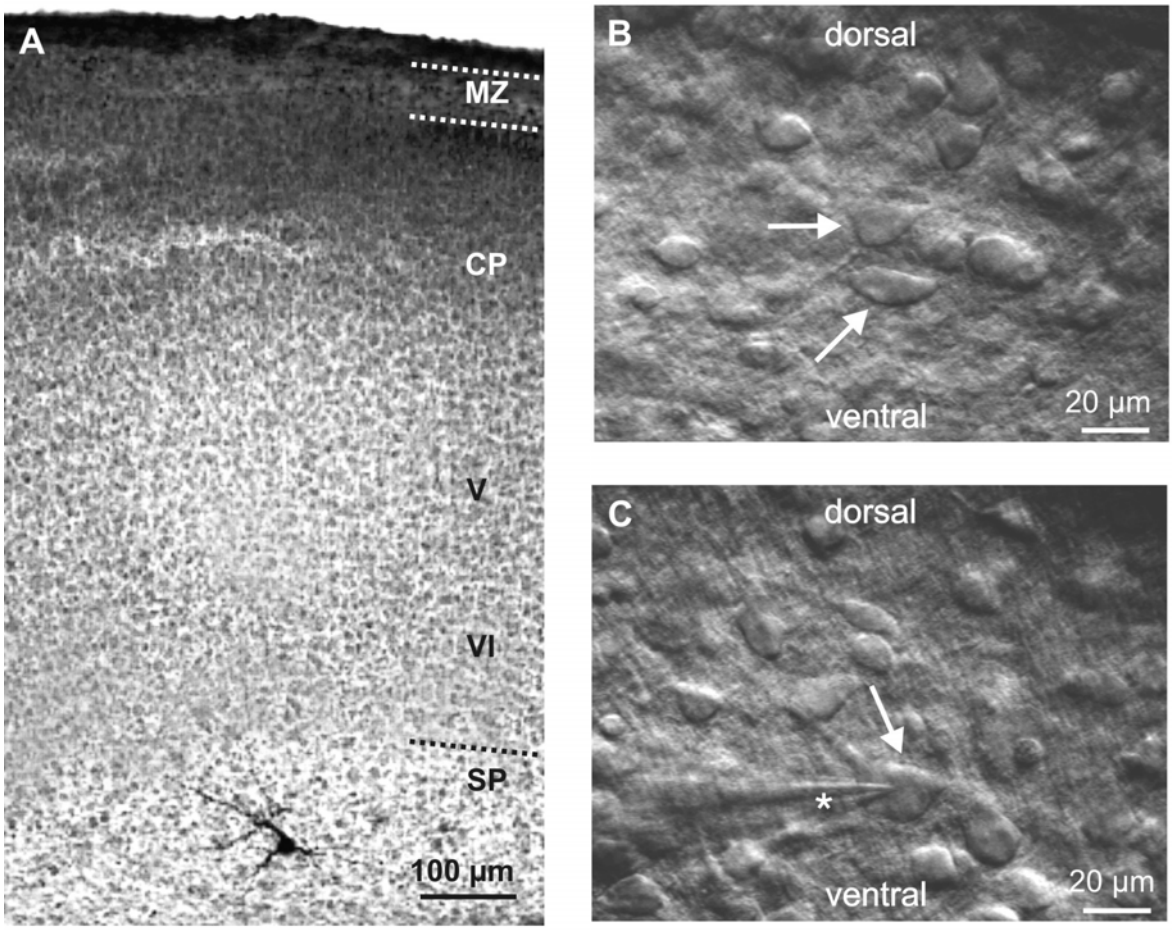

Figure 4. Location of the subplate in the developing cortex and appearance of SPn under video-assisted Nomarski microscopy. **A.** Photomicrograph of Nissl-stained coronal section with biocytin-labeled SPn in a P2 rat. Nissl and biocytin co-staining revealed the location of the cell-sparse subplate (SP) and of densely cell-packed CP and layers V/VI as well as the position of biocytin-filled SPn within the subplate. **B.** Digital infrared-videomicroscopic image of SPn in a 400 µm thick coronal slice from a P2 rat. Arrows point to focused SPn showing horizontal and triangular forms of the soma. **C.** Digital infrared-videomicroscopic image of the patch pipette tip (marked by asterisk) during seal formation on a P2 SPn (marked by arrow).

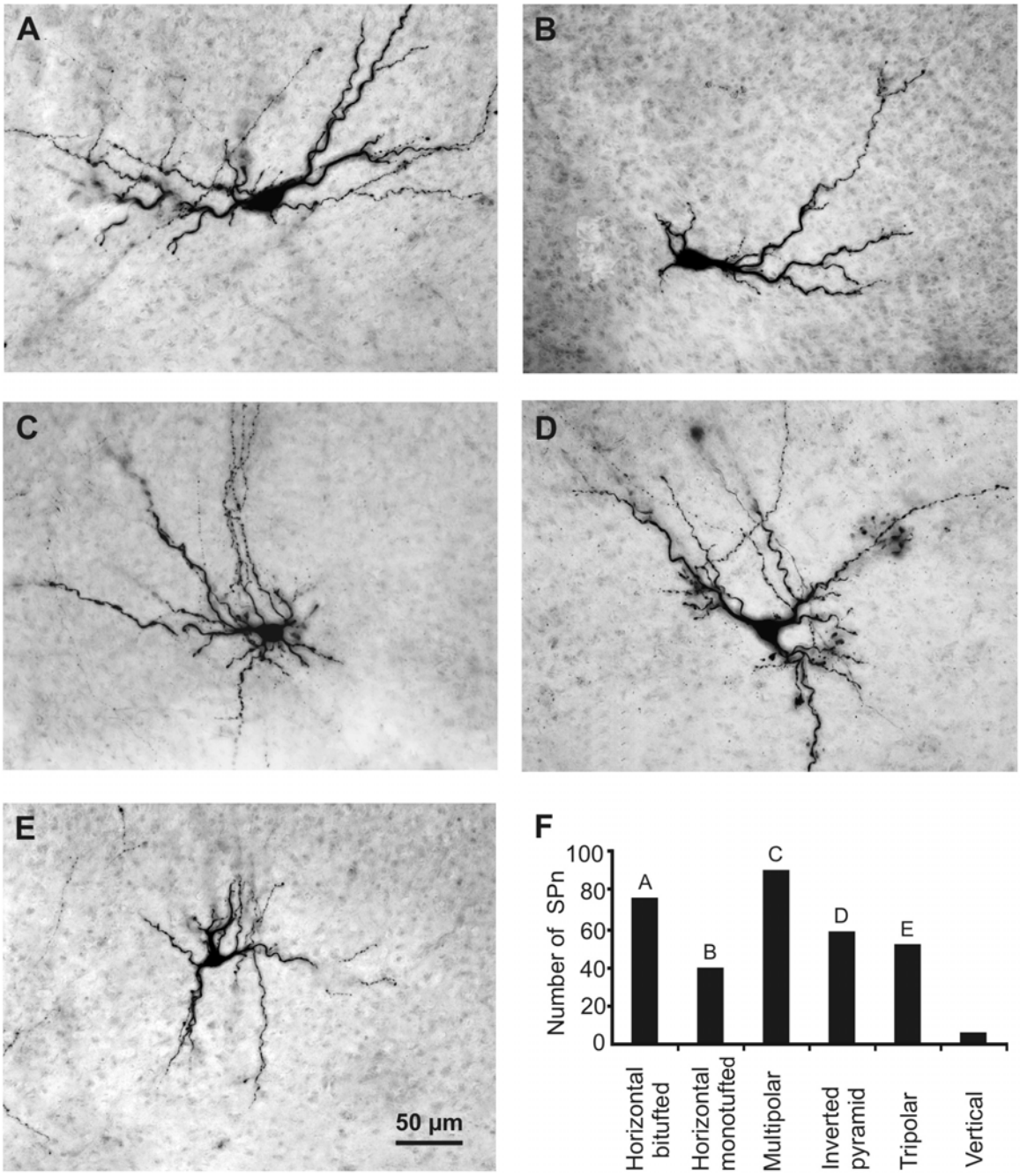

Figure 5. Morphological classification of biocytin-stained SPn. **A.** P3 horizontal bitufted SPn with large fusiform soma and primary dendrites oriented parallel to the pial surface. **B.** P2 horizontal monotufted SPn. **C.** P3 multipolar SPn with extensive dendritic arborization within SP and layers V/VI. **D**. P2 inverted pyramidal SPn with triangular soma and major dendrite oriented towards white matter. **E.** P3 tripolar SPn with triangular soma and the major dendrite oriented to the pial surface. Scale bar in **E** corresponds to **A**-**E** and pial surface is located toward the top in all photomicrographs. **F.** Bar diagram illustrating number of biocytin-stained SPn in the six morphological classes. Letters refer to the corresponding photomicrograph.

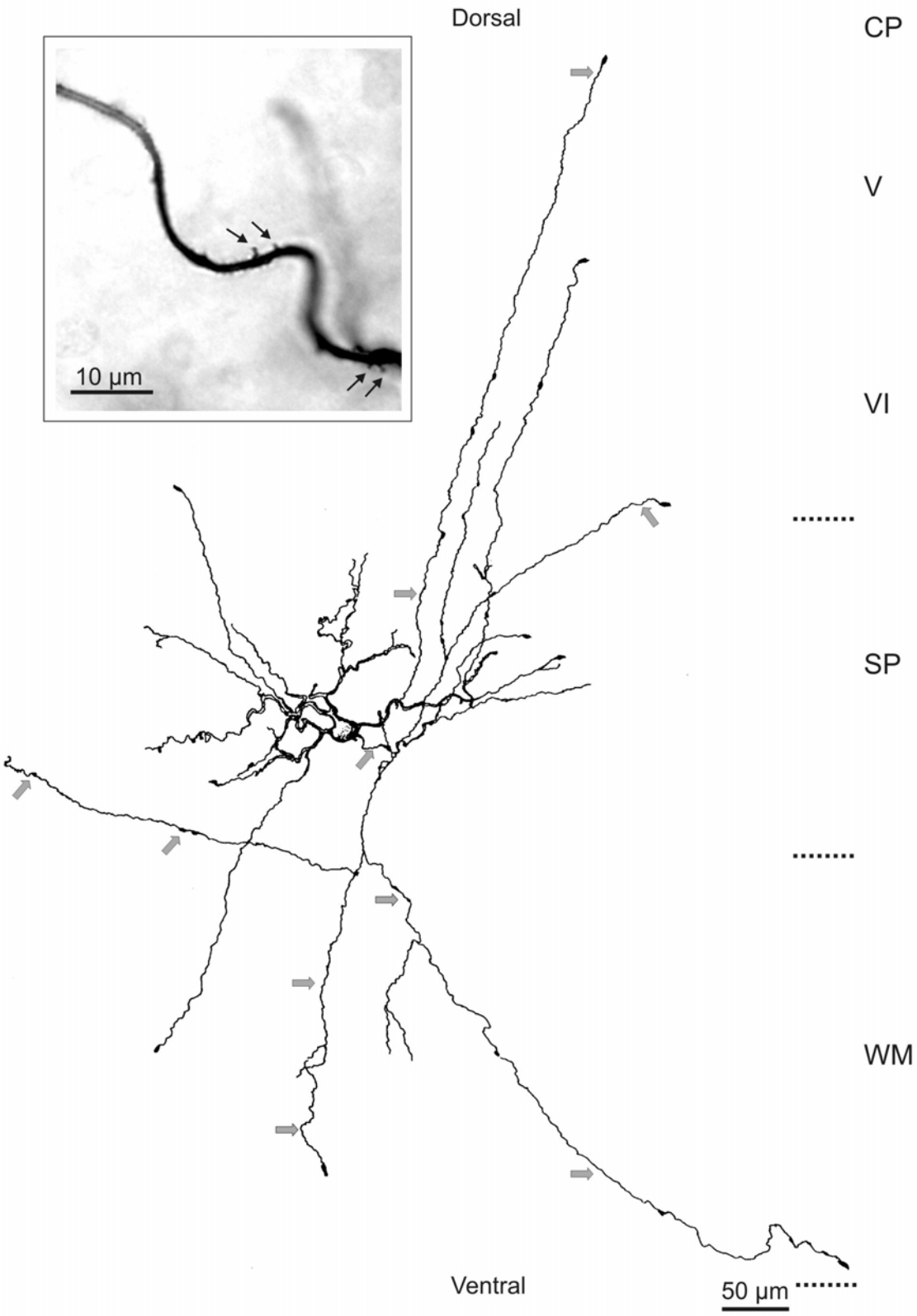

Figure 6. Morphological properties of SPn. Camera lucida reconstruction of a P1 SPn stained for biocytin. Note the ramified dendritic tree and the ascending and descending axonal collaterals marked by grey arrows. The inset shows a small axonal fragment from a P3 SPn displayed at high magnification. Note the presence of spines marked by black arrows.

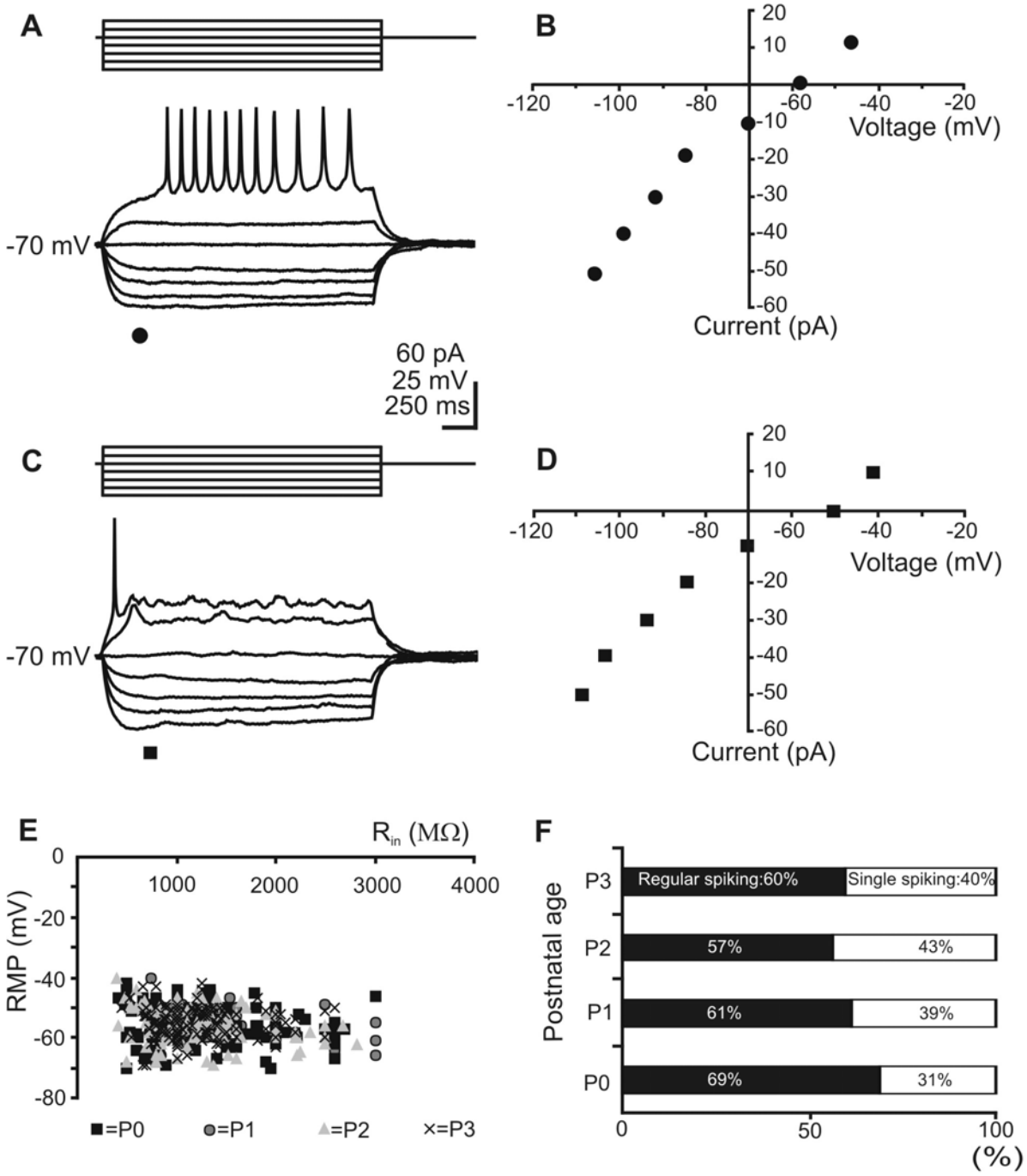

Figure 7. Membrane properties of *regular spiking* and *single spiking* SPn. **A.** Current-clamp recordings from a *regular spiking* SPn. Voltage responses to injection of hyper- and depolarizing current pulses at a holding membrane potential of -70 mV were recorded. A suprathreshold current pulse elicited repetitive action potentials. Resting membrane potential (RMP) was -59 mV. **B.** Current-voltage relationship of the SPn shown in **A**. Voltage responses were measured 300 ms after the onset of the pulse. The plot reveals a linear dependence of the voltage from the injected current. **C.** Current-clamp recording from a *single spiking* SPn at a holding membrane potential of -70 mV. RMP was -50 mV. **D.** Current-voltage relationship of the SPn shown in **C**. For both IV plots the current axis represents the total (holding and pulse) current. **E.** Relationship between RMP and input resistance (R_{in}) for all investigated SPn. Note the absence of age-dependent differences in RMP and R_{in}. **F.** Relationship between firing patterns and age. The proportion of *regular* and *single spiking* SPn remains relative constant over P0-P3 age interval.

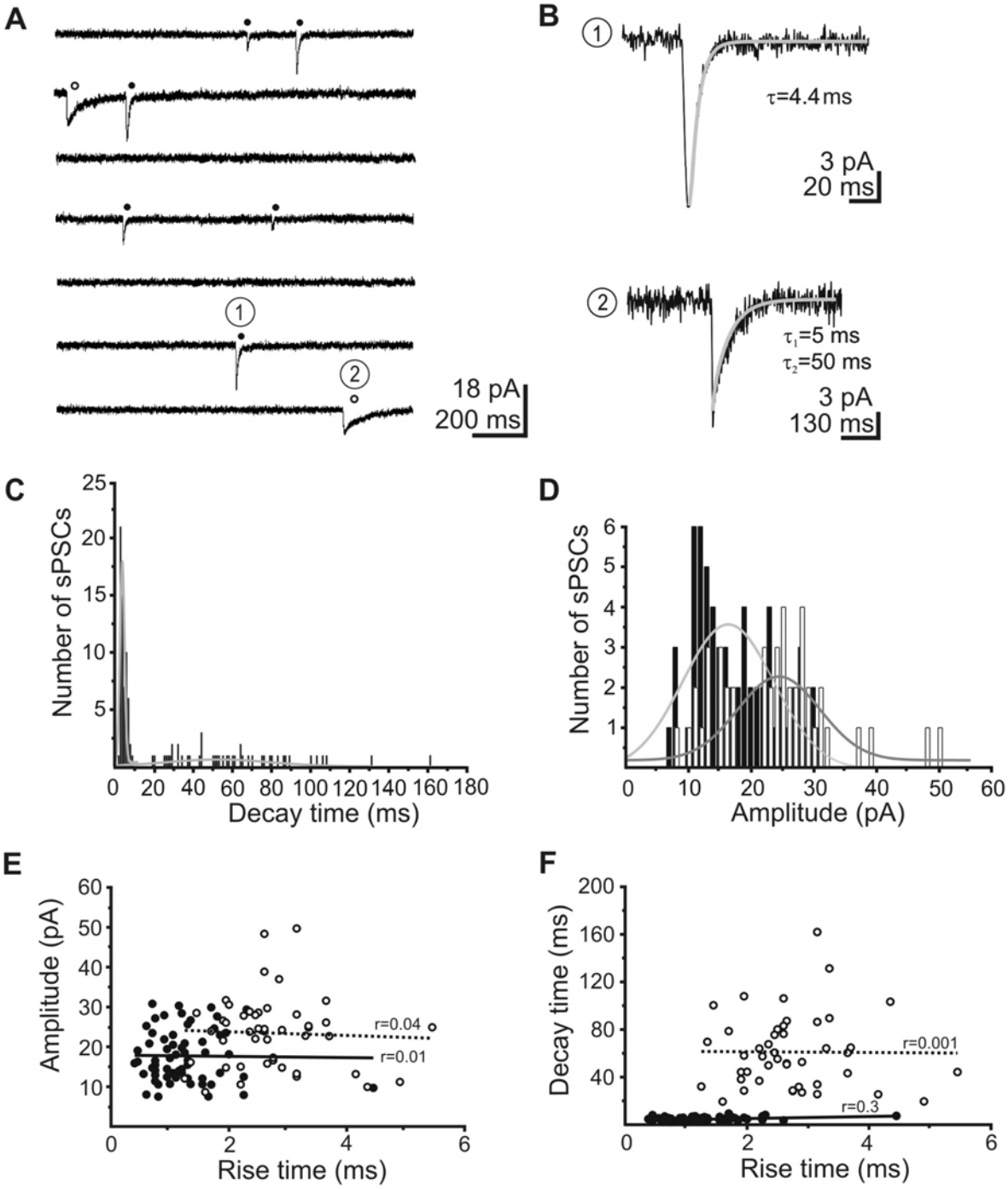

Figure 8. Fast and slow spontaneous postsynaptic currents (sPSCs) recorded at -70 mV in neonatal rat SPn. **A.** Seven consecutive traces recorded in a P1 SPn show fast (•) and slow (○) sPSCs occurring at low frequency. **B.** Example of a fast (①) and slow (②) sPSC from the traces shown in **A**. The decay of the fast sPSC was fitted with a monoexponential function and of the slow sPSC with a biexponential function. The fits are displayed as gray lines. Note different time scales. **C.** Decay-time distribution histogram obtained from the sPSCs recorded from a single SPn. Note the two peaks corresponding to fast and slow sPSCs. The limit between the two populations of sPSCs is 15 ms. **D.** Amplitude distribution of the fast (filled bars) and slow (open bars) sPSCs. For **C** and **D** the gray lines superimposed on the histogram represent the Gaussian distribution which best fits the data. **E.** Plot of sPSC amplitude versus rise-time for the fast (•) and slow (○) sPSCs. **F.** Plot of sPSC decay-time versus rise-time. For **E** and **F** the correlation coefficients obtained from regression analyses for fast (solid line) and slow (doted line) sPSCs indicate lack of correlation between rise-time and amplitude and between rise-time and decay-time. Data shown in **C**-**F** were obtained from the same P1 SPn.

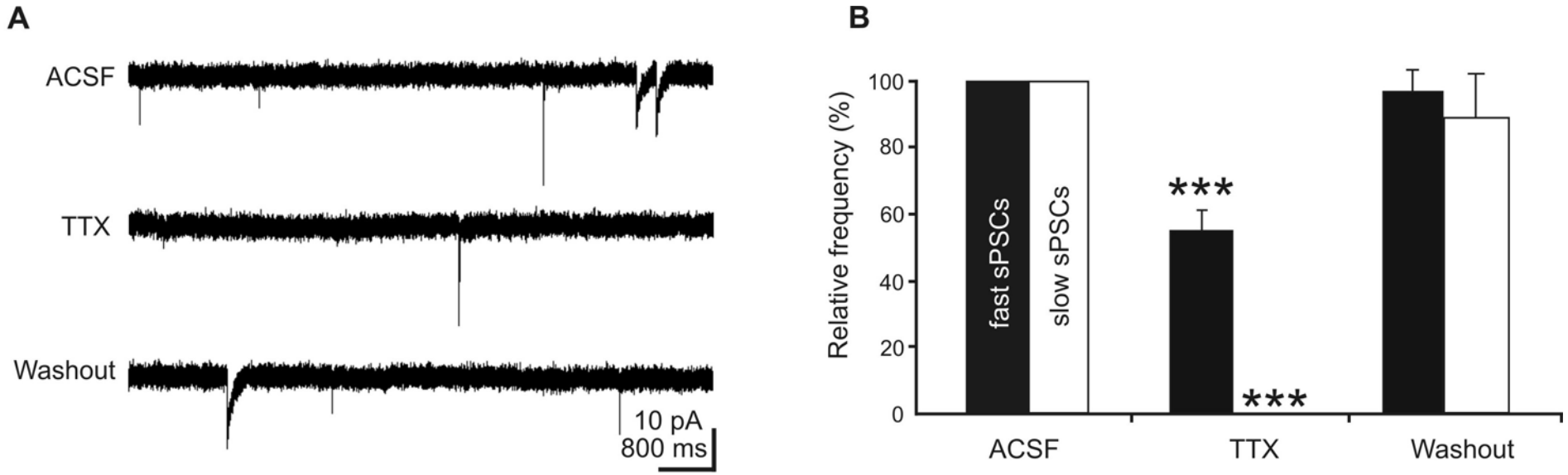

Figure 9. Effect of TTX on sPSCs. **A.** Fast and slow sPSCs recorded at -70 mV in a P1 SPn under control conditions, during 1 μM TTX application and after washout of TTX. Fast sPSCs were significantly reduced and slow sPSCs were completely abolished in TTX. **B.** TTX effect on relative frequency of fast (filled bars) and slow (open bars) sPSCs (n=8 cells).

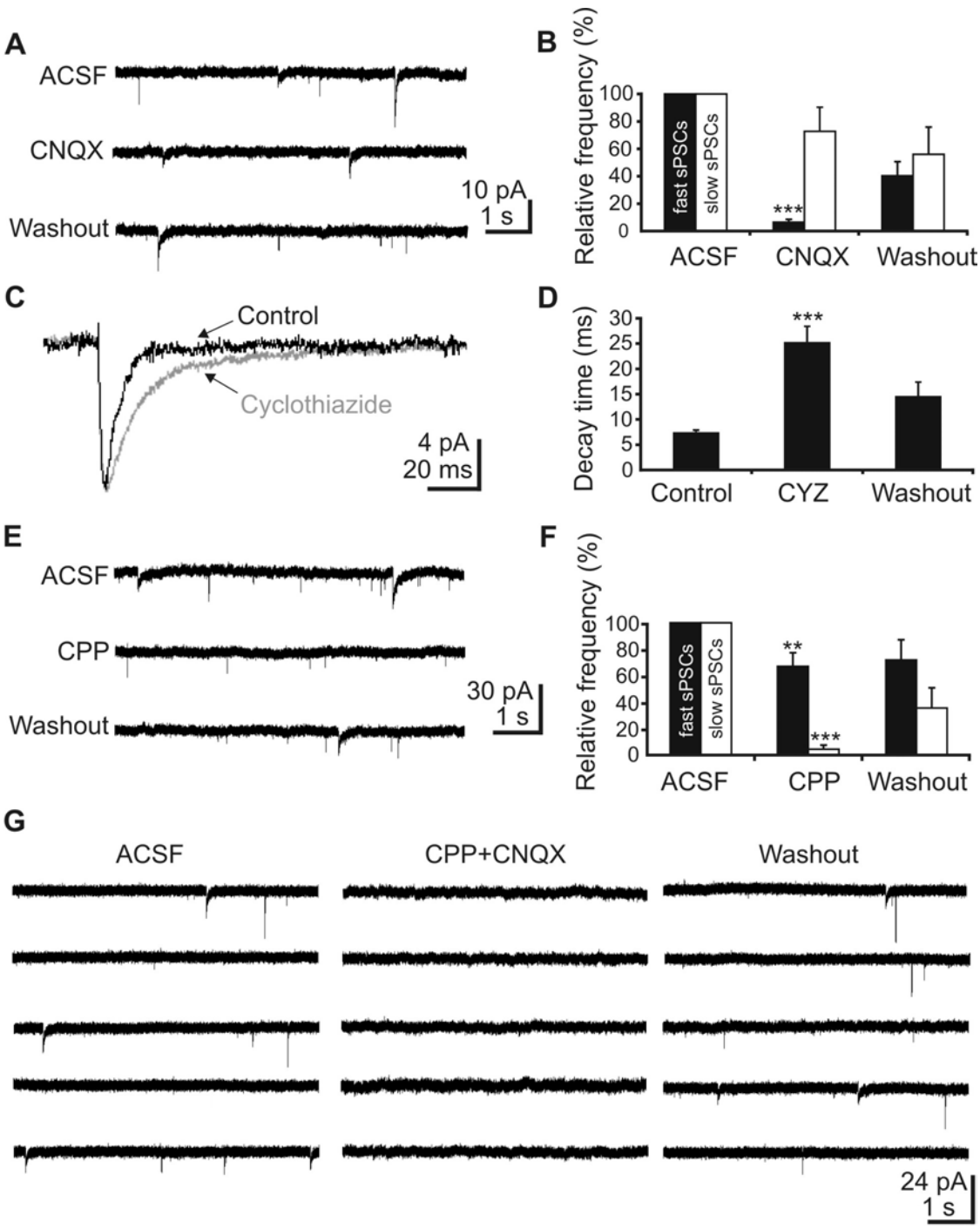

Figure 10. Role of ionotropic glutamate receptors for the mediation of sPSCs in SPn. **A.** Current traces from a P0 SPn recorded at -70 mV before, during and after bath application of 10 μM CNQX. Fast sPCS were completely blocked in CNQX, whereas slow sPCS remained unaffected. **B.** Effect of CNQX on the relative frequency of fast (filled bars) and slow (open bars) sPCS (n=12 cells). **C.** Superimposed averaged fast sPSC recorded from a P1 SPn under control condition (n=21 sPSCs) and in 100 μM cyclothiazide (n=24 sPSCs). Note the prolongation of decay-time of fast sPSCs in cyclothiazide. **D.** Effect of cyclothiazide on the decay-time of the fast sPSCs (n=6 cells). For **C** and **D** control recordings were performed in the presence of 20 μM CPP and 50 μM gabazine. **E.** Current traces from a P2 SPn recorded at -70 mV before, during and after bath application of 10 μM CPP. The slow sPSCs were abolished by CPP. **F.** Effect of CPP on the frequency of fast (filled bars) and slow (open bars) sPSCs (n=8 cells). **G.** Four consecutive current traces recorded at -70 mV before, during and after combined application of 10 μM CNQX and 10 μM CPP. Note complete blockade of fast and slow sPSCs in the mixture of CNQX and CPP.

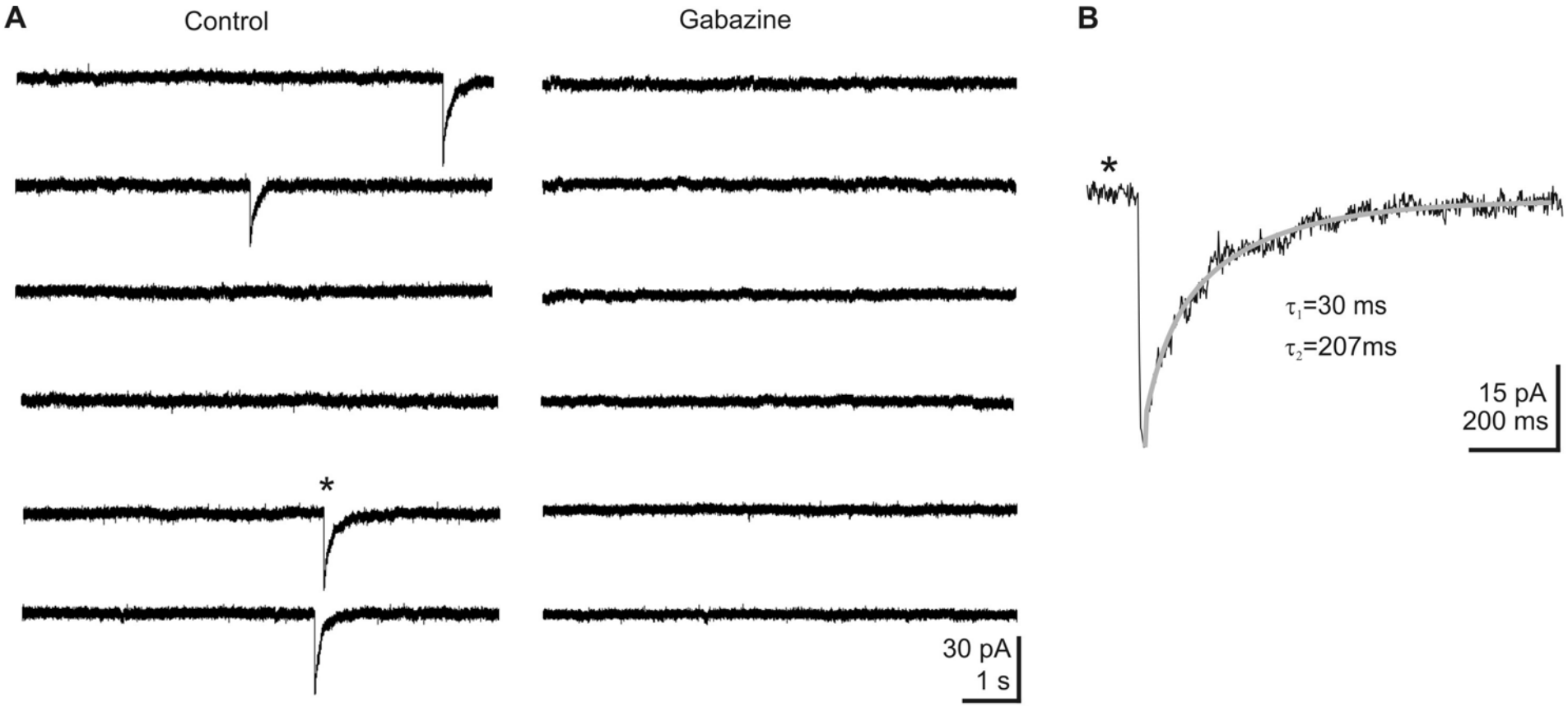

Figure 11. $GABA_A$ receptor-mediated sPSCs recorded with high-chloride pipette solution when the bath solution contained 20 μM CPP and 10 μM CNQX (control). **A.** Six consecutive traces recorded from a P1 SPn under control conditions and during bath application of 100 μM gabazine. Note the complete abolishment of the sPSCs by gabazine. **B.** Example of $GABA_A$ receptor-mediated sPSC from traces shown in **A** (*). The slow decay of the sPSC was fitted with a biexponential function.

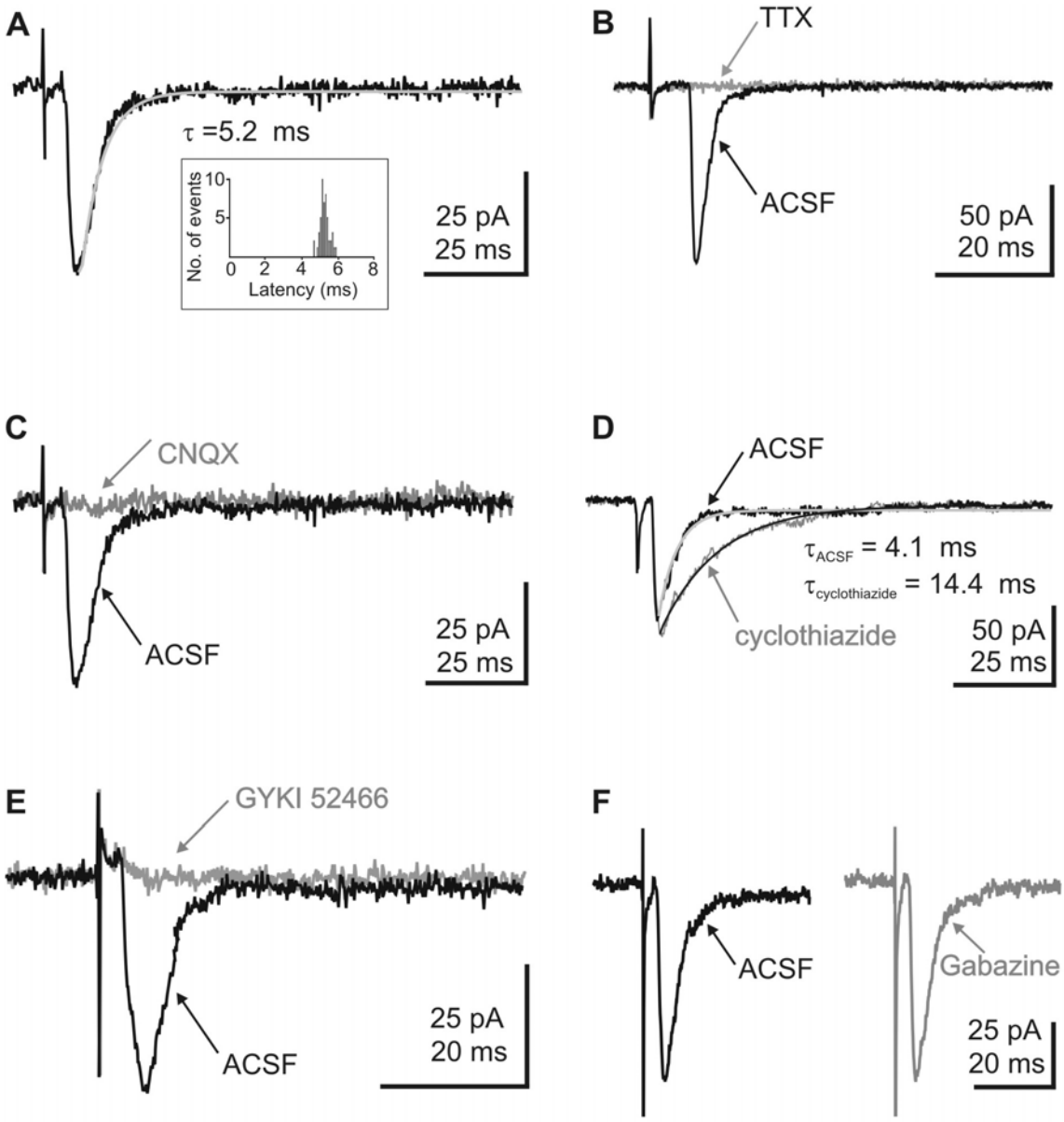

Figure 12. Postsynaptic currents elicited by electrical stimulation of the thalamocortical afferents (TA-PSCs) at a holding potential of -70 mV. **A.** TA-PSCs recorded in a P3 SPn. The PSC decay could be fitted with a monoexponential function (grey line). The inset shows the unimodal latency distribution of 50 TA-PSCs recorded from one SPn. **B.** TA-PSCs recorded in a P2 SPn in ACSF and in the presence of 1 μM TTX. TTX completely blocked the TA-PSC. **C.** TA-PSCs recorded in a P1 SPn in ACSF and in 10 μM CNQX. CNQX abolished the TA-PSC. **D.** TA-PSCs recorded in a P3 SPn in ACSF and in 100 μM cyclothiazide causing a pronounced prolongation of the response. **E.** TA-PSCs recorded in a P3 SPn in ACSF and in 80 μM GYKI 52466 causing the complete blockade of the response. **F.** TA-PSCs recorded in a P3 SPn in ACSF and in 100 μM gabazine. Neither the amplitude nor the kinetic of the TA-PSC were affected by gabazine.

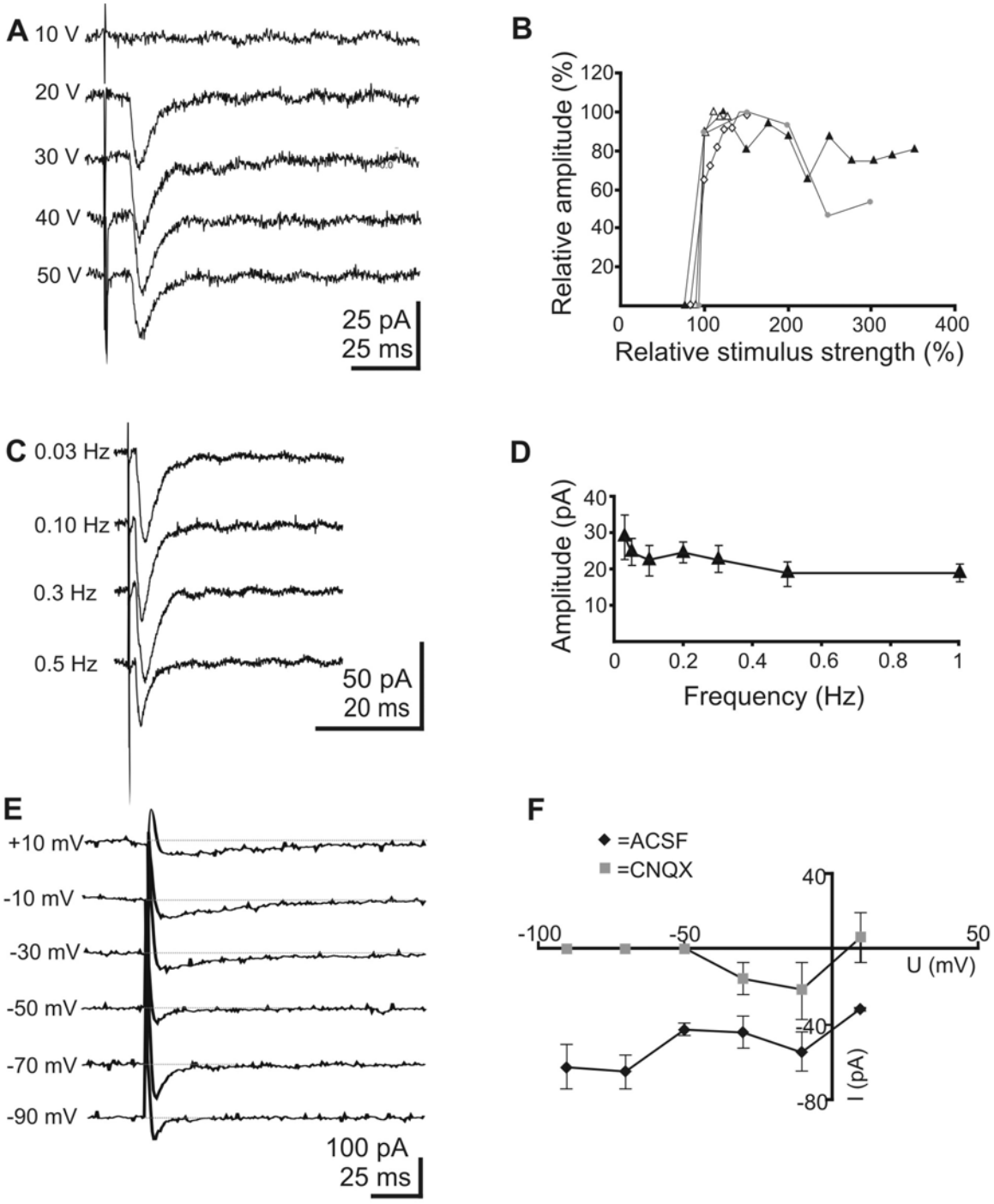

Figure 13. Properties of TA-PSCs. **A.** TA-PSCs recorded in a P3 SPn at stimulus intensities ranging from 10 to 50 V. Stimuli were delivered at 0.03 Hz. Note the constancy of the TA-PSCs once a critical threshold of stimulus intensity was reached. **B.** Relationship between relative TA stimulation intensity and relative response amplitude of TA-PSCs obtained from 4 SPn. TA-PSCs amplitudes and stimulus intensities are normalized to maximal amplitude and lowest suprathreshold stimulus intensity, respectively. **C.** TA-PSCs recorded in a P3 SPn at different stimulation frequencies. The amplitude and the kinetic of TA-PSCs were not affected by increased stimulation frequency. **D.** Relationship between TA stimulation frequency and amplitude of TA-PSCs obtained from 7 SPn. **E.** TA-PSCs recorded in a P3 SPn at different holding potentials using QX-314-containing pipette solution. Note the changes in the kinetics of TA-PSCs with increasing depolarization. **F.** Current-voltage relationship of the TA-PSCs recorded from 5 SPn under control conditions (◆) and after application of 10μM CNQX (■). Note the presence of the CNQX-insensitive component at membrane potentials positive to -50 mV.

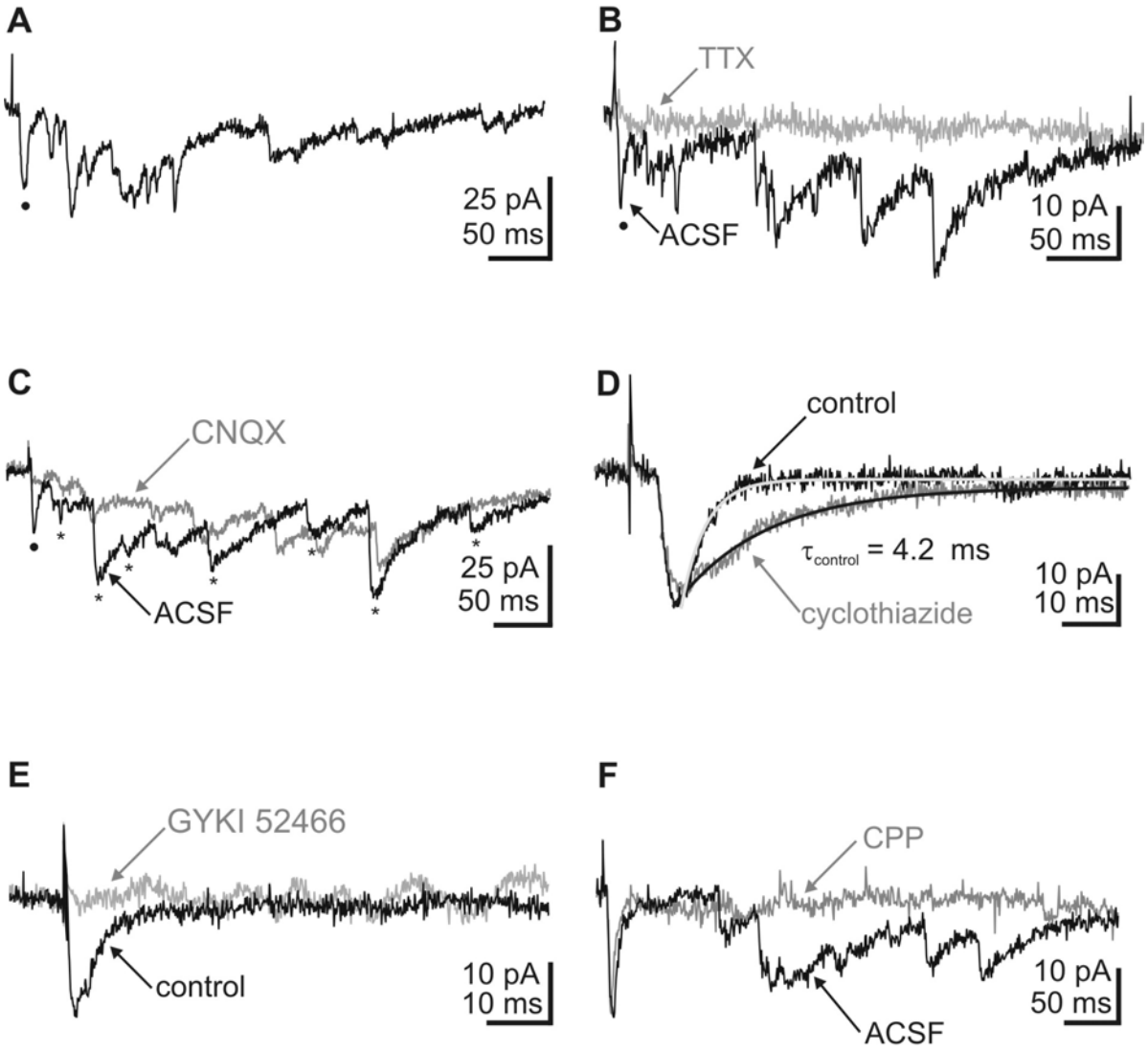

Figure 14. Postsynaptic currents elicited by electrical stimulation of the CP including layers V/VI (CP-PSCs). **A.** Monosynaptic (CP-monoPSC, •) and polysynaptic (CP-polyPSCs) responses recorded in a P2 SPn at -70 mV to electrical stimulation of the CP including layers V/VI. **B.** CP-PSCs recorded in a P0 SPn in ACSF and in the presence of 1 μM TTX. TTX abolished both CP-monoPSC (•) and CP-polyPSC. **C.** CP-PSCs recorded in a P0 SPn in ACSF and in the presence of 10 μM CNQX. Note the blockade of initial CP-monoPSC (•) and reduced amplitudes of CP-polyPSC (*) in CNQX. **D.** CP-monoPSCs recorded in a P3 SPn in 20 μM CPP (control) and after addition of 100 μM cyclothiazide. Note the cyclothiazide-induced prolongation of the CP-monoPSC. **E.** CP-monoPSCs recorded in a P2 SPn in 20 μM CPP (control) and in 80 μM GYKI 52466. **F.** CP-PSCs recorded in a P3 SPn in ACSF and in 20 μM CPP. CP-monoPSC was not affected, whereas CP-polyPSC was completely blocked by CPP.

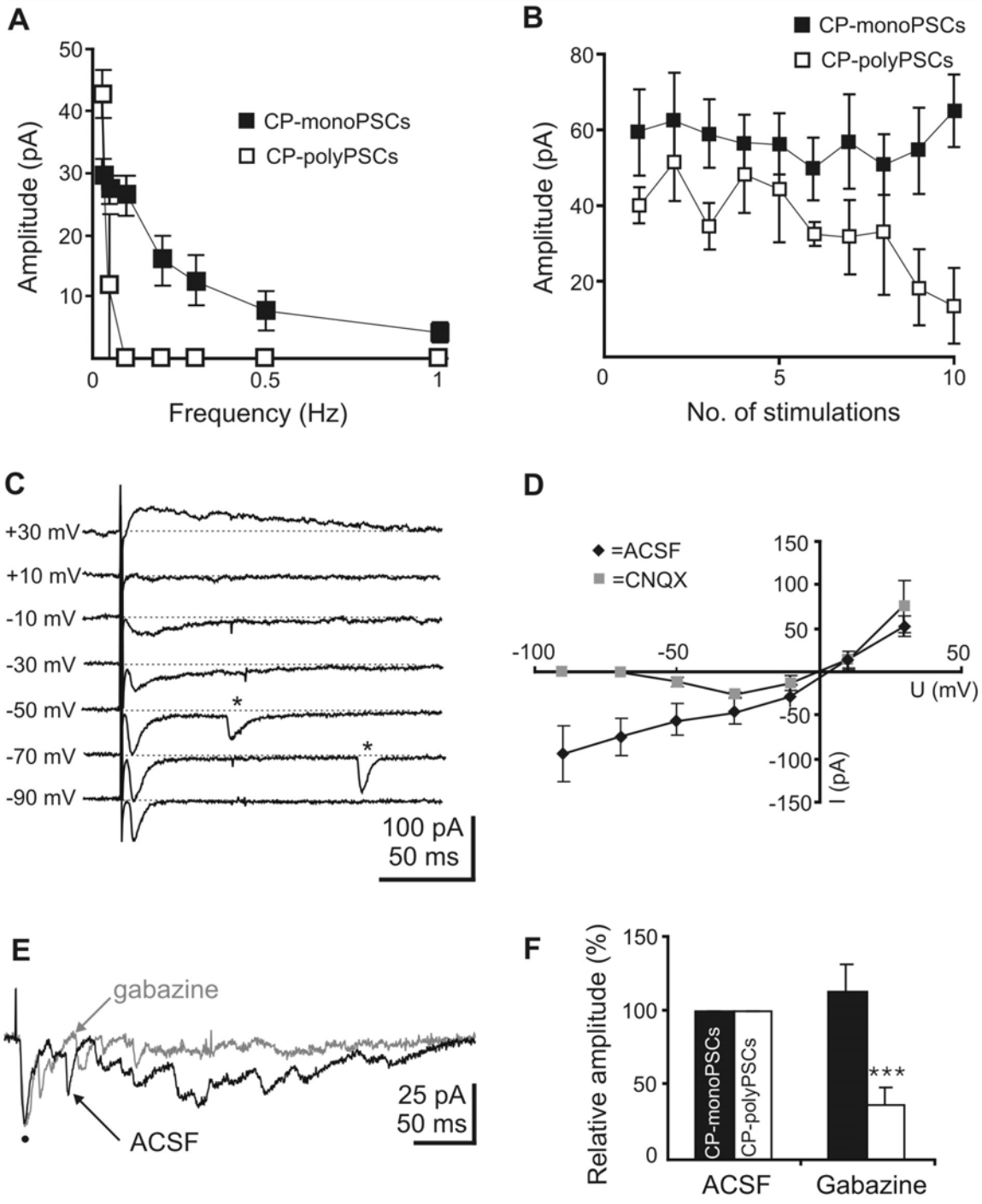

Figure 15. Properties of CP-PSCs. **A.** Relationship between stimulation frequency and amplitude of CP-monoPSCs (n=11 cells) and CP-polyPSCs (n=2 cells). Note the decreased amplitude of both CP-monoPSCs and CP-polyPSCs with increased stimulus frequency. **B.** Average amplitude of CP-monoPSCs (n=7 cells) and CP-polyPSCs (n=6 cells) to 10 consecutive stimulations at 0.03 Hz. Note the relative constant amplitude of CP-monoPSCs and the gradual decrease of CP-polyPSCs in response to repetitive stimulation. **C.** CP-monoPSCs recorded in a P1 SPn at different holding potentials using QX-314-containing pipette solution. Note the changes in the kinetics of CP-monoPSCs with increasing depolarization. Asterisks mark sPSCs. **D.** Current-voltage relationship of CP-monoPSCs recorded from 8 SPn under control conditions (◆) and after addition of 10 μM CNQX (■). **E.** CP-PSCs recorded in a P3 SPn in ACSF and in 100 μM gabazine. CP-monoPSC (•) were not affected by gabazine, whereas the maximal amplitude of CP-polyPSC was significantly reduced. **F.** Effect of 100 μM gabazine on the relative amplitude of CP-PSCs recorded from 5 SPn.

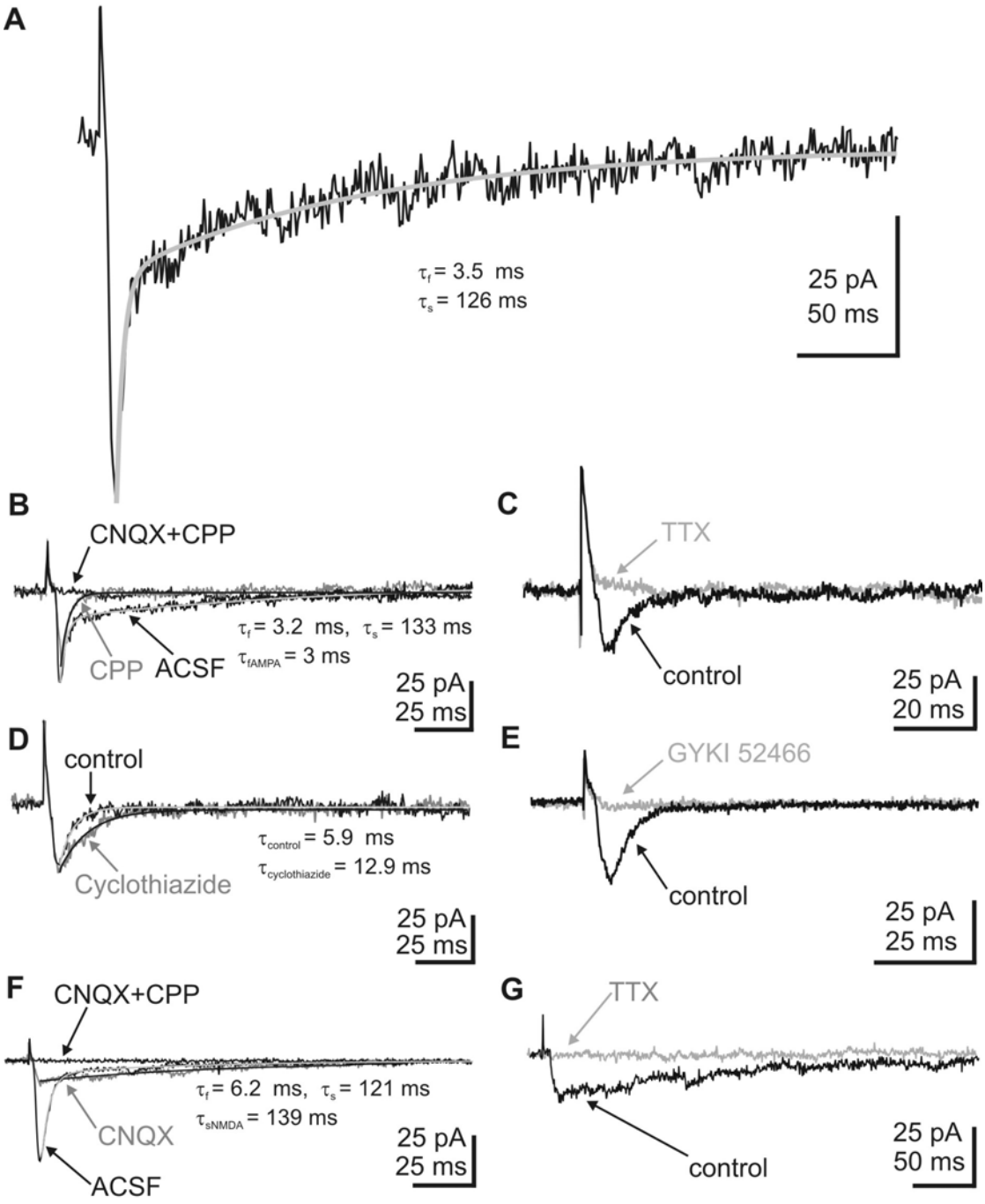

Figure 16. Dual-component monosynaptic PSCs elicited by electrical stimulation of the subplate (dual-component SP-monoPSCs). **A.** Dual-component SP-monoPSC recorded in a P2 SPn at -70 mV. The SP-PSC was fitted with a biexponential function (grey line) corresponding to the fast and the slow decaying component. **B.** Pharmacological isolation of the fast decaying component by application of 20 μM CPP. The CPP-insensitive component could be fitted with a monoexponential function and was blocked by addition of 10 μM CNQX. **C.** Fast decaying component of the dual-component SP-monoPSC recorded in 20 μM CPP (control) and after addition of 1 μM TTX. **D.** Fast decaying component recorded in 20 μM CPP (control) and 100 μM cyclothiazide. Cyclothiazide prolonged the fast decaying component. **E.** Fast decaying component recorded in 20 μM CPP (control) and after addition of 80 μM GYKI 52466. **F.** Pharmacological isolation of the slow decaying component of the dual-component SP-monoPSC by application of 10 μM CNQX. The CNQX-insensitive component could be fitted with a monoexponential function and was blocked by addition of 20 μM CPP. **G.** Slow decaying component of the dual-component SP-monoPSC recorded in 10 μM CNQX and 1 μM TTX.

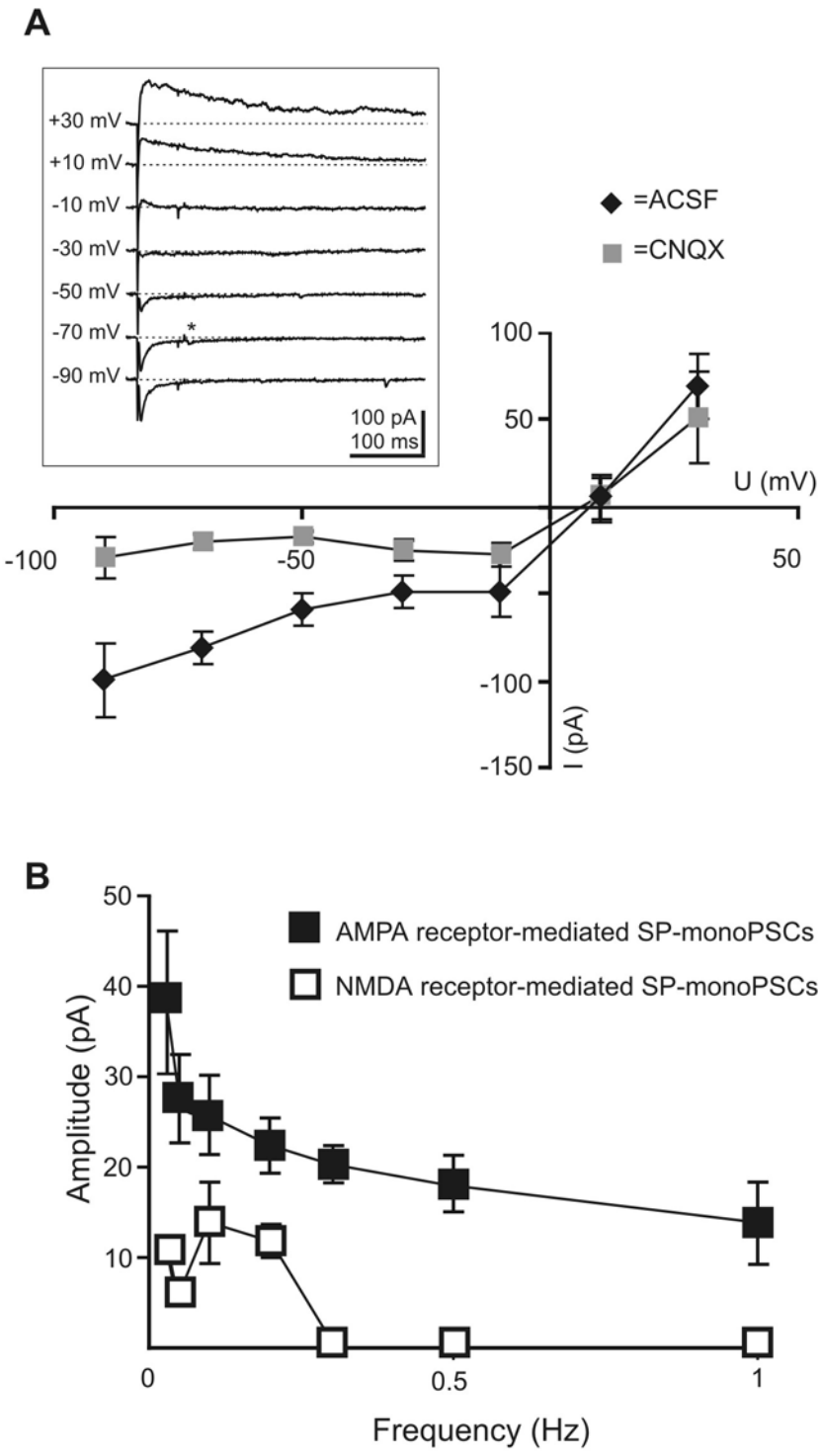

Figure 17. Properties of dual-component SP-monoPSCs. **A.** Current-voltage relationship of dual-component SP-monoPSCs recorded from 5 SPn under control conditions (◆) and after application of 10 μM CNQX (■). Recordings were performed with QX-314-containing pipette solution. Inset shows dual-component SP-monoPSCs recorded in a P1 SPn at different holding potentials. Asterisk marks sPSCs. **B.** Relationship between stimulation frequency and amplitude of fast decaying component (n=5 cells) and slow decaying component (n=2 cells) of the dual-component SP-monoPSCs. Note the decreased amplitude of both fast decaying and slow decaying component with increased stimulation frequency.

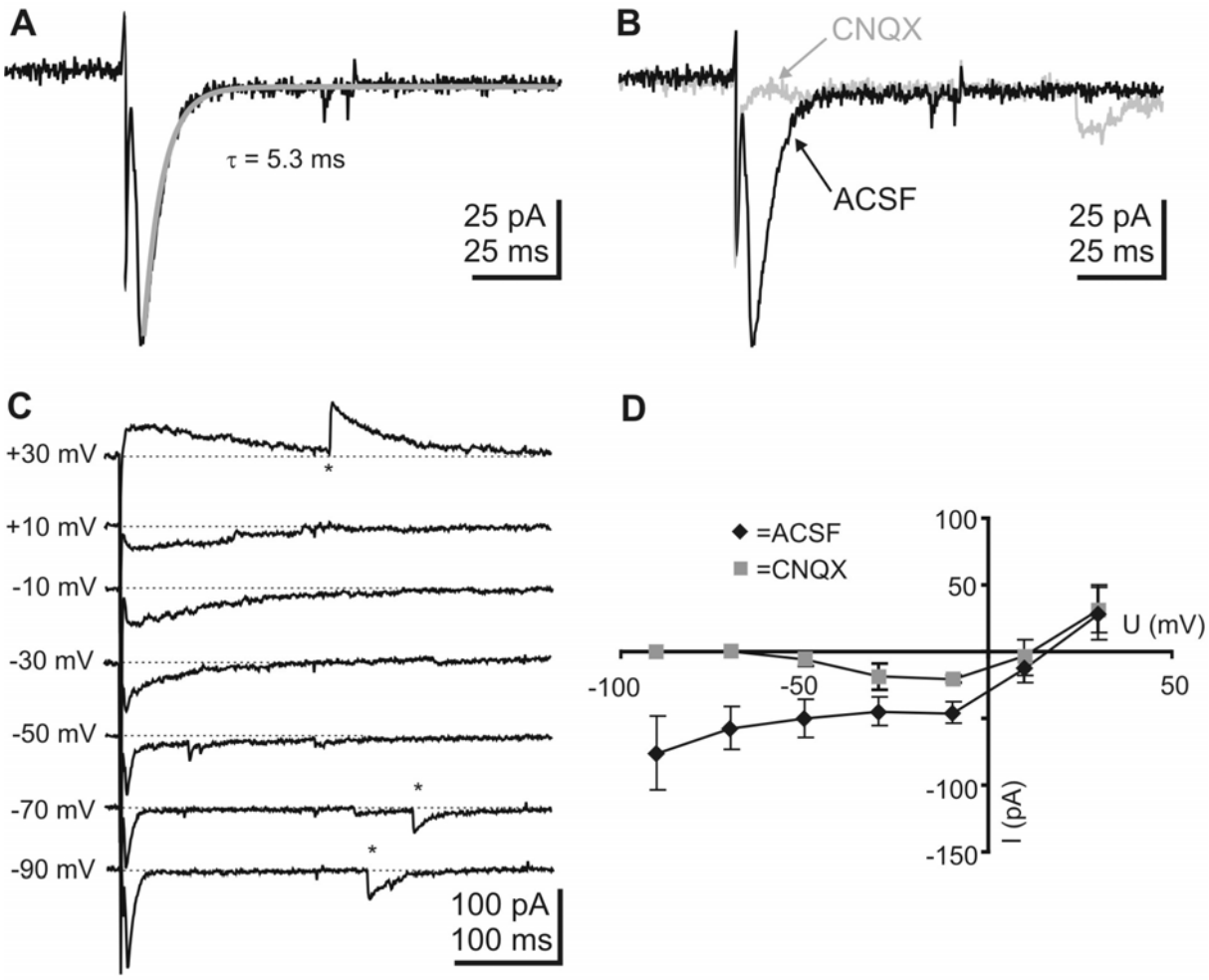

Figure 18. Single-component monosynaptic PSCs elicited by electrical stimulation of the subplate (single-component SP-monoPSCs). **A.** Single-component SP-monoPSC recorded in a P3 SPn at -70 mV was fitted with a monoexponential function (grey line). **B.** Single-component SP-monoPSC recorded in ACSF and after addition of 10 μM CNQX. The single-component SP-monoPSC was abolished by CNQX. **C.** Single-component SP-monoPSCs recorded in a P2 SPn at different holding potentials using QX-314-containing pipette solution. Note the changes in the kinetics of the single-component SP-monoPSCs with increasing depolarization. Asterisks mark sPSCs. **D.** Current-voltage relationship of single-component SP-monoPSCs recorded from 3 SPn under control conditions (◆) and after addition of 10 μM CNQX (■). Note the presence of additional CNQX-insensitive component at depolarized membrane potentials.

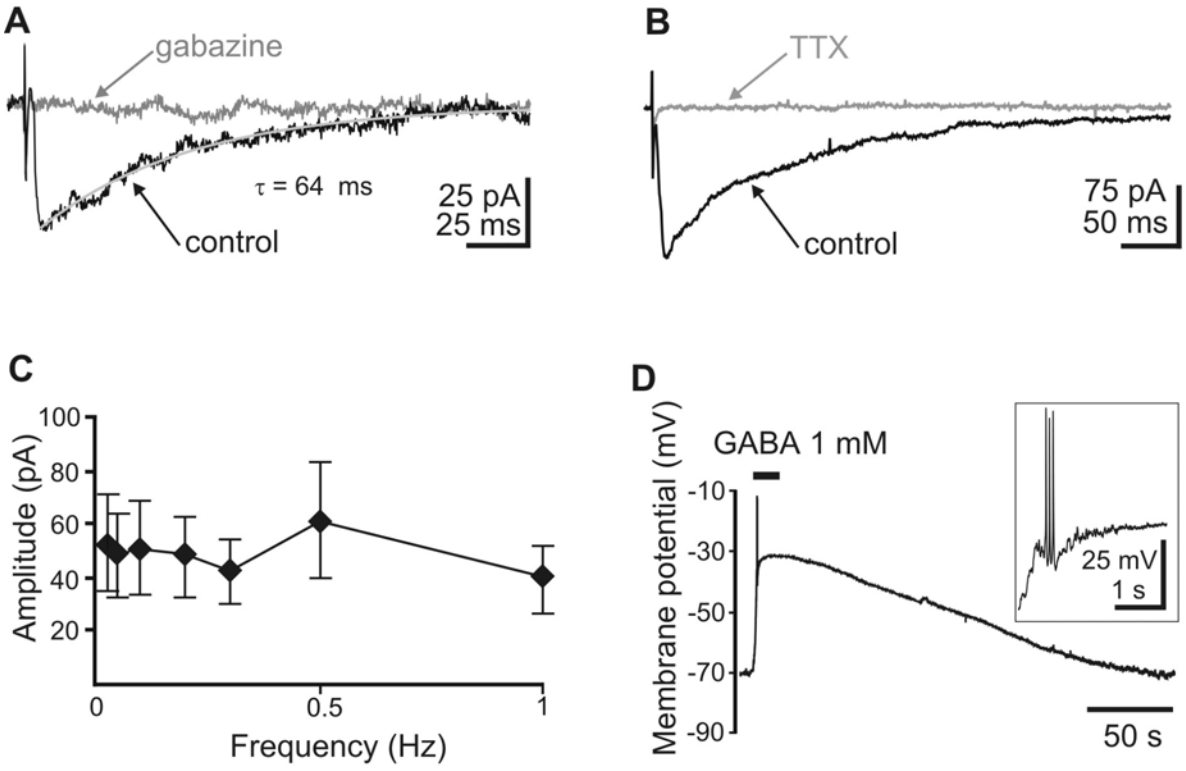

Figure 19. Chloride-driven monosynaptic PSCs elicited by stimulation of the subplate and mediated by $GABA_A$ receptors with depolarizing action in SPn. **A**. $GABA_A$ receptor-mediated SP-monoPSC recorded in 10 μM CNQX and 20 μM CPP (control) and in 100 μM gabazine when high-chloride pipette solution was used. The GABAergic SP-monoPSC revealed a long decay-time constant and could be fitted with a monoexponential function (grey line). **B.** $GABA_A$ receptor-mediated SP-monoPSC recorded in a P3 SPn in 10 μM CNQX and 20 μM CPP (control) and after addition of 1 μM TTX. **C.** Relationship between stimulation frequency and amplitude of $GABA_A$ receptor-mediated SP-monoPSCs (n=4 cells). Note the constancy of the PSCs amplitude even at high stimulation frequency. **D.** Depolarizing response to bath-applied GABA recorded in gramicidin perforated patch conditions in a P1 SPn. GABA was applied for 15 s. Note GABA evoked action potentials displayed at a larger scale in the inset.

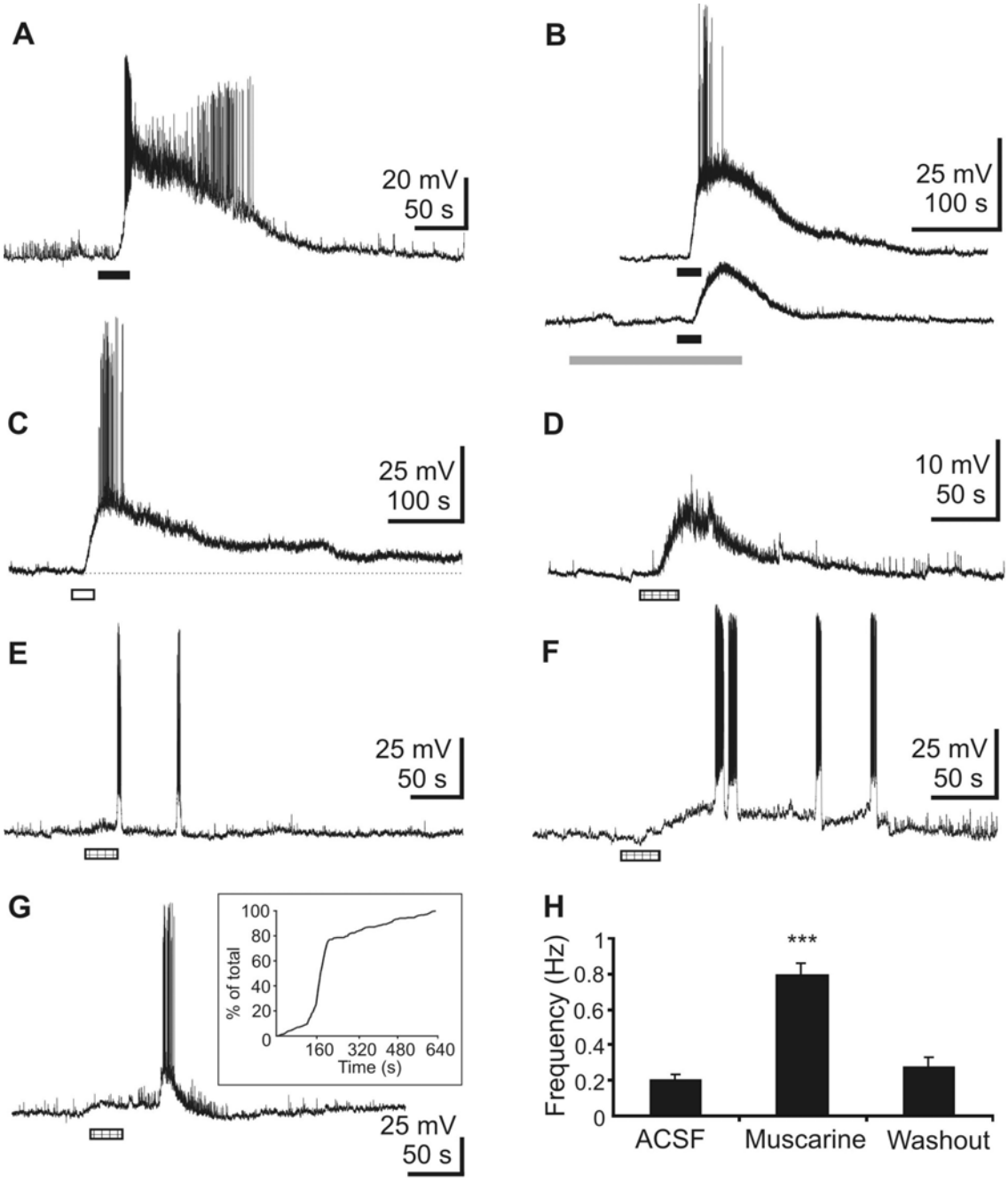

Figure 20. Activation of muscarinic and nicotinic receptors on SPn. **A.** Depolarizing response to carbachol (100 μM) recorded in current-clamp mode in a P1 SPn. Carbachol was bath-applied (black bar). Note the barrage of APs. **B.** Carbachol (black bar) effects recorded on a P2 SPn in ACSF and in a mixture of 1 μM TTX, 10 μM CNQX and 20 μM CPP (grey bar) reducing the carbachol-induced depolarization. **C.** Long-lasting depolarizing response to nicotine (100 μM) recorded in current-clamp mode in a P3 SPn. Nicotine was bath-applied (open bar). **D.** Depolarizing response to muscarine (30 μM) recorded in current-clamp mode in a P2 SPn. Muscarine-induced depolarization was not of sufficient amplitude to trigger APs. **E.** Oscillation-like changes in the membrane potential accompanied by APs recorded in current-clamp mode in response to muscarine (30 μM). Note the absence of muscarine-induced depolarization. **F.** Oscillation-like changes in the membrane potential accompanied by APs and depolarization recorded in current-clamp mode in response to muscarine (30 μM). **G.** Muscarine (30 μM) increased the frequency of spontaneous postsynaptic potentials (sPSPs) recorded in a P2 SPn. Inset displays the cumulative frequency distribution of the sPSPs recorded from the same SPn. In **D-G** muscarine was bath-applied (hatched bar). **H.** Effect of muscarine on the frequency of sPSPs (n=10 cells).

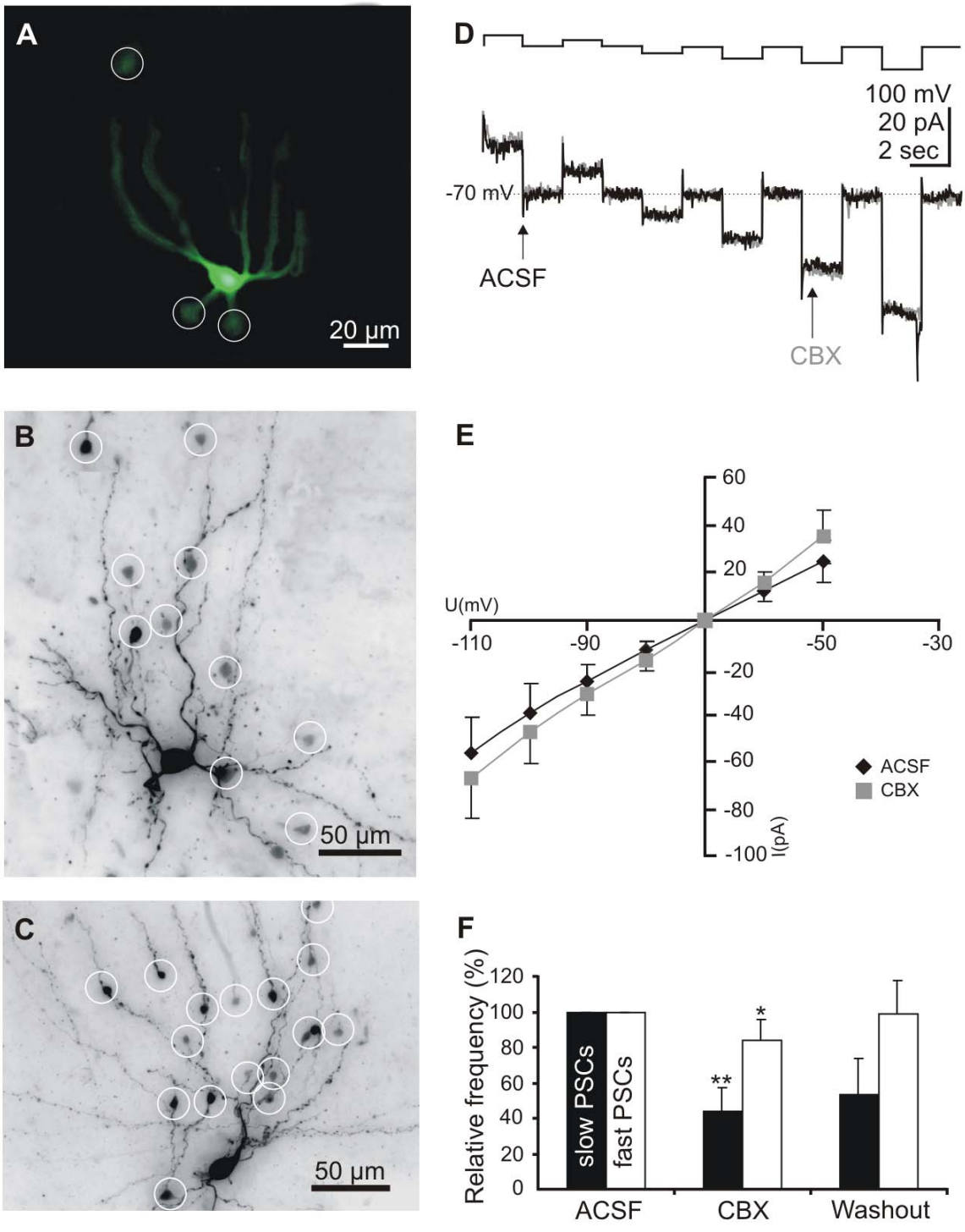

Figure 21. Gap junction coupling in the subplate. **A.** Lucifer yellow-stained SPn. Lucifer yellow injection leads to intense staining of the injected SPn and to weaker staining of 3 neighboring SPn (marked by white circles). **B.** and **C.** Biocytin-stained SPn. Injection of biocytin into one SPn stained several other neighboring neurons (marked by white circles). **D.** Hyper-and depolarizing current steps recorded in a P3 SPn in ACSF and in the presence of 100 µM carbenoxolone (CBX). Note the absence of CBX effects. **E.** Current-voltage relationship recorded from 22 investigated SPn in ACSF (◆) and CBX (■). **F.** Effect of CBX on the frequency of the fast (filled bars) and slow (open bars) sPSCs. Note the decreased frequency of both fast and slow sPSCs in CBX.

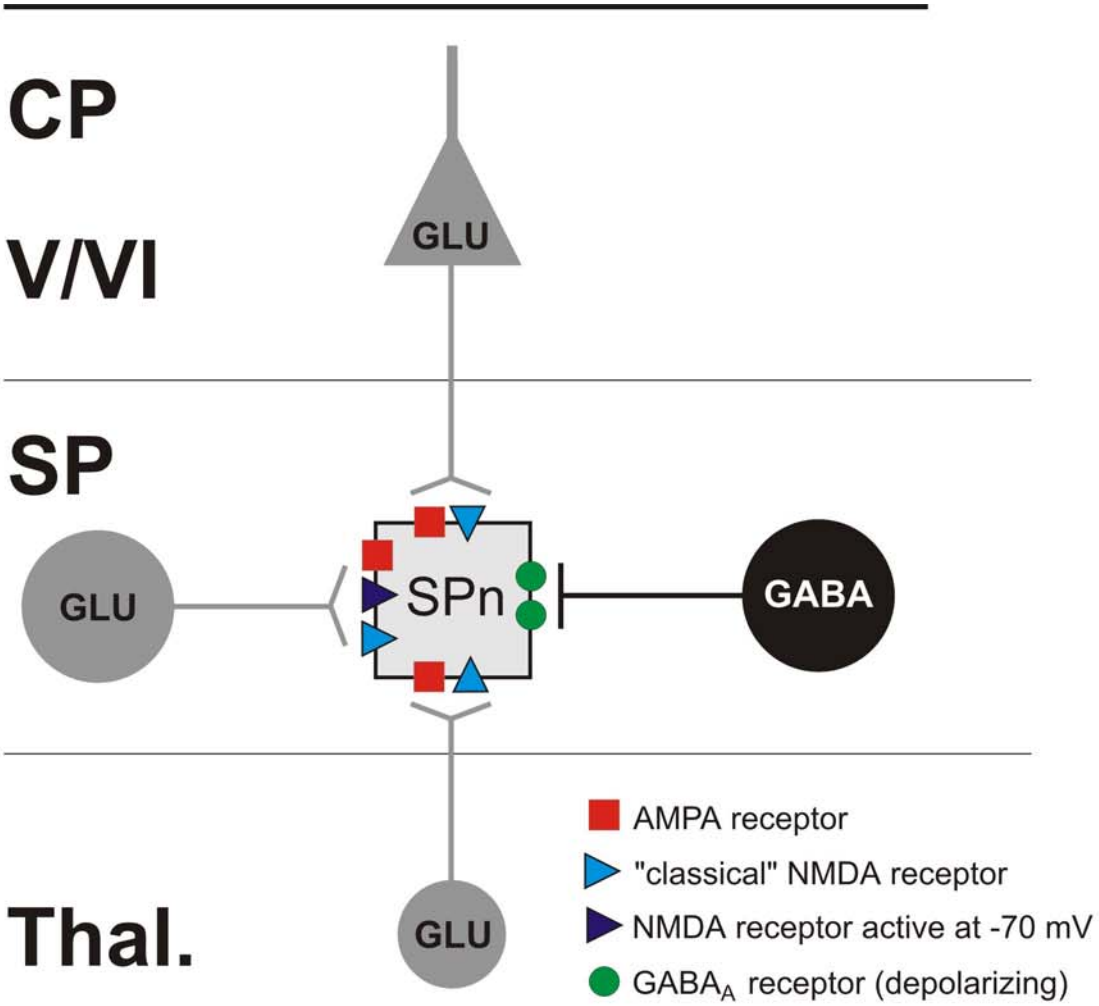

Figure 22. Schematic diagram illustrating the distribution of postsynaptic receptors on SPn for monosynaptic inputs arising from thalamus (Thal.), CP including layers V/VI and subplate (SP). Note that only synaptic inputs from the other SPn can lead to activation of $GABA_A$ receptors and NMDA receptors active at negative membrane potentials. Polysynaptic activity mediated by NMDA and $GABA_A$ receptors may be predominantly generated within the subplate.

8. List of abbreviations

ACh **= acetylcholine**

ACSF **= artificial cerebrospinal fluid**

AMPA **= (±)-α-amino-3-hydroxy-5-methylisoxazole-4-propionic acid**

APs **= action potentials**

BX **= carbenoxolone**

NQX **= 6-cyano-7-nitroquinoxaline-2,3-dione**

P **= cortical plate**

CPP = R(-)-3-(2-carboxypiperazin-4-yl)-propyl-1-phosphonic acid

DAB = 3,3-diaminobenzidine

DMSO = dimethylsulfoxide

EGTA = ethylene glycol-bis(2-aminoethylether)-N,N,N',N'-tetraacetic acid

GABA = γ-amino-butyric acid

GYKI 52466 = 1-(4-aminophenyl)-4-methyl-7,8-methylenedioxy-5*H*-2,3-benzodiazepine

HEPES = N-(2-hydroxyethyl) piperazine-N'-(2-ethanesulfonicacid)

MW = molecular weight

NMDA = N-methyl-D-aspartate

QX-314 = lidocaine N-ethyl bromide

BS **= phosphate-buffered saline**

P **= preplate**

SCs **= postsynaptic currents**

$\boldsymbol{R_{in}}$ = input resistance

RMP = resting membrane potential

SPn = subplate neurons

sPSCs = sponatneous postsynaptic currents

sPSPs = spontaneous postsynaptic potentials

TA = thalamocortical afferents

TTX = tetrodotoxin citrate

VZ = ventricular zone

WM = white matter

Acknowledgments

First of all, I would like to thank Prof. Dr. Heiko Luhmann for offering me the possibility to achieve this study, for his continuous and friendly support, for the helpful discussions and observations during all project phases and especially, for the mediated scientific enthusiasms.

I would like to thank Prof. Dr. Wolf-Rüdiger Schlue for his friendly support and helpful comments on the present study.

A special thank is addressed to Dr. Werner Kilb for the helpful discussions and for his friendly support during all project phases.

I would also like to thank Brigitte Hellmuth and Petra Schwarz for the excellent technical support.

Dr. Jochen Staiger I would like to thank for his competent help in morphological cell classification and Dr. Ildiko Világi for kindly providing GYKI 52466.

I would like to thank Dr. Iris Flagmayer for helpful discussions and Dirk Schubert for his help when computers had a bad day.

And last but not least, I would like to thank my parents Mariana and Nicolae Hanganu and grandparents Elena and Valeriu Ploae for always being my soul support. This work is dedicated to them.

This project was supported by DFG grant Lu 375/3 and the neuroscience graduate program GRK 320.